THE TRIPLET STATE OF BENZENE
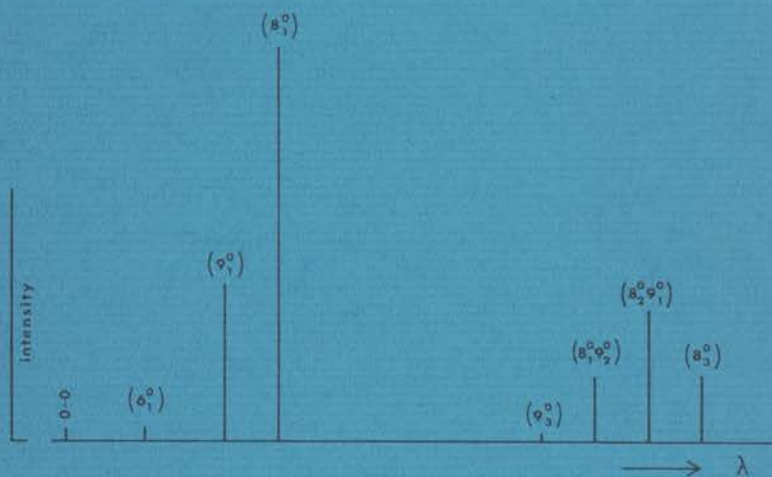
AN INVESTIGATION BY THE ZEEMAN EFFECT
AND MICROWAVE INDUCED DELAYED PHOSPHORESCENCE


J. van EGMOND

STELLINGEN

1. De resultaten van de experimenten in hoofdstuk V leveren een direct experimenteel bewijs van de $^3B_{1u}$-symmetrie van de laagste triplet-toestand van benzeen.

2. Katz et al.'s vibratieanalyse van het benzeen-absorptiespectrum rond 2100 Å, waaruit zou blijken dat de tweede singulettoestand van benzeen toegekend moet worden aan een $\pi\pi^*-^1B_{1u}$-toestand, is aanvechtbaar.

   Katz, B., Brith, M., Sharf, B., en Jortner, J., 1970, J. Chem. Phys., 52, 88.

3. Het is niet noodzakelijk dat bij Fermi-resonantie in een vibronisch geïnduceerd spectrum de betrokken banden elkaar "afstoten".

4. Mizushima en Koide's beschrijving van de spin-baankoppeling in het benzeenmolecule wordt ten onrechte door Hameka en Oosterhoff als onjuist bestempeld.

   Mizushima, M., en Koide, S., 1952, J. Chem. Phys., 20, 765.
   Hameka, H.F., en Oosterhoff, L.J., 1958, Mol. Phys., 1, 358.

5. Sixl meent ten onrechte dat de individuele relaxatietijden tussen de subniveaus van een electronische triplettoestand experimenteel niet onafhankelijk van elkaar te bepalen zijn.

   Sixl, H., 1971, Proefschrift, Stuttgart, p 124.

6. Bloom ziet, bij zijn voorstel om met behulp van een "level-crossing"-experiment de "tunnelling-frequency" in een CH_3-groep te bepalen, over het hoofd dat de spin-rooster-relaxatietijd ter plaatse van de "crossingen" veel korter kan zijn dan in een normaal NMR-experiment.

   Bloom, M., 1971, 4th Magnetic Resonance Conference, Israël.
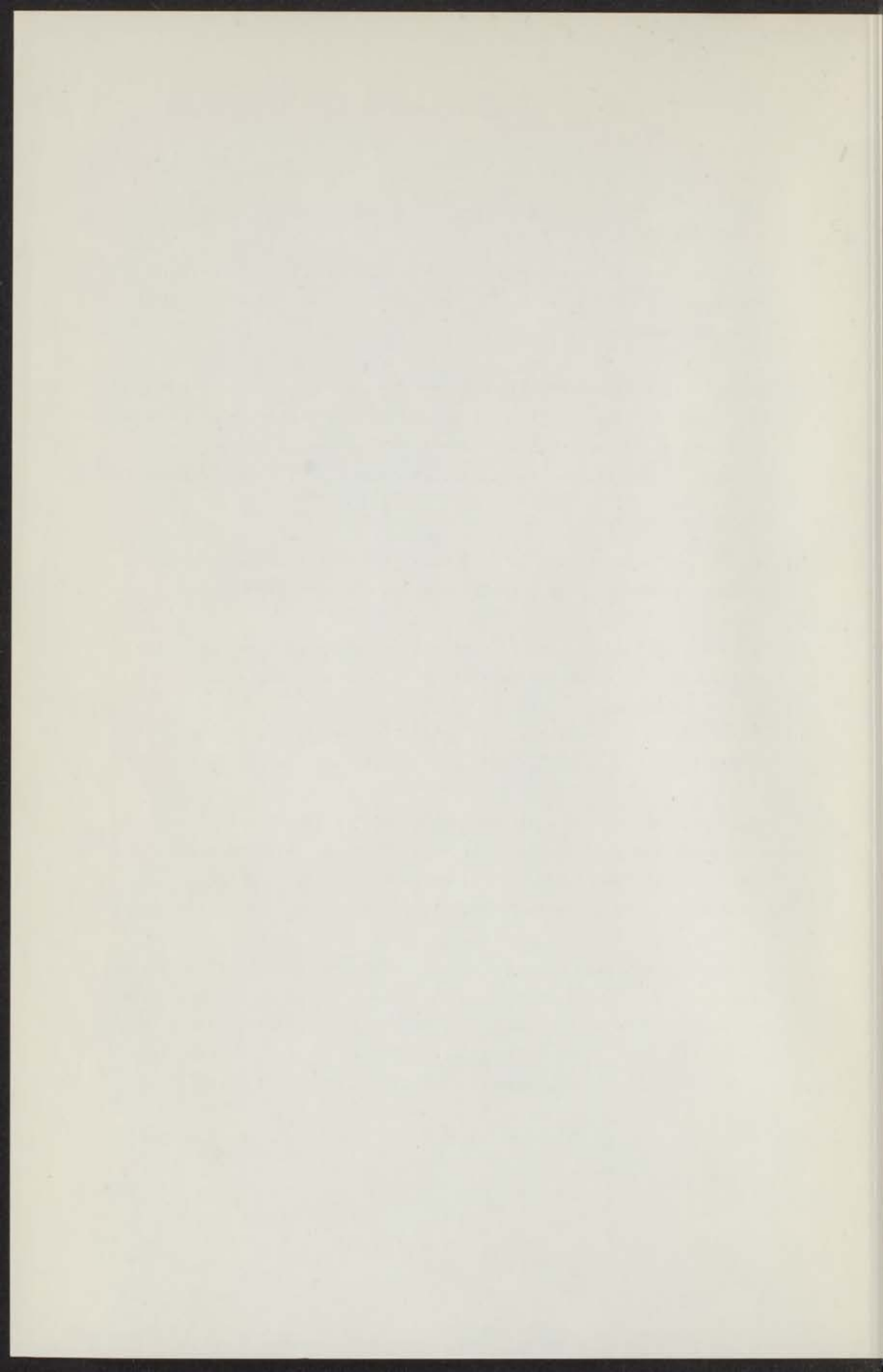
7. De verklaring, die door Stenberg en Dutton gegeven wordt voor het
   meta-richtende effect van de nitro-groep in een aangeslagen nitro-
   benzeenmolecule, is onbevredigend.

   Stenberg, V.I., en Dutton, D.R., 1972, Tetrahedron, <u>28</u>, 4635.

8. Terecht wordt door Douma in de kwestie van de euthanasie onderscheid
   gemaakt tussen beëindigen van het leven en beëindigen (of ook: het
   niet-aanvangen) van de behandeling.

   Douma, J., 1973, Euthanasie, De Vuurbaak, Groningen, p 28.

9. Schilders interpretatie van Openbaring 1:10 verdient de voorkeur boven
   die van Greydanus.

   Schilder, K., De Openbaring van Johannes en het Sociale Leven,
   Ton Bolland, Amsterdam, p 21.

   Greydanus, S., Korte Verklaring van de Heilige Schrift, Kok, Kampen.

10. Het verdient aanbeveling in onze moderne tijd de emancipatie ook door
    te voeren in de hockeyspelregels.

11. Nu uit recente onderzoekingen is komen vast te staan dat roken de
    hersenfuncties nadelig beïnvloedt is tevens duidelijk waarom acties
    tegen het roken altijd zo weinig opleveren.

J. van Egmond   Leiden, 7 juni 1973

THE TRIPLET STATE OF BENZENE

AN INVESTIGATION BY THE ZEEMAN EFFECT
AND MICROWAVE INDUCED DELAYED PHOSPHORESCENCE

JAN VAN EGMOND

THE TRIPLET STATE OF BENZENE

An investigation by the Zeeman effect
and Microwave Induced Delayed Phosphorescence

JAN van EGMOND
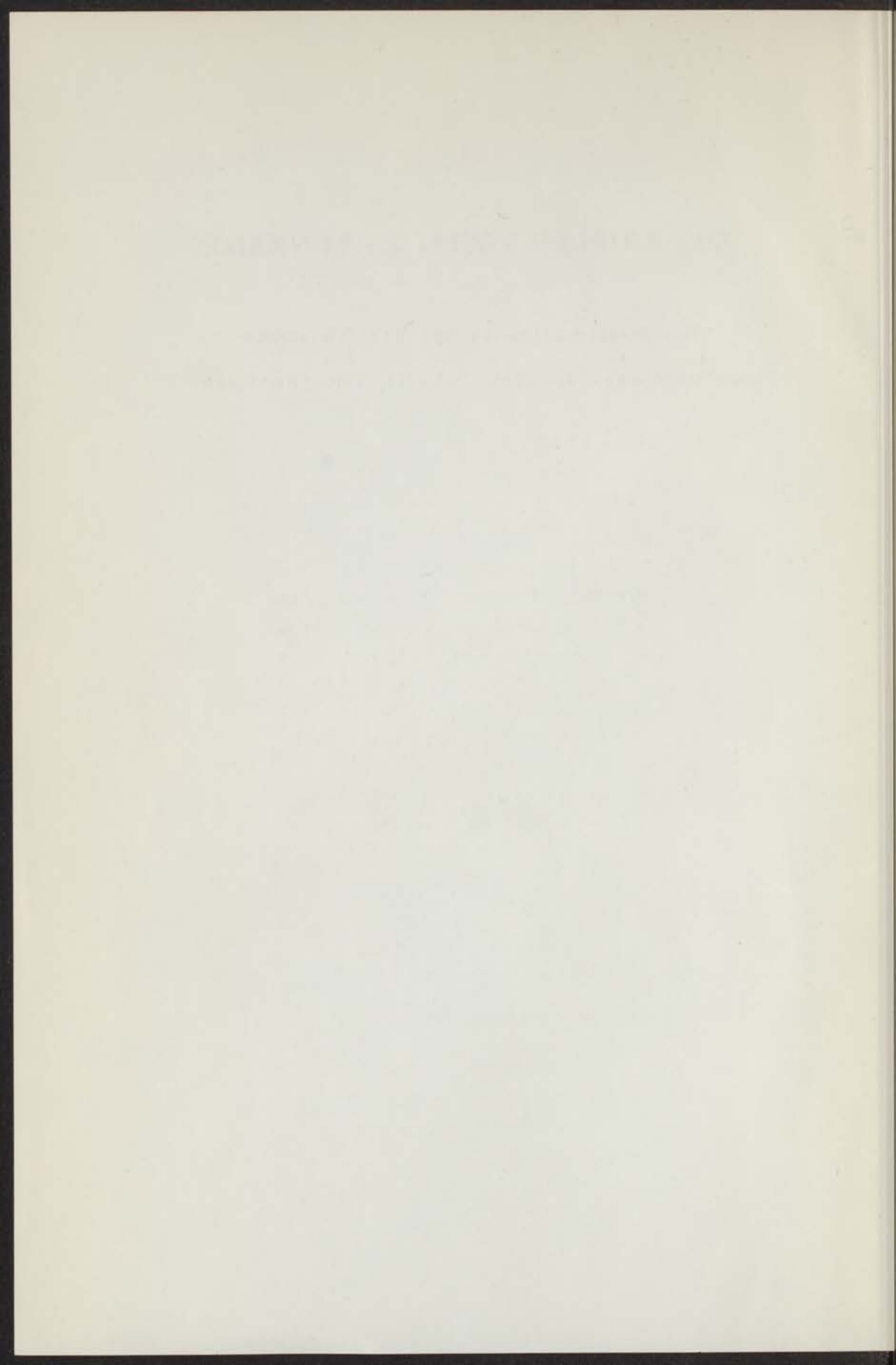
Geboren te Hillegom in 1945

PROMOTOR: PROF.DR. J.H. VAN DER WAALS

*Aan de nagedachtenis
van mijn vader*

aan mijn moeder

CONTENTS

CHAPTER I

Introduction.

After the pioneering work of Lewis and Kasha [1] in which they
recognized the phosphorescence of organic molecules as coming from the lowest
triplet state, numerous investigations have supported the existence of such
a paramagnetic metastable state. Microwave transitions between the three sub-
levels were first observed by Hutchison and Mangum [2] in ESR experiments on
a durene crystal doped with naphthalene in a field of 2-4 kGauss. These
electron spin resonance transitions in first approximation correspond to a
change of ± 1 in the magnetic quantum number m. Soon also the $\Delta m = 2$
transition was found by van der Waals and de Groot [3] of the same molecule
diluted in a glass. These experiments prove that the phosphorescent state is
indeed paramagnetic, having a spin angular momentum S = 1.

Owing to the low symmetry of aromatic molecules as compared to atoms,
group theory does not require the triplet state to be triply degenerate;
spin-spin and spin-orbit interactions lift, in most cases, the degeneracy
completely, giving a zero-field splitting. The existence of this splitting,
which became clear from the ESR experiments also permits microwave
transitions to occur in the absence of an external magnetic field, as first
observed by Erickson [4] for inorganic ions, and later by Hutchison [5] for
the phenanthrene molecule.

Later, it was shown that such microwave transitions, with or without a
field, can be determined by looking at changes in the phosphorescence
intensity. In 1967 Sharnoff [6] in this way detected the $\Delta m = 2$ transition in
naphthalene in an external field, while in 1968 Schmidt [7] observed changes
in the phosphorescence of quinoxaline due to resonant microwaves in zero-
field. These variations in the intensity brought about by microwave
transitions are caused by the difference in decay characteristics of the
three triplet sublevels.

In fig. 1.1 we show the scheme – the origin of which goes back to the work of Jablonski [8] – that provides the basis for explanation of all these experiments. We have chosen naphthalene as an example. The triplet state can be prepared by exciting the molecule with light of the appropriate wavelength from the ground state S_o to the first excited singlet state S_1. From there part of the molecules cross to the lowest triplet state T_o, loosing the excess of energy by radiationless processes.

It has been found that the substates of T_o are not prepared with the same rate, nor do they radiate back to the ground state with the same probability [9,10]. These differences are now understood. The spin system of an organic molecule is weakly coupled to an anisotropic environment, the molecule itself. Thus spin dependent interactions are different for different orientations of the spin angular momentum. If the symmetry of the molecule is sufficiently high (at least C_{2v}) then in each of the three distinct substates of T_o the spin is aligned in one of the three principal planes of the molecule [10]. The state can therefore be characterized by the notation used in fig. 1.1 at the right, where the zero-field splitting is shown on an enlarged scale and the substates are denoted by $|x\rangle$, $|y\rangle$ and $|z\rangle$ indicating that for the state $|x\rangle$ the spin is aligned in the plane x = 0. Because spin-orbit interaction is different for the three substates selective population and depopulation occurs. A further important consequence is that the phosphorescence is highly polarized.

In the case of naphthalene it is observed [9] that the upper state of T_o is the most radiative one. Under certain conditions, for instance when Boltzmann equilibrium prevails, the population of the three substates is such that there are more molecules in the bottom level than in the top one. Interaction of the system with microwaves of the correct frequency (3.4 GHz in the case of fig. 1.1) will then take molecules from the bottom to the upper state. This can be measured as an absorption of microwaves, but will also appear as an increase of the phosphorescence intensity.

The splitting, which is of the order of 0.1 cm^{-1} in zero-field, changes through interaction of the spins with an external magnetic field. By applying the appropriate field the separation can be made equal to a quantum of energy in the ESR region (0.3 – 1.0 cm^{-1}). The strength of the field for which this happens depends on the orientation of the molecule and the zero-field splitting. In fig. 1.1 the transitions are indicated for a magnetic field parallel to the molecular y-axis.
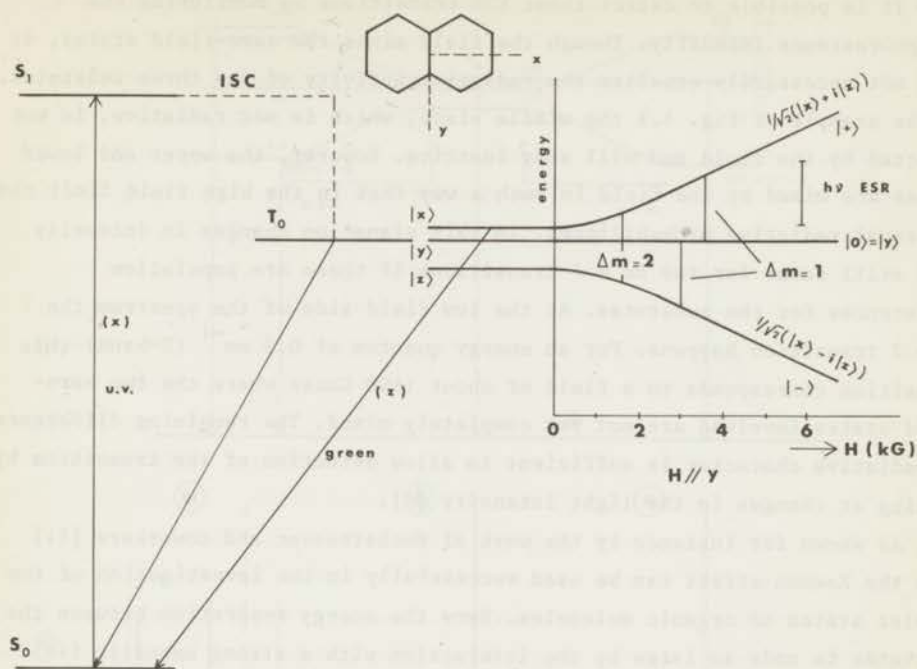
Fig. 1.1. Energy diagram of naphthalene.

The molecule is excited to the first excited singlet state S_1 by u.v. light. The absorption is x-polarized. (For choice of axes see top part of the figure). By intersystem crossing (ISC) the molecule goes over into the triplet manifold. Here the excess of (vibrational) energy is lost by radiationless processes and the molecule arrives in one of the components of the lowest triplet state T_0. In the case of naphthalene the upper state of T_0 is mostly populated and also has the strongest radiative character. The phosphorescence is green and z-polarized.

In a magnetic field parallel to the y-axis the upper and lower states are mixed, while the middle one is not affected (right hand part of the figure). At three different magnetic field strengths ESR transitions occur as indicated, which can be measured by looking at the absorption of microwaves or by monitoring the phosphorescence intensity (optical detection of ESR [6,7]).

It is possible to detect these ESR transitions by monitoring the phosphorescence intensity. Though the field mixes the zero-field states, it does not necessarily equalize the radiative activity of the three substates. In the example of fig. 1.1 the middle state, which is not radiative, is not affected by the field and will stay inactive. However, the upper and lower states are mixed by the field in such a way that in the high field limit they get equal radiative probabilities. In this situation changes in intensity will still occur for the $\Delta m = 1$ transitions if there are population differences for the substates. At the low field side of the spectrum the $\Delta m = 2$ transition happens. For an energy quantum of 0.3 cm^{-1} (X-band) this transition corresponds to a field of about 1600 Gauss where the two zero-field states involved are not yet completely mixed. The remaining difference in radiative character is sufficient to allow detection of the transition by looking at changes in the light intensity [6].

As shown for instance by the work of Hochstrasser and coworkers [11] also the Zeeman effect can be used successfully in the investigation of the triplet states of organic molecules. Here the energy separation between the substates is made so large by the interaction with a strong magnetic field that one sees the phosphorescence lines split into their three Zeeman components when using a spectrograph with sufficient resolution. A schematic example of the Zeeman effect is given in fig. 1.2, where we show the influence of a magnetic field on the o-o transition of the phosphorescence of naphthalene. In the absence of a field (situation b) the o-o transition occurs at a wavelength λ_o. On the left (a) we show what happens in a strong field along the y-axis and at the right (c) we give the situation for a field along the x-axis.

The difference between the spectra may be understood with reference to our discussion of fig. 1.1. In fig. 1.2 (a) the magnetic field is parallel to the y-axis, as in fig. 1.1; the state $|y\rangle$ is not affected while $|x\rangle$ and $|z\rangle$ are mixed. In the high-field limit the eigenfunctions are as shown in the figure with the result that the $m = \pm 1$ states obtain equal amounts of radiative character. Consequently, the phosphorescence line is split into two components which are approximately symmetrically displaced from the original position by an amount proportional to the field strength. Although the two lines correspond to equal transition probabilities they appear with different intensities in the spectrum because of the difference in population of the three Zeeman states at low temperature. In fig. 1.2 (c), where the field is

12
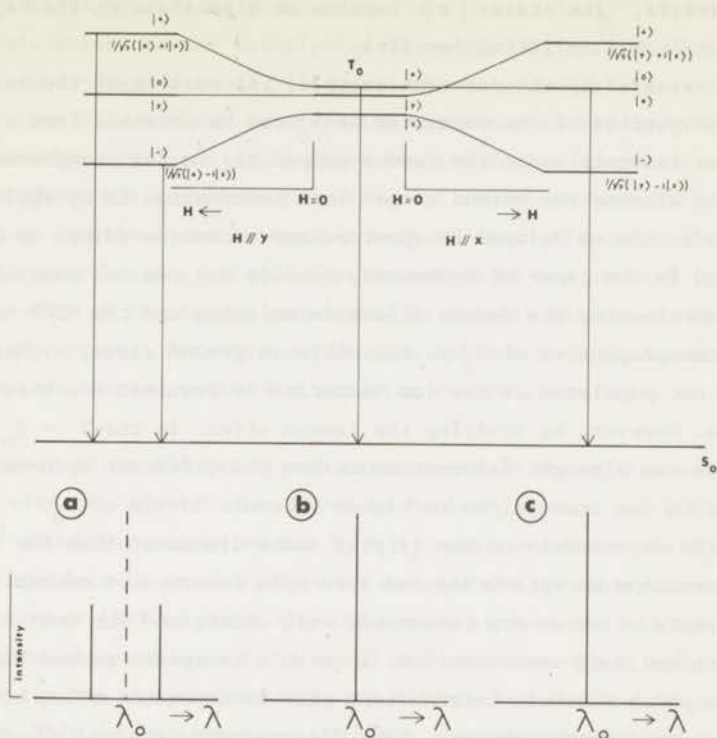
Fig. 1.2. The effect of a magnetic field on the phosphorescence spectrum of naphthalene.

Only the o-o transition is considered. This transition happens at a wavelength λ_o in the absence of the field (b). The spectrum does not change when the magnetic field is applied along the x-axis of the molecule (c), but a field along the y-axis mixes the radiative $|x\rangle$ level with the non-radiative $|z\rangle$ level. This results at high field in two states ($|+\rangle$ and $|-\rangle$) possessing half of the radiative character of $|x\rangle$ in zero-field. The phosphorescence line is then split into two components that are symmetrically displaced from the original position and have the same transition probabilites (a). (The intensities observed in an emission spectrum, however, may vary appreciably because of the population differences of the Zeeman levels.)

Similar results will be obtained for transitions to higher vibronic levels of the ground state if such transitions originate from the same zero-field component.

13

along the x-axis, the state $|x\rangle$ remains an eigenstate in the high-field limit and no Zeeman splitting results.

As illustrated by the previous example, information on the relative radiative properties of the substates of T_o can be obtained from a study of the relative intensities of the Zeeman components in the phosphorescence spectrum. An alternative method to get this information is by application of the Microwave Induced Delayed Phosphorescence technique (MIDP) as described for instance in the paper of Antheunis, Schmidt and van der Waals [12]. Both types of experiments, the Zeeman effect in emission and the MIDP technique, relate to the properties of T_o in its vibronic ground state; higher vibronic levels are not populated at the low temperatures required for these experiments. However, by studying the Zeeman effect in the $T_o \leftarrow S_o$ <u>absorption</u> spectrum one can also get information on how the different spin components participate in the transitions to higher vibronic levels of T_o.

From the experiments on the triplet state discussed thus far one can derive information on spin-orbit and spin-spin interaction mechanisms, the general aspects of which are reasonably well understood for most aromatic hydrocarbons and some aza-aromatics. A notable exception seemed benzene, a molecule in which vibronic interactions play an important role, both in fluorescence and phosphorescence. Here disagreement remained about the assignment of the lower vibronic levels of the triplet state [13,14]; this assignment is essential for a proper understanding of vibronic coupling in benzene. Further, the polarization of its phosphorescence as reported by Russell and Albrecht [15] is anomalous in the context of current ideas about spin-orbit coupling in aromatic hydrocarbons.

The present investigation was initiated to settle these outstanding questions. We began by using the Zeeman technique to obtain insight into the mechanisms of vibronic coupling and spin-orbit interaction for the lower triplet levels of benzene. It appeared that for the particular case of the benzene crystal, with four molecules in the unit cell, the Zeeman technique cannot yield unambiguous data on the radiative characteristics of the three zero-field components. Hence, to complete the answer we also have used the MIDP technique, adapted for the special situation found in benzene.

A theoretical introduction to the problems is given in chapter II. Selection rules for the benzene molecule are deduced from group theory, including the effects of spin-orbit interaction and vibronic coupling. Subsequently we review the description of vibronic coupling in the lower

14

triplet states of benzene as given by van der Waals et al. [19,20]. These calculations, which use the description introduced by Moffitt and Thorson [16] and Longuet-Higgins et al. [17], will be extended in chapter VI.

In chapter III we first describe the experimental set-up. Then in a brief mathematical analysis it is shown how the Zeeman spectra yield information about the radiative properties of the three zero-field states. The resulting equations can be applied both to absorption and emission studies. The complicating effect of polarization of the optical transitions on the intensity of the Zeeman components is briefly discussed. Finally it is shown that the crystal structure of benzene introduces a fundamental ambiguity in the Zeeman method for studying the relative rates of the spin-levels.

In chapter IV we discuss Zeeman experiments in absorption on the remarkable vibronic doublet discovered by Burland, Castro and Robinson [13] at 245 cm^{-1} above the origin of the $T_o \leftarrow S_o$ spectrum. Since the $T_o \leftarrow S_o$ absorption spectrum is exceedingly weak we used the phosphorescence excitation method [18] in which the absorption is detected via the phosphorescence it produces. It is found that the zero-field spin sublevel responsible for the absorption intensity differs for the two components of the doublet. This is in accordance with the theoretical predictions that follow from the assignment of Burland et al. [13], who explained the two lines as the two components of the transition to a degenerate vibrational level of the e_{2g} mode ν_8. Our results confirm that the frequency of this mode in the triplet state is reduced in a spectacular way as compared to the ground state by "pseudo-Jahn-Teller" vibronic coupling and that the splitting must be attributed to the crystal field [19,20]. The results of these experiments have already been published [21] and we return to the underlying theoretical problem in chapter VI.

In chapter V we describe experiments set up to determine along which paths individual bands of the phosphorescence spectrum of benzene acquire their intensity. It follows that two spin sublevels are responsible for the radiation emitted in the two strongest phosphorescence lines which correspond to different vibrational modes of the same symmetry (e_{2g}). It is concluded that for these lines vibronic interactions are involved that occur in the triplet manifold.

Finally we give in chapter VI the results of some calculations on vibronic coupling in the triplet manifold. Here we consider the simultaneous

15

interaction through two modes of e_{2g} symmetry (ν_8 and ν_9). It is shown that the appearance of "combination bands" of these two modes in the phosphorescence spectrum can be explained quantitatively by our model. These calculations also prove Katz et al's contention [22] that the inclusion of an additional mode in the vibronic coupling problem has a marked effect on the frequency of the strong doublet in the $T_o \leftarrow S_o$ absorption spectrum [13].

References.

[1] Lewis, G.N., and Kasha, M., 1944, J. Am. Chem. Soc., 66, 2100.
     Lewis, G.N., and Kasha, M., 1945, J. Am. Chem. Soc., 67, 994.
[2] Hutchison, C.A., and Mangum, B.W., 1958, J. Chem. Phys., 29, 952.
[3] Van der Waals, J.H., and de Groot, M.S., 1959, Mol. Phys., 2, 333.
[4] Erickson, L.E., 1966, Phys. Rev., 143, 295.
[5] Hutchison, C.A., 1967, The Triplet State, Cambridge University Press,
     p. 63.
[6] Sharnoff, M., 1967, J. Chem. Phys., 46, 3263.
[7] Schmidt, J., and van der Waals, J.H., 1968, Chem. Phys. Lett., 2, 640.
[8] Jablonski, A., 1933, Nature, 131, 839.
[9] Schwoerer, M., and Sixl, H., 1969, Z. für Naturf., 24a, 952.
[10] Van der Waals, J.H., and de Groot, M.S., 1967, The Triplet State,
     Cambridge University Press, p. 101.
[11] Castro, G., and Hochstrasser, R.M., 1968, J. Chem. Phys., 48, 637.
     Hochstrasser, R.M., and Lin, T.S., 1968, J. Chem. Phys., 49, 4929.
[12] Antheunis, D.A., Schmidt, J., and van der Waals, J.H., 1970, Chem. Phys.
     Lett., 6, 255.
[13] Burland, D.M., Castro, G., and Robinson, G.W., 1970, J. Chem. Phys.,
     52, 4100.
[14] Lopez-Delgado, R., Thèse, Faculté des Sciences d'Orsay, Université de
     Paris (1969).
[15] Russell, P.G., and Albrecht, A.C., 1964, J. Chem. Phys., 41, 2536.
[16] Moffitt, W., and Thorson, W.R., 1958, Rec. Mém., C.N.R.S., Paris,
     November.
[17] Longuet-Higgins, H.C., Öpik, U., Pryce, M.H.L., and Sack, R.A., 1958,
     Proc. R. Soc. A, 244, 1.
[18] Avakian, P., Abramson, E., Kepler, R.G., and Caris, J.C., 1963, J. Chem.
     Phys., 39, 1127.
     Castro, G., and Robinson, G.W., 1969, J. Chem. Phys., 50, 1159.
[19] Van der Waals, J.H., Berghuis, A.M.D., and de Groot, M.S., 1967, Mol.
     Phys., 13, 301.
[20] Van der Waals, J.H., Berghuis, A.M.D., and de Groot, M.S., 1971, Mol.
     Phys., 21, 497.
[21] Van Egmond, J., Burland, D.M., and van der Waals, J.H., 1971, Chem.
     Phys. Lett., 12, 206.

17

Hochstrasser, R.M., Wessel, J.E., and Zewail, A.H., 1971, J. Chem. Phys. 55, 3596.

[22] Katz, B., Brith, M., Sharf, B., and Jortner, J., 1970, J. Chem. Phys., 52, 88.

C H A P T E R   II

SOME THEORETICAL CONSIDERATIONS
CONCERNING THE LOWER EXCITED STATES OF BENZENE.

1. Form of the Hamiltonian and its approximate eigenfunctions.

We first consider the "adiabatic approximation" proposed by Born and and Oppenheimer [1]. The Hamiltonian of a molecule is written as

$$\mathcal{H} = T_e(q) + V(q,Q) + T_k(Q) + \mathcal{H}(s,q;Q). \tag{2.1}$$

In this notation q and Q denote the ensembles of positional parameters of the electrons and nuclei respectively, and s stands for the spin coordinates. The kinetic energy of the electrons $T_e(q)$ is an operator that relates to the q only, but the potential energy $V(q,Q)$, describing the Coulomb interactions of the charged particles, contains both q and Q and makes a strict separation of the electronic and nuclear variables impossible. In the first instance we shall neglect the small spin-dependent term $\mathcal{H}(q,s;Q)$.

Because the motion of the nuclei is slow relative to that of the electrons one may approximate the eigenfunctions of (2.1) by so called Born-Oppenheimer product functions of the form

$$\Psi = \psi(q,s;Q)\ \chi(Q). \tag{2.2}$$

If we define the "electronic" Hamiltonian $\mathcal{H}_e$ as the first part of (2.1)

$$\mathcal{H}_e = T_e(q) + V(q,Q), \tag{2.3}$$

then $\psi(q,s;Q)$ is a solution of this Hamiltonian for a fixed value of Q,

19

$$\mathcal{H}_e \; \psi(q,s;Q) = U(Q) \; \psi(q,s;Q).$$ (2.4)

There will be many solutions of (2.4) which, when necessary, we shall characterize by a set of labels as

$$\prescript{\mu}{\nu}{\psi}_i(q,s;Q).$$ (2.5)

Here μ denotes the multiplicity $(2S + 1)$; we only consider singlet $(\mu = 1)$ and triplet $(\mu = 3)$ states. The three components of a triplet are distinguished by the subscript ν, and i may be used as a further specification of states having the same μ and ν. In a strong magnetic field we characterize the substates of a triplet by the component of spin angular momentum along the direction of the field $(\nu = 1,0,-1)$; in zero-field the states are characterized by the plane in which the spin angular momentum is located $S_\nu \{ \prescript{\mu}{\nu}{\psi}_i(q,s;Q)\} = 0$ $(\nu = x, y, z)$.

. The potential $U(Q)$ in (2.4) is a function of the positions of the nuclei and the function $\chi(Q)$ describes the motion of the nuclei in this potential. In order to find $\chi(Q)$ one has to solve a second eigenvalue problem

$$\{T_k(Q) + U(Q)\} \; \chi(Q) = E \; \chi(Q).$$ (2.6)

It is now clear that the functions (2.2) only are eigenfunctions of the total Hamiltonian with eigenenergy E if one assumes

$$T_k(Q) \; \psi(q,s;Q) = \psi(q,s;Q) \; T_k(Q).$$ (2.7)

For non-degenerate states the terms neglected are of a relative magnitude equal to the ratio of the masses of the electron and the nucleus which is of the order of 10^{-4}, and the Born-Oppenheimer approximation then in most cases works nicely. Exceptions are found for degenerate and near-degenerate states.

For actual calculations on polyatomic molecules, however, the Born-Oppenheimer method in the above form still is not of great practical use. Even if the electronic problem (2.4) can be solved by assuming a simple model, one then obtains $U(Q)$ in a non-analytical form and the nuclear problem (2.6) may become quite complex.

For this reason extensive use is made of perturbation methods based on the following, even simpler model. In what has come to be known as the "Crude Born-Oppenheimer" approximation the electronic wave functions are considered as Q-independent,

$$\psi(q,s;Q) = \psi(q,s;0) = \psi^{\circ}(q,s) . \qquad (2.8)$$

These functions often are called Crude-Born-Oppenheimer (CBO) functions and the superscript $^{\circ}$ indicates that the function (or operator) concerned is to be taken for a specified nuclear conformation chosen as the origin of Q. For benzene in its ground state the origin may be chosen at the absolute minimum of U(Q) for this state, which in this case corresponds to the hexagonal "equilibrium" conformation. For the $^{3}B_{1u}$ state in which we are interested we choose the origin at that conformation for which U(Q) is lowest under the constraint that it is hexagonal; this conformation need not be an "equilibrium" conformation as non-hexagonal conformations may have lower energies [2,3].

   If the potential in which the nuclei move is approximated by a sum of harmonic potentials along the normal coordinates Q_i,

$$U(Q) = \sum_i \lambda_i Q_i^2 \qquad (2.9)$$

then the vibrational wave function $\chi(Q)$ takes the form of a product of harmonic oscillator functions

$$\chi(Q) = \prod_{3N-6} \eta_i(Q_i). \qquad (2.10)$$

Here η_i describes the motion along Q_i and for non-degenerate vibrations it can be characterized by a single energy quantum number. Whenever degeneracy occurs the two relevant η_i's in (2.10) can be combined into an eigenfunction of an isotropic two-dimensional harmonic oscillator [4].

   A CBO product of the form

$$\psi_i^{\circ}(q,s) \prod_j \eta_j(Q_j) \qquad (2.11)$$

in general will not be a very good approximation for a molecular eigenstate.

21

However, as discussed for instance by Longuet-Higgins [5] a set of such products may form a very convenient basis for finding approximate solutions by a variational procedure, in particular for degenerate and near-degenerate states. The advantage of the variational method over the construction of adiabatic solutions (2.2) is twofold. First, by taking a linear combination of products of the type (2.11) with two or more electronic factors ψ_i^o the dynamic coupling of the electrons and nuclei (i.e. the effect of $T_k(Q)$ on the electronic wave function $\psi(q,s;Q)$, see (2.7)) is more properly taken into account [5]. Secondly, one gets rid of the mathematical inconvenience of the non-analytical form of the potential $U(Q)$ in the nuclear problem (2.6).

As long as the spin-dependent term $\mathcal{H}(q,s;Q)$ in (2.1) is neglected, one can further separate the orbital and spin coordinates of the electrons. Consequently, the electronic wave functions take the form

$$\,^\mu_\nu\psi^o(q,s) = A \,^\mu\theta^o(q) \,^\mu_\nu\zeta(s). \tag{2.12}$$

Here the antisymmetrizing operator A takes care of the permutation symmetry of the electrons. All $\theta^o(q)$ for different permutations of the electrons belong to the same representation of the point group of the molecule, as is the case for the different permutations of $\zeta(s)$. Consequently, for the derivation of selection rules for matrix elements it suffices to look at the point group symmetry of the factors θ^o and ζ in the single term written in (2.12).

The total wave function takes the form

$$\,^\mu_\nu\psi^o(q,s;Q) = A \,^\mu\theta^o(q) \,^\mu_\nu\zeta(s) \, \chi(Q). \tag{2.13}$$

The Hamiltonian being invariant under all symmetry operations of the point group of the molecule, the functions θ, ζ and χ have to belong to irreducible representations of this group. If we denote the representation to which a function f belongs by Γ_f we find for the symmetry of the total wave function

$$\Gamma_\psi = \Gamma_\theta \otimes \Gamma_\zeta \otimes \Gamma_\chi. \tag{2.14}$$

22

Table 2.I

D_{6h}	E	$2C_6$	$2C_3$	C_2	$3C_2'$	$3C_2''$	i	$2S_3$	$2S_6$	σ_h	$3\sigma_d$	$3\sigma_v$	
A_{1g}	1	1	1	1	1	1	1	1	1	1	1	1	
A_{2g}	1	1	1	1	-1	-1	1	1	1	1	-1	-1	R_z
B_{1g}	1	-1	1	-1	1	-1	1	-1	1	-1	1	-1	
B_{2g}	1	-1	1	-1	-1	1	1	-1	1	-1	-1	1	
E_{1g}	2	1	-1	-2	0	0	2	1	-1	-2	0	0	R_x, R_y
E_{2g}	2	-1	-1	2	0	0	2	-1	-1	2	0	0	
A_{1u}	1	1	1	1	1	1	-1	-1	-1	-1	-1	-1	
A_{2u}	1	1	1	1	-1	-1	-1	-1	-1	-1	1	1	z
B_{1u}	1	-1	1	-1	1	-1	-1	1	-1	1	-1	1	
B_{2u}	1	-1	1	-1	-1	1	-1	1	-1	1	1	-1	
E_{1u}	2	1	-1	-2	0	0	-2	-1	1	2	0	0	x,y
E_{2u}	2	-1	-1	2	0	0	-2	1	1	-2	0	0	

Table 2.I.   Character table of D_{6h}, the point group of the benzene molecule.
  The various twofold axes are defined in fig. 2.1. It is indicated at the right to which representations the translation and rotation operators belong.

Table 2.II

$A \otimes B = B$ $\quad 1 \otimes 1 = 1$	
$A \otimes A = A$ $\quad 1 \otimes 2 = 2$	
$B \otimes B = A$ $\quad 2 \otimes 2 = 1$	$u \otimes u = g \otimes g = g$
	$u \otimes g = g \otimes u = u$
$E_1 \otimes E_1 = E_2 \otimes E_2 = A_1 + A_2 + E_2$	
$E_1 \otimes E_2 = E_2 \otimes E_1 = B_1 + B_2 + E_1$	
$A \otimes E_1 = E_1$, $A \otimes E_2 = E_2$	
$B \otimes E_1 = E_2$, $B \otimes E_2 = E_1$	

Table 2.II.   Multiplication table of the point group D_{6h}.

2. Electric dipole transitions in benzene.

From hereon we shall restrict ourselves to the benzene molecule, which is known to belong to the group D_{6h} in its ground state. The character table of this group is given in table 2.I, while a multiplication table is found in table 2.II. The axes are chosen in the molecule as in fig. 2.1, where also the various symmetry elements used in table 2.I are depicted. The x-axis of the molecule passes through opposite carbon atoms, while the y-axis intersects carbon-carbon bonds. The z-axis is perpendicular to the molecular plane.
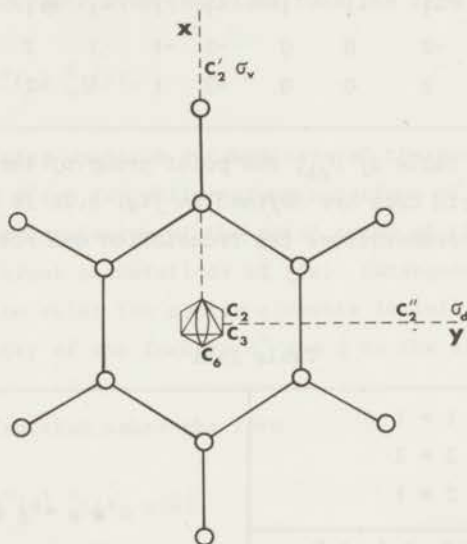
Fig. 2.1 Choice of axes in benzene.

The x- and y-axes are the in-plane axes. The z-axis is perpendicular to the molecular plane. The various C_2 axes of table 2.I are indicated. The molecular plane is the σ_h reflection plane. The positions of the other reflection planes are indicated.

The probability for a molecule to be excited from a state Ψ_1 to a state Ψ_2 by the absorption of light, or to go from Ψ_2 to Ψ_1 by spontaneous emission, is proportional to the square of the length of the transition

moment vector $\vec{M}$, defined as [6]

$$\vec{M} = \langle \Psi_1 | \vec{\mu} | \Psi_2 \rangle . \tag{2.15}$$

The dipole moment operator $\vec{\mu} = e \sum_i \vec{q}_i$ is dependent on the position $\vec{q}_i$ of the electrons only, which allows one to write in the CBO description

$$\vec{M} = \langle A \, {}^{\mu}\theta_1^o(q) \, {}^{\mu}_{\nu}\zeta_1(s) | \vec{\mu} | A \, {}^{\mu'}\theta_2^o(q) \, {}^{\mu'}_{\nu'}\zeta_2(s) \rangle \langle \chi_1(Q) | \chi_2(Q) \rangle \, \delta_{\mu\mu'} \, \delta_{\nu\nu'} . \tag{2.16}$$

The first factor at the right hand side of (2.16) is the "electronic transition moment" and the second factor an overlap integral known as the Franck-Condon factor. Since the operator $\vec{\mu}$ does not affect the spin coordinates the "overlap" integrals for the spin lead to the Kronecker functions corresponding to the spin selection rules

$$\mu = \mu' \quad \text{and} \quad \nu = \nu', \tag{2.17}$$

where the spin quantum numbers μ and ν are those defined in the discussion following (2.5).

For spontaneous emission the radiation intensity is given by $|M|^2$ multiplied by a proportionality factor containing the cube of the emission frequency ν^3. The integrated intensity

$$I = \int_\nu I(\nu) \, d\nu,$$

which is derived by integrating over a band in the spectrum, therefore is not a direct measure for the corresponding transition moment, but the reduced intensity I/ν^4 is. For comparison of calculated and experimental intensities one therefore often uses the reduced intensity instead of the integrated intensity.

The electronic transition moment in (2.16) can only be non-zero if the product of the three representations of the parts in the integrand which depend on the coordinates q contains the totally symmetric representation,

$$\Gamma_{\theta_1}^* \otimes \Gamma_{\vec{\mu}} \otimes \Gamma_{\theta_2} \quad \text{must contain } A_{1g} . \tag{2.18}$$

In the point group D_{6h} we are only concerned with real representations and for this reason the star in (2.18) can be omitted. In the cases which arise in our studies one of the functions Θ, say Θ_1, represents the electronic ground state and belongs to A_{1g} in D_{6h}. Then (2.18) reduces to

$$\Gamma_{\vec{\mu}} \otimes \Gamma_{\Theta_2} \quad \text{must contain } A_{1g}. \tag{2.18a}$$

As can be read from table 2.I the dipole operators transform like E_{1u} (x and y in-plane components) and A_{2u} (z out-of-plane component). This, and the spin selection rules (2.17) imply that, in the first instance, only singlet states with electronic symmetry A_{2u} or E_{1u} can be reached by absorption of light from the ground state. Conversely, it means that in the present simple picture these states are the only ones that can loose their excitation energy by radiative decay to the ground state.

3. The lower excited states of benzene.

In the LCAO-MO description of benzene one finds that, because of the hexagonal symmetry of the molecule, the Molecular Orbitals (MO's) of the π electrons may be cast in the form [7,8]

$$\phi_k = \frac{1}{N} \sum_{l=0}^{5} \omega^{kl} \, p_l \qquad \omega = \exp(2\pi i/6) \qquad k = 0, \pm 1, \pm 2, 3.$$

In this notation the $2p_z$ orbital of the l'th carbon atom is denoted by p_l. The value of k labels the representation to which ϕ belongs in the group C_6. The energy scheme of the MO's is given in fig. 2.2. In this simple description the ground state is obtained by putting the six π electrons in the lower three MO's as indicated in the figure. The first excited state then corresponds to promotion of an electron from an MO with $k = \pm 1$ to one with $k = \pm 2$ and therefore, in this simple picture, it is fourfold degenerate. However, according to group theory there are no irreducible representations of dimensionality greater than 2 in D_{6h}, and as shown in the famous work of Goeppert-Mayer and Sklar [8] electron-electron repulsion will lift this fourfold degeneracy partly, yielding four states belonging to B_{1u}, B_{2u} and E_{1u} in D_{6h}. These states can be singlets as well as triplets and, as has been shown in section 2, the $^1E_{1u}$ state is the only one of them that is

connected by an "allowed" electric dipole transition to the ground state.

$$b_{2g} \quad\quad 3$$

$$e_{2u} \quad -2 \quad\quad\quad e_{2u} \quad\quad 2$$

$$e_{1g} \quad -1 \quad\quad\quad e_{1g} \quad\quad 1$$

$$a_{2u} \quad\quad 0$$
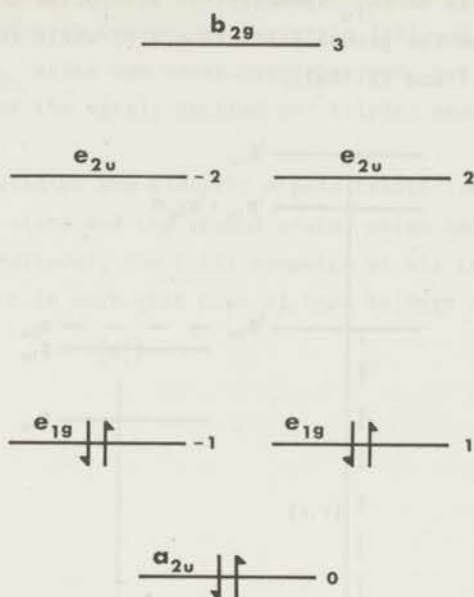
Fig. 2.2. Schematic diagram of the molecular π orbitals of benzene. The k-value is given at the right, while the symmetry labels in D_{6h} are above the levels. Six electrons are put in the three lower orbitals to form the ground state.

From experiments and calculations it is now known that the energy levels of these states are as drawn in the diagram of fig. 2.3. The lowest excited singlet state is $^1B_{2u}$. The absorption to this state from the ground state is forbidden in the CBO picture, but it is induced by vibronic coupling via e_{2g} vibrational modes [9]. Considerations given by Moffitt [10] make clear that the assignment $^1B_{2u}$ rather than $^1B_{1u}$ agrees with the experimental fact that the absorption is mostly induced by ν_6 (Wilson's numbering of the modes [11]). This is a bending mode which is expected to mix the $^1B_{2u}$ and $^1E_{1u}$ electronic states, the latter to which the transition is allowed.

The second singlet state is generally thought to be of $^1B_{1u}$ symmetry. However, calculations sometimes predict [12] a "doubly" excited state of $^1E_{2g}$ symmetry in the same region. The assignment of the diffuse spectrum in this region [13] is still not unquestionable because both $^1B_{1u}$ and $^1E_{2g}$

states can borrow intensity from the higher $^1E_{1u}$ pair. The next higher state in fig. 2.3 undoubtly is of $^1E_{1u}$ symmetry; in absorption it is seen as an allowed transition from the ground state ($f = 0.9$) while the polarization is in-plane (see table 2.I and (2.18a)).
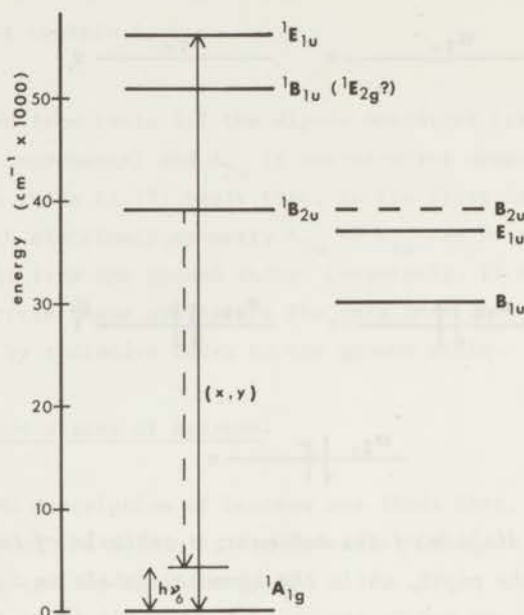
Fig. 2.3. The lower excited ππ* states of benzene. On the right hand side one finds the triplet states, which generally are of lower energy than the corresponding singlet states. Full lines correspond to observed states. The position of $^3B_{2u}$ is as calculated by Pariser [27]. The assignment of the second excited singlet state is questionable.

The only state that corresponds to an allowed transition from the ground state is the $^1E_{1u}$ state, which is indicated by the full line. This absorption is in-plane polarized. The fluorescence from the $^1B_{2u}$ state is of a forbidden type and vibronically induced by e_{2g} vibrations. Because of this mechanism the emission goes to the vibronic level of the ground state corresponding to one quantum of the active mode (broken line). The energy quantum of this mode is exaggerated.

The lowest triplet state is generally assigned to have $^3B_{1u}$ electronic

symmetry. This assignment is in accordance with the predictions of all calculations, see [14] for a review. The next higher triplet state has been observed in absorption by Colson and Bernstein [15] and is assigned as a $^3E_{1u}$ state. The $^3B_{2u}$ state has never been observed, but has been calculated to be the highest of the singly excited $\pi\pi^*$ triplet states [14] here considered.

We are interested in the electric dipole transitions between the lowest triplet electronic state and the ground state, which because of (2.17) are "spin forbidden". Moreover, the total symmetry of all three spin components of the triplet state is such that none of them belongs to E_{1u} or A_{2u} (see
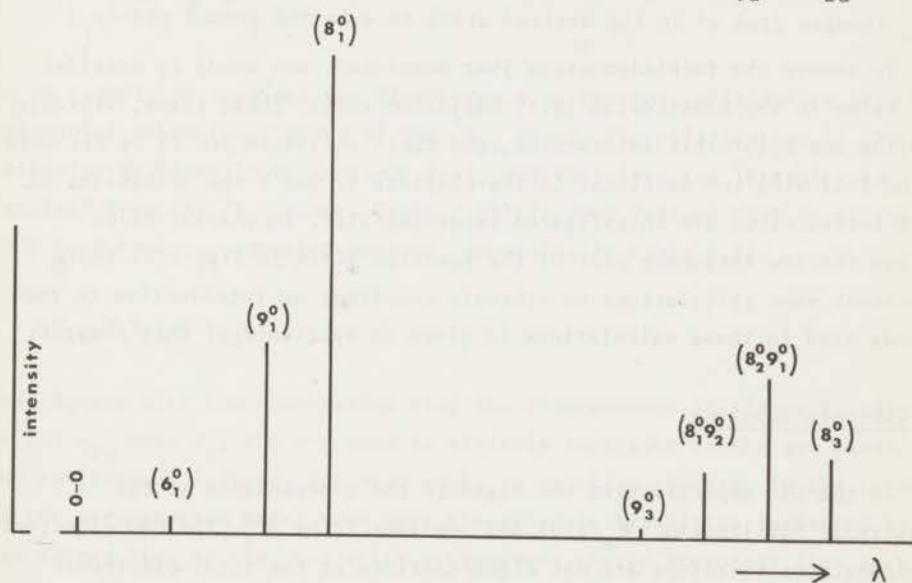
Fig. 2.4. *Part of the phosphorescence spectrum of benzene (schematically).*
The heights of the sticks correspond to the reduced intensities of the bands involved. Only those lines that involve e_{2g} *vibrations are indicated. Benzene has four* e_{2g} *modes;* ν_6, ν_7, ν_8 *and* ν_9, *the latter two are most active in the spectrum;* ν_6 *appears only weakly;* ν_7 *is very weak and has been omitted.*

Very characteristic for the benzene phosphorescence spectrum is the low-frequency part of the spectrum where we see the bands involving 3 quanta of ν_8, *3 quanta of* ν_9, *and combination bands with two quanta of one mode and one quantum of the other vibration.*

section 5) and thus because of (2.18a) the $^1A_{1g} \leftrightarrow {}^3B_{1u}$ transitions are also symmetry forbidden. In the structure of the spectra the latter forbiddenness is reflected in the very weak o-o transitions relative to those lines that involve non-totally symmetric vibrations of e_{2g} symmetry; the spectra are "vibronically induced". In fig. 2.4 we schematically show that part of the phosphorescence spectrum of interest for the present study. The intensity is mostly induced by the vibrations ν_8 and ν_9 and the very weak o-o transition only appears by the distortions induced by the environment of the molecule. We make use of the notation introduced by Callomon et al. [28].; $(n_\nu^{v'})$ is the band for which the energy quantum number of ν_n changes from v' in the excited state to v in the ground state.

To remove the forbiddennesses just mentioned, one needs to consider some terms in the Hamiltonian (2.1) neglected sofar. These terms, vibronic coupling and spin-orbit interaction, and their influence are to be discussed in the following two sections. In the chapters IV and V the mechanisms of these interactions are investigated experimentally. In chapter VI we discuss the low-frequency part of the spectrum given in fig. 2.4. There we present some calculations on vibronic coupling; an introduction to the methods used in these calculations is given in section 7 of this chapter.

4. Vibronic coupling.

In the CBO approximation one neglects the Q-dependence of the "electronic Hamiltonian" $\mathcal{H}_e(q,Q)$ and replaces it by $\mathcal{H}_e^o$. The CBO electronic eigenfunctions therefore are not eigenfunctions of the total electronic Hamiltonian $\mathcal{H}_e(q,Q)$. By using perturbation theory in the basis (2.13) with the perturbation $\mathcal{H}_e(q,Q) - \mathcal{H}_e^o$ one is able to get better eigenfunctions of $\mathcal{H}_e(q,Q)$ expressed as a linear combination of functions of the type (2.13). This perturbation will give matrix elements of the type

$$\langle \, {}_\nu^\mu \psi_1^o(q) \, \chi_1(Q) \mid \mathcal{H}_e(q,Q) - \mathcal{H}_e^o \mid {}_{\nu'}^{\mu'} \psi_2^o(q) \, \chi_2(Q) \, \rangle \quad ; \qquad (2.19)$$

the operator does not act on the spin and (2.19) vanishes if $\mu \neq \mu'$ and (or) $\nu \neq \nu'$. Or, in other words, if we remember (2.12) that the electronic functions ψ_i are antisymmetric products of orbital functions Θ_i and spin functions ζ_i then the spin factors ζ_1 and ζ_2 at the left and right in (2.19)

must belong to the same irreducible representation of the group D_{6h}. Consequently, it follows that the perturbation operator, which is totally symmetric, only mixes states for which

$$\Gamma_{\theta_1} \otimes \Gamma_{\chi_1} = \Gamma_{\theta_2} \otimes \Gamma_{\chi_2} . \tag{2.20}$$

If for one of the states concerned, for instance in the bra of (2.19), the lowest vibronic level is involved then χ_1 is a totally symmetric vibrational wave function and (2.20) reduces to

$$\Gamma_{\theta_1} = \Gamma_{\theta_2} \otimes \Gamma_{\chi_2} . \tag{2.21}$$

As an example we consider the fluorescence of benzene, originating from the zero-point vibrational level of the $^1B_{2u}$ state. The polarization of the emisssion is known to be in-plane [16], and therefore the intensity is "stolen" from the $^1E_{1u}$ state. From (2.21) it then follows that an active mode most have e_{2g} symmetry because, according to table 2.II

$$E_{1u} = B_{2u} \otimes e_{2g} .$$

This agrees with the observation that the fluorescence is strongly induced by the e_{2g} mode ν_6; the o-o band is strictly forbidden in the gas phase and environment induced, but very weak, in solution spectra. In the terms of the perturbation model used here the vibronic transition indicated by the dotted line in fig. 2.3 which corresponds to the strongest line in the fluorescence spectrum appears in the following way. If $\psi_1 \chi_1$ represents the vibrationless $^1B_{2u}$ state then by vibronic coupling some of the wave function $\psi_2 \chi_2$ will be mixed in, where ψ_2 represents the $^1E_{1u}$ electronic state and χ_2 a vibrational wave function corresponding to one quantum of vibrational energy of the e_{2g} mode ν_6. In the vibronic transition the vibrational quantum number does not change (2.16) and hence emission occurs to the ground state plus one quantum of ν_6.

5. Spin-orbit coupling.

We shall now consider the influence of the term $\mathcal{H}(q,s;Q)$ in (2.1). By the motion of the electrons around the nuclei their magnetic moment

interacts with the magnetic field produced by their angular motion. This interaction is known as the spin-orbit coupling, and a review of this phenomenon and its description is given e.g. by Hameka [17]. The vibrational motion of the nuclei is relatively slow and thus unimportant. Also, it is known that spin-orbit interaction is most effective very close to the nuclei, because of which it is thought to be not very sensitive to the exact nuclear conformation. For the moment we shall therefore neglect the Q-dependence of $\mathcal{H}(q,s;Q)$ and replace it by $\mathcal{H}^o_{so}$. Similarly to what happened by the vibronic coupling term in section 4 there now will be non-zero matrix elements of $\mathcal{H}^o_{so}$ in the basis (2.13). One finds for these matrix elements

$$\langle \, {}^{\mu}_{\nu}\psi^o_1(q) \; \chi_1(Q) \mid \mathcal{H}^o_{so} \mid {}^{\mu'}_{\nu'}\psi^o_2(q) \; \chi_2(Q) \rangle =$$

$$= \langle A \; {}^{\mu}\theta^o_1(q) \; {}^{\mu}_{\nu}\zeta_1(s) \mid \mathcal{H}^o_{so} \mid A \; {}^{\mu'}\theta^o_2(q) \; {}^{\mu'}_{\nu'}\zeta_2 \,(s) \rangle \; \langle \, \chi_1(Q) \mid \chi_2(Q) \rangle \qquad (2.22)$$

because of the Q-independence of the perturbation. Therefore, in the first instance, there will be no spin-orbit interaction between states of different vibrational parentage. As a second selection rule we find that the symmetry of the product of the electronic wave function θ and the spin factor ζ must be equal for both states,

$$\Gamma_{\theta_1} \otimes \Gamma_{\zeta_1} = \Gamma_{\theta_2} \otimes \Gamma_{\zeta_2} \,. \qquad (2.23)$$

We restrict ourselves to considering singlet and triplet states. The spin function for a singlet state belongs to the representation $D^{(o)}$ of the continuous rotation group, which means that it is invariant under all symmetry operations of this group and therefore also under those of the sub-group D_6. The singlet spin function for this reason can be taken to belong to A_{1g} in D_{6h} [18]. We shall denote the singlet spin functions further by σ, while the triplet spin functions will be indicated by τ_ν. The latter functions belong to the three dimensional representation $D^{(1)}$ of the continuous rotation group. A threefold degeneracy does not occur in D_{6h} and will be partly lifted. By inspection of the characters of the representation $D^{(1)}$ for the operations of the sub-group D_6 one finds that $D^{(1)}$ splits into E_{1g} and A_{2g} in D_{6h}.

We shall use this result for the ${}^3B_{1u}$ phosphorescent triplet state of

benzene. The total symmetry of the three triplet components of the lowest vibronic level then are

$$\Gamma_\Theta \otimes \Gamma_{\tau_z} = B_{1u} \otimes A_{2g} = B_{2u} \quad \text{for the } |z\rangle \text{ level,}$$

(2.24)

$$\text{and } \Gamma_\Theta \otimes \Gamma_{\tau_{x,y}} = B_{1u} \otimes E_{1g} = E_{2u} \quad \text{for the triplet } |x,y\rangle \text{ pair.}$$

We use the notation $|x,y\rangle$ to indicate that in the free molecule not only $|x\rangle$ and $|y\rangle$ are eigenstates, but also any normalized linear combination, as long as there is no distortion from hexagonal symmetry. This result is visualized in fig. 2.5. The splitting between $|z\rangle$ and $|x,y\rangle$ is caused by spin-spin and spin-orbit interactions [19]. From (2.23) it now follows that the triplet components can only spin-orbit couple with singlet states of B_{2u} or E_{2u} electronic symmetry. However, these states cannot radiate to the ground state because of (2.18a) nor can they be reached from the ground state by the absorption of light. The transitions $^1A_{1g} \leftrightarrow {}^3_\nu B_{1u}$ ($\nu = x,y,z$) are therefore "symmetry forbidden".
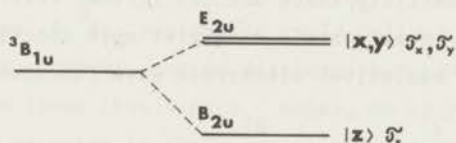
Fig. 2.5. *The spin sub-levels of the lowest triplet state of benzene.*
    The splitting is mainly caused by spin-spin interaction. The spin functions are denoted by τ_ν, the states by $|\nu\rangle$. In the benzene crystal the degeneracy of $|x\rangle$ and $|y\rangle$ is lifted, but on most of the effects discussed in this study this has a minor effect.

6. Combination of perturbations, general selection rules.

A combination of vibronic coupling and spin-orbit interaction can bring A_{2u} or E_{1u} electronic singlet character into the lowest triplet state of benzene, which in our description is necessary for "allowed" emission. This scheme was already proposed by Craig [20] and also by Mizushima and Koide [21] in their calculations on spin-orbit coupling in benzene. Albrecht [22] analyzed these interactions to interpret his results of photoselection

experiments on the benzene phosphorescence [16]. We shall discuss the various possibilities suggested by him in chapter V.

It is possible to deduce general selection rules for the vibrational symmetry of the modes that are active in the phosphorescence spectrum without knowing the exact mechanism by which the intensity is acquired. (The same vibrations then should be active in the absorption spectrum because of the similarity of (2.20) and (2.23) for absorption and emission.) These selection rules follow from the symmetry of the states involved.

When thinking in terms of a basis of the type (2.13) the wave function of the spin component $|\nu\rangle$ of the phosphorescent triplet state can be written as

$$|^3_\nu B_{1u}\rangle = A\{ |^3\Theta_{B_{1u}} \chi_o \tau_\nu\rangle + \sum_k \lambda_k |k\rangle \} \tag{2.25}$$

where χ_o is the zero-point vibrational wave function and $|k\rangle$ stands for a product of the type $\Theta^o_k \chi_k \zeta_k$. Since all intra-molecular interactions are totally symmetric the total symmetry of all $|k\rangle$ must be equal to that of the the triplet component involved; B_{2u} for $|z\rangle$ and E_{2u} for $|x,y\rangle$. To have non-vanishing transition probability there are two further restrictions. At least one of the states $|k\rangle$ must contain a singlet spin function $^\mu_\nu\zeta = \sigma$ and at the same time have a "radiative" electronic wave function $^1\Theta_i$ of $^1A_{2u}$ or $^1E_{1u}$ symmetry.

So there are the following possibilities:

i) $\Gamma_{|k\rangle} = B_{2u}$ and $\Gamma_{\Theta_k} = A_{2u}$

In this case the induced intensity originates from the $|z\rangle$ component and is out-of-plane polarized. In this situation

$$\Gamma_{\Theta_k} \otimes \Gamma_{\chi_k} \otimes \Gamma_{\zeta_k} = A_{2u} \otimes \Gamma_{\chi_k} \otimes A_{1g} = B_{2u}$$

and it follows that $\Gamma_{\chi_k} = B_{2u} \otimes A_{2u} = b_{1g}$. $\tag{2.26a}$

ii) $\Gamma_{|k\rangle} = B_{2u}$ and $\Gamma_{\Theta_k} = E_{1u}$, for which in-plane polarized emission originates from the $|z\rangle$ component. This results in

$$\Gamma_{\Theta_k} \otimes \Gamma_{\chi_k} \otimes \Gamma_{\zeta_k} = E_{1u} \otimes \Gamma_{\chi_k} \otimes A_{1g} = B_{2u}$$

and $\Gamma_{\chi_k} = B_{2u} \otimes E_{1u} = e_{2g}$. $\tag{2.26b}$

34

iii)   For emission from the $|x,y\rangle$ components which is out-of-plane polarized one finds

$$\Gamma_{\Theta_k} \otimes \Gamma_{\chi_k} \otimes \Gamma_{\zeta_k} = A_{2u} \otimes \Gamma_{\chi_k} \otimes A_{1g} = E_{2u}$$

and $\Gamma_{\chi_k} = E_{2u} \otimes A_{2u} = e_{2g}$ (2.26c)

iiii)   Finally for in-plane polarized intensity from these $|x,y\rangle$ components one gets

$$\Gamma_{\chi_k} = E_{2u} \otimes E_{1u} = b_{1g} + b_{2g} + e_{1g} \, .$$
          (2.26d)

So, group theoretically, four symmetries are allowed for the vibrational wave functions: b_{1g}, b_{2g}, e_{1g} and e_{2g}. For benzene, however, there are no b_{1g} modes [11], thus leaving only three different symmetries. In experiment just these symmetries are found in the phosphorescence spectrum [23].

As already shown by Craig [20] and Albrecht [22] the appearance of just these symmetries is not a proof of the $^3B_{1u}$ assignment of the lowest triplet state of benzene. A $^3B_{2u}$ assignment would deliver the same symmetries. These two assignments, however, can be distinguished by the polarization of the emission in the lines involving b_{2g} modes, or by the zero-field component(s) from which the emission in these bands originates. In chapter V it is shown that only the $^3B_{1u}$ assignment is compatible with the experimental results there presented.

7.   <u>Vibronic coupling in degenerate and near-degenerate states.</u>

In this section we turn to the quantitative description of vibronic coupling in degenerate or near-degenerate states as first applied by Moffitt and Thorson [24] and Longuet-Higgins, Öpik, Pryce and Sack [25]. This method later was extended to the pseudo-Jahn-Teller interaction between the lower triplet states of benzene by van der Waals, Berghuis and de Groot [2]. As an introduction to chapter VI we here give a short review of the work of van der Waals et al. [2], in which is described the interaction between the $^3B_{1u}$ and $^3E_{1u}$ states by a single e_{2g} mode ν_8. In chapter VI we then present the results of calculations on the simultaneous interaction by two modes of e_{2g} symmetry. For a more detailed discussion of these methods we refer to the

review article by Longuet-Higgins [5] and to reference [2].

The approximate eigenfunctions of the total Hamiltonian are expressed in the basis set formed by the products of CBO electronic wave functions and harmonic oscillator functions corresponding to the active vibrational mode ν_8

$$\substack{\mu \\ \nu}\psi_\Lambda^o \; \eta(\rho,\phi) \; . \tag{2.27}$$

Whereas in (2.11) all vibrational degrees of freedom appear in the wave functions, one only considers here the normal coordinates ρ and ϕ of the active mode; it is assumed that the other vibrational coordinates are separable from the electronic problem [5] (for the expression of the normal coordinates of a two-dimensional isotropic harmonic oscillator in polar form see [4]). Since we have seen that vibronic coupling occurs only between states with the same spin quantum numbers, we may for the time being omit the labels μ and ν in the vibrational problem.

Because of the presence of the hexagonal axis the electronic wave functions can be characterized by the quantum number Λ related to the angular momentum of the electronic motion, which also describes the behaviour under a rotation over $2\pi/6$. Denoting such a rotation by R one has

$$R \, \psi_\Lambda = \omega^\Lambda \, \psi_\Lambda \, , \text{ where } \omega = \exp(2\pi i/6), \tag{2.28}$$

and for the states of present interest

$$
\begin{aligned}
R \; \psi_{E_{1u}^+} &= \omega \, \psi_{E_{1u}^+} & \Lambda &= 1 \\
R \; \psi_{B_{1u}} &= \omega^3 \psi_{B_{1u}} & \Lambda &= 3 \\
R \; \psi_{E_{1u}^-} &= \omega^{-1} \psi_{E_{1u}^-} = \omega^5 \psi_{E_{1u}^-} & \Lambda &= 5 \; .
\end{aligned}
\tag{2.29}
$$

In (2.27) the eigenfunctions $\eta_{v\ell}(\rho,\phi)$ of the two dimensional isotropic harmonic oscillator of a single e_{2g} mode are characterized by the two quantum numbers v and ℓ. The first relates to the vibrational energy and defines the number of vibrational quanta ε_o according to

$$E = (v + 1)h\nu_8 = (v + 1)\varepsilon_o \; . \tag{2.30}$$

36

The angular motion of the vibration is described by l, which also determines the behaviour of $\eta_{vl}(\rho,\phi)$ under rotation over $2\pi/6$,

$$R\,\eta_{vl}(\rho,\phi) = \omega^{2l}\eta_{vl}(\rho,\phi), \tag{2.31}$$

where $l = v, v-2, \ldots\ldots, -v+2, -v.$ \hfill (2.32)

The factor 2 in the exponent in (2.31) arises because of the e_{2g} character of the vibration. It is seen that for the product function (2.27), further abbreviated as $|B\,;\,v,l\rangle$ or $|E\underline{+}\,;\,v,l\rangle$, or if not explicit as $|\Lambda\,;\,v,l\rangle$, one has

$$R\,|\Lambda\,;\,v,l\rangle = \omega^{\Lambda}\omega^{2l}\,|\Lambda\,;\,v,l\rangle = -\omega^{2j}\,|\Lambda\,;\,v,l\rangle . \tag{2.33}$$

Defining the quantum number j as $j = 1/2(\Lambda - 3) + 2l$ it is found that, though Λ and l separately are no constants of the motion, j is a good quantum number because of (2.33) and the fact that R and $\mathcal{H}$ commute. Thus because of the hexagonal symmetry of the molecule, interaction occurs only between states with the same j (or in higher order $j \pm 3$).

Following Longuet-Higgins [5] one expands the electronic part of the Hamiltonian as a Taylor series in the nuclear coordinate ρ (the displacement from the symmetrical nuclear conformation). Because of the invariance of the Hamiltonian under the operation of R, only a few terms in the expansion can give rise to non-vanishing matrix elements in the basis (2.27). In what is called the pseudo-cylindrical approximation [2] (for which j is a good quantum number and there is no mixing of terms that differ a multiple of 3 for j) one keeps the terms up to ρ^2 in the elements that are diagonal in the electronic quantum number Λ and the terms linear in ρ in the non-diagonal elements. When further assuming a single force constant λ for the active mode in the excited electronic states involved one finds [2] that the total Hamiltonian can be written as

$$\mathcal{H} = \mathcal{H}^o_e + [T_k(\rho,\phi) + \tfrac{1}{2}\lambda\rho^2] + K\rho U(\phi). \tag{2.34}$$

The pair of terms in square brackets represents the Hamiltonian of an isotropic two dimensional harmonic oscillator with eigenfunctions η_{vl} and energies defined in (2.30). The last term expresses the vibronic coupling of the B_{1u} state with the members of the E_{1u} pair; K is the coupling parameter and in the basis of the electronic functions (2.29) the operator

$U(\phi)$ is represented by the matrix

$$U = \begin{pmatrix} . & \exp(-i\phi) & . \\ \exp(i\phi) & . & \exp(-i\phi) \\ . & \exp(i\phi) & . \end{pmatrix} .$$
(2.35)

The matrix elements of the Hamiltonian (2.34) in the basis of the CBO products (2.27) follow from the known expressions for the integrals [25]

$$\langle n_{v l}(\rho,\phi) \mid \rho \exp(\pm i\phi) \mid n_{v'l'}(\rho,\phi) \rangle .$$

One finds for the <u>elements diagonal in Λ</u>

$$\langle B ; v, l \mid \mathcal{H} \mid B ; v', l' \rangle = \delta_{vv'} \, \delta_{ll'} \, (v + 1)\epsilon_o$$

$$\langle E\pm ; v, l \mid \mathcal{H} \mid E\pm ; v', l' \rangle = \{C\epsilon_o + (v + 1)\epsilon_o\} \, \delta_{vv'} \, \delta_{ll'} ,$$
(2.36a)

where C is equal to the electronic energy difference $U^o_{E_{1u}} - U^o_{B_{1u}}$
expressed in units of the vibrational quantum ϵ_o.
Similarly for <u>non-diagonal elements in Λ</u> one gets

$$\langle B ; v+1, l+1 \mid \mathcal{H} \mid E_- ; v, l \rangle = \langle B ; v, l \mid \mathcal{H} \mid E_+ ; v+1, l+1 \rangle = K[\tfrac{1}{2}(v+l+2)]^{\frac{1}{2}} \epsilon_o$$
(2.36b)

$$\langle B ; v-1, l+1 \mid \mathcal{H} \mid E_- ; v, l \rangle = \langle B ; v, l \mid \mathcal{H} \mid E_+ ; v-1, l+1 \rangle = K[\tfrac{1}{2}(v-l)]^{\frac{1}{2}} \epsilon_o .$$

By diagonalization of the Hamiltonian matrix with the aid of (2.36) one obtains the eigenvectors in the basis (2.27). The eigenvalues then correspond to the vibronic spacing in the excited states. From the eigenvector of the eigenstate with lowest energy (parentage $\mid B ; 0,0 \rangle$) intensities are deduced for the emission spectrum originating from this level. As will be outlined in chapter V experiments prove that the phosphorescence intensity of the lines involving ν_8 is stolen by vibronic coupling between ${}^3E_{1u}$ and ${}^3B_{1u}$ states with subsequent spin-orbit coupling between ${}^3E_{1u}$ and ${}^1A_{2u}$ states. From the calculations of van der Waals et al. [2] it follows that, when considering the vibronic coupling due to ν_8 the vibrationally unexcited state T_o of the ${}^3B_{1u}$ triplet in the basis (2.27) takes the form

$$|T_o \; ; \; 0,0\rangle = a_1 \; |B \; ; \; 0,0\rangle + a_2 \; \{|E_+ \; ; \; 1,1\rangle + |E_- \; ; \; 1,-1\rangle \}$$

$$+ \; a_3 \; |B \; ; \; 2,0\rangle + a_4 \; \{|E_+ \; ; \; 3,1\rangle + |E_- \; ; \; 3,-1\rangle \} + \ldots \quad (2.37)$$

Because of the orthogonality of the harmonic oscillator functions $\eta_{v\ell} \; (\rho,\phi)$ the terms $|E_{\pm}, \; 1, \; \pm 1\rangle$ are responsible for the emission to the electronic ground state plus one quantum of ν_8. Similarly the emission to the level with three quanta of ν_8 is proportional to $(a_4)^2$. In this description the ratio of the reduced intensities in these bands is determined by

$$I(8_3^o) / \; I(8_1^o) = (a_4)^2 / \; (a_2)^2 \; . \qquad\qquad (2.38)$$

From the results of [2] it appears that this quantity depends strongly on K and the experimental value of this intensity ratio is a good check on the value of the coupling parameter K.

The effect of the vibronic coupling on the energy of the vibronic levels is depicted in fig. 2.6. In part (a) we show schematically the imaginary situation where there is no coupling. The energy quantities are all given in units of ε_o. By arrows the various interactions are indicated. It can be seen that in three steps the functions $|E_{\pm} \; ; \; 3, \pm 1\rangle$ are mixed into the lowest triplet state from which the phosphorescence originates.

The most striking result of the calculations of [2] is the shift of the vibronic level of parentage $|B \; ; \; 1, \pm 1\rangle$ in the lowest triplet state. With values for the parameters C and K that fit the experimental values of Γ (the distance between the two o-o transitions in the absorption spectra, see fig. 2.6) and the intensity ratio (2.38) it is found that the energy quantum of ν_8 is lowered from ε_o to as little as 0.35 ε_o. The experimental value from the absorption spectrum [26] is about 0.17 ε_o and it is felt that, qualitatively at least, the model predicts quite nicely the great reduction of the frequency of the active mode when going from the $^1A_{1g}$ ground state to the $^3B_{1u}$ excited state. In chapter VI we shall show that the introduction of a second active vibration reduces this vibrational quantum even more and the calculated value then comes quite close to the experimental one.
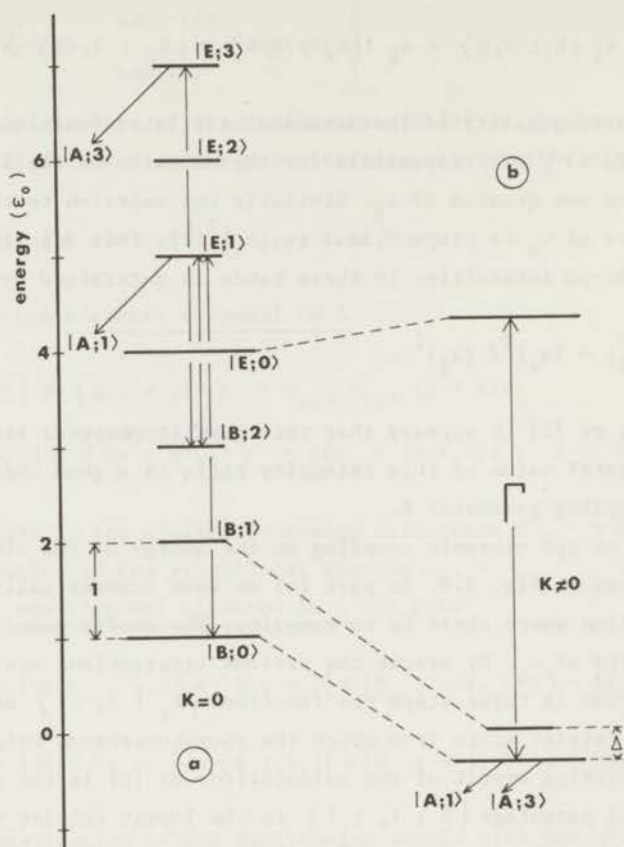
Fig. 2.6.   Schematic diagram of the energy levels with and without vibronic coupling.

(a) The case of no coupling (K = 0). The various parameters are indicated in the figure. All energies are expressed in units of ε_o, the vibrational quantum of ν_8. Levels between which vibronic coupling takes place are connected by arrows. The levels containing more quanta of ν_8 have high degeneracies and coupling does not occur between all of these levels. We also omit the vibrational quantum number l.

(b) The case for K = 1.2. The experimental observables are indicated. Γ is the energy gap between the o-o transitions to the two electronic states from the ground state. The energy quantum of ν_8 is decreased to a value of Δ.

References.

[1] Born, M., and Oppenheimer, R., 1927, Ann. Physik, 84, 457.

[2] Van der Waals, J.H., Berghuis, A.M.D., and de Groot, M.S., 1967,
     Mol. Phys., 13, 301.
     Van der Waals, J.H., Berghuis, A.M.D., and de Groot, M.S., 1971,
     Mol. Phys., 21, 497.

[3] Liehr, A.D., 1961, Z. Naturforsch., 16 a, 641.

[4] Herzberg, G., 1951, Molecular Spectra and Molecular Structure,
     Vol II (D. van Nostrand).

[5] Longuet-Higgins, H.C., 1961, Adv. Spectrosc., Vol II, p 428.

[6] Eyering, H., Walter, J., and Kimball, G.E., 1947, Quantum Chemistry,
     (Wiley, New York).

[7] Salem, L., 1966, The Molecular Orbital Theory of Conjugated Systems
     (W.A. Benjamin).

[8] Goeppert-Mayer, M., and Sklar, A.L., 1938, J. Chem. Phys., 6, 645.

[9] Herzberg, G., 1966, Molecular Spectra and Molecular Structure, Vol III,
     p 555 (D. van Nostrand).

[10] Moffitt, W., 1954, J. Chem. Phys., 22, 320.

[11] Wilson, E.B., 1934, Phys. Rev., 45, 706.

[12] Bloor, J.E., Lee, J., and Gartside, S., 1960, Proc. Chem. Soc., 413.

[13] Katz, B., Brith, M., Sharf, B., and Jortner, J., 1970, J. Chem. Phys.,
     52, 88.

[14] Kearns, D.R., 1962, J. Chem. Phys., 36, 1608.

[15] Colson, S.D., and Bernstein, E.R., 1965, J. Chem. Phys., 43, 2661.

[16] Russell, P.G., and Albrecht, A.C. 1964, J. Chem. Phys., 41, 2536.

[17] Hameka, H.F., The Triplet State, 1967, ed. A.B. Zahlan (Cambridge Univ.
     Press, London).

[18] Tinkham, M., Group Theory and Quantum Mechanics, Chapter V (McGraw-Hill
     Book Company, London).

[19] Van der Waals, J.H., and de Groot, M.S., 1967, The Triplet State,
     ed. A.B. Zahlan (Cambridge Univ. Press, London).

[20] Craig, D.P., 1950, J. Chem. Phys., 18, 236.

[21] Mizushima, M., and Koide, S., 1952, J. Chem. Phys., 20, 765.

[22] Albrecht, A.C., 1963, J. Chem. Phys., 38, 354.

[23] Bernstein, E.R., Colson, S.D., Tinti, D.S., and Robinson, G.W., 1968,
     J. Chem. Phys., 48, 4632.

[24] Moffitt, W., and Thorson, W.R., 1958, Rec. Mém., C.N.R.S., Paris, November.

[25] Longuet-Higgins, H.C., Öpik, U., Pryce, M.H.L., and Sack, R.A., 1958, Proc. R. Soc., A 244, 1.

[26] Burland, D.M., Castro, G., and Robinson, G.W., 1970, J. Chem. Phys., 52, 4100.

[27] Pariser, R., 1956, J. Chem. Phys., 24, 250.

[28] Callomon, J.H., Dunn, T.M., and Mills, I.M., 1966, Phil. Trans. R. Soc., A 259, 499.

CHAPTER III

EXPERIMENTAL METHODS.

1. The Zeeman spectrometer.

1.1 Absorption measurements.

In fig. 3.1 we give a schematic diagram of the experimental set-up used for measuring absorption Zeeman spectra of benzene with the phosphorescence photo-excitation method. A 1000 Watts Osram HBO-1000 high pressure mercury arc acts as a light source. The light is first filtered by a 5 cm solution filter which contains an aqueous solution of 240 g $NiSO_4.6H_2O$ and 45 g $CoSO_4.7H_2O$ per litre and finally by a Chance Pilkington OX-7 or Schott und Gen. UG-5 optical glass filter. A monochromator (Jarrell-Ash 0.75 m Czerny-Turner) selects the wavelength after which the light is focussed on the first chopper of a variable-frequency chopper assembly. The choppers are driven by a sinewave oscillator via a power amplifier and are normally used at about 45 Hertz. The light is then focussed on the crystal in the cryostat. The crystal is placed in the center of a superconducting Niobium-Titanium solenoid (Oxford Instruments), the bore of which is placed vertically. To keep boiling helium away between the innermost window and the crystal, an evacuated milk-bottle shaped quartz device is placed on the window.

The phosphorescence of the crystal is gathered by a telescopic array of lenses (suprasil), which are mounted in a stainless steel tube that is suspended from the top of the cryostat and ends just above the sample. The bottom of this tube is sealed with a flat suprasil window and an Indium ring. The top of the tube is sealed off by the last of the seven lenses, made slightly larger in diameter than the others, and a teflon covered "O" ring. (The use of this kind of "O" rings is necessary because of the high vacuum

[13] McGlynn, S.P. and Kasha, M., 1956 ... ...

[14] Siegel, S. ...

[15] Kortland, ... Carlson, ... and Robinson ... ... 1962.

[16] Porter, G.... 1963.

[17] Robinson, G.W. ... 30, 333.

[18] Galloway, ... Hilsch, ... 1963 ... ... p. 212, 1964.
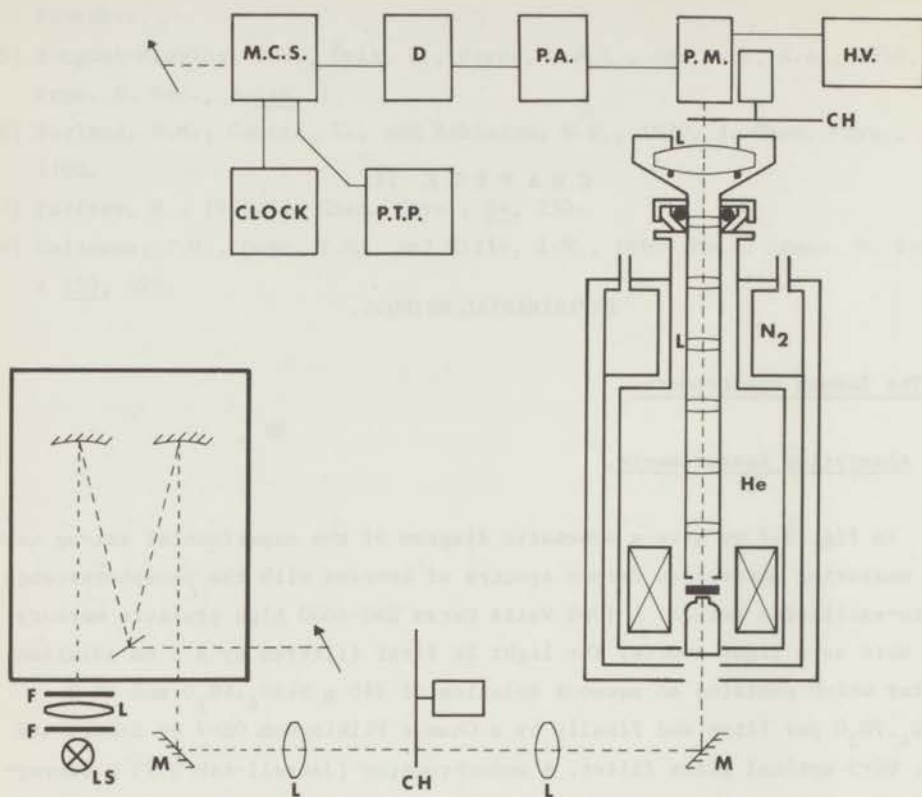
Fig. 3.1. The Zeeman spectrometer as used for absorption measurements.

The exciting light of the light source LS passes a filter combination F and is focussed on the monochromator. Via mirrors M, choppers CH and lenses L it is focussed on the crystal. The phosphorescence is gathered by the lens tube and finally reaches the photomultiplier behind the second chopper. The detection system exists of a pre-amplifier PA, a discriminator D and a Multi-Channel-Scaler MCS. The spectra are punched on paper tape by a punch unit PTP. A clock takes care of the simultaneous scanning of the monochromator and the MCS.

created inside the tube when placed in liquid helium. When normal "O" rings were used "plasticizer" was found to diffuse out of the rings and cover the lenses.) All seven lenses are of the same strength and they are spaced with a mutual distance of twice their focal length.(Three of them act as field lenses which reduce light losses to the walls of the tube.) The actual sample holder is fastened with its top to the bottom of the tube and carries a device which causes the crystal to rotate about a horizontal axis when the lens tube is turned about its vertical axis inside the cryostat. The angle of rotation can be read on a dial on the top of the cryostat.

A schematic diagram of the sample holder is given in fig. 3.2. It consists of three parts, the top one of which is fastened to the stainless steel tube. The bottom part can rotate freely around the upper one, but is anchored in the magnet coil by two pins on the magnet that fall into appropriate holes in the sample holder. The third part is allowed to turn freely about a horizontal axis which is perpendicular to the magnetic field direction. Two gears take care of the correlation between the rotation of the tube and that of the inner part of the sample holder. A small brass cup, which holds the crystal, fits in a predetermined way in the rotating part and can be tightened with a small screw.

Above the tube the second chopper is mounted to permit anti-phase chopping. The phosphorescence light is then focussed on the cathode of a cooled photomultiplier, if necessary after filtering by an optical glass filter to select the phosphorescence of the crystal and to prevent emission from other objects in the light path from reaching the detection system.

1.2 Photo-excitation technique.

For the absorption measurements we have made use of the phosphorescence photo-excitation method as used before by several experimentalists [1]. The power of this technique is for instance demonstrated by the work of Burland, Castro and Robinson [2], who detected the o-o transition in the triplet←singlet absorption of benzene in a small crystal in this manner. On the other hand, attempts to find the same transition in a direct way in a liquid cell with an optical path length of 22.5 m have been reported as unsuccessful [3].

The principle of the method rests on the migration of the excitation energy through the crystal. The absorbed photons finally are "trapped" on

Fig. 3.2. The sample holder.

The upper part I of the sample holder is fastened on the lens tube. Part II rotates freely around I, but is anchored in the magnet coil. By turning I in II part III, which carries the crystal, rotates about a horizontal axis. The angle of rotation is determined from a dial D on the tube by the pointer P on the cryostat.

The light passes through a suprasil rod and a flat window in the bottom of the lens tube (S).
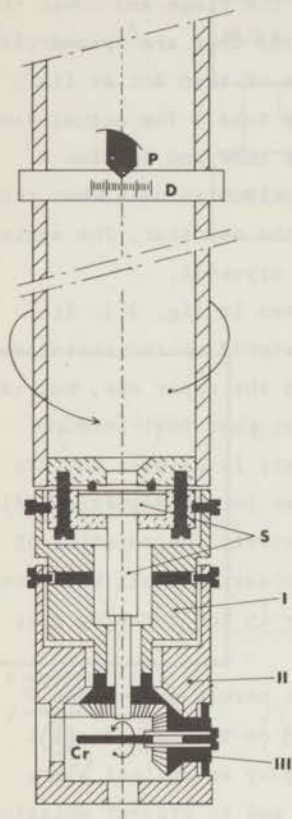
guest molecules that have lower excitation energy, or on host molecules the excitation energy of which is lowered by interaction with a dislocation or impurity. Finally the absorbed energy is lost by the crystal partly as phosphorescence from the "traps". The assumption is made that this phosphorescence is proportional to the energy which has been absorbed in the first instance.

The advantage of the phosphorescence photo-excitation method is that one transforms the difficulty of the experiment from determining very small changes in a high light intensity to the detection of a small amount of phosphorescence against a dark background. In this way one does not need to stabilize the light source, nor does the boiling helium around the sample affect the measurements too seriously. Also, phase sensitive detection is not necessary: all photons that reach the photomultiplier — if needed after some filtering — belong to the signal.

Because of the success of this method in experiments on the benzene absorption mentioned above [2] we measured the Zeeman spectra with the same technique. We have used benzene crystals doped with 0.01 % by weight of toluene as a "trap". The system in this way gets a response time equal to the phosphorescence lifetime of the emitting trap; in the case of toluene about 5 seconds. Of course the scanning speed of the measurements has to be chosen slow relative to the rate of response.

1.3 Emission experiments.

To be able to measure Zeeman spectra in the phosphorescence of benzene the experimental set-up of fig. 3.1 has to be changed to some extent, as shown in fig. 3.3. For this type of experiments the light source and the detection system are interchanged so that the detecting beam instead of the exciting beam now passes through the monochromator. In this case a Philips SP-1000 high pressure mercury arc acts as the light source, because of its relatively high intensity in the region of the first absorption band of benzene at about 2600 Å. The excitation light is filtered through the same filters as under 1.1 to put as little heat into the liquid helium as possible. To permit chopping at very low frequencies the choppers are replaced by electrical shutters. An external clock is used for opening and closing the shutters.

1.4 The detection system.

The phosphorescence, in absorption as well as emission experiments, is detected by a cooled photomultiplier (EMI-9634 or EMI-6256) and the signal is fed into a Nuclear-Data Pulse-Height-Analyser, which is used as Multi-Channel-Scaler. The signal is first amplified by a pre-amplifier and then passed through a discriminator. By discrimination it is possible to improve the signal to noise ratio because of the difference in pulse height distribution of the pulses originating from the dark-current and those from the signal. Dark-current is relatively rich in low pulses and by discrimination of the lower pulses it can be limited to 25 counts per second for the EMI-9634 without loosing much of the signal pulses.(For the EMI-6256 we were left with about one count per second under the same conditions. These numbers will of course vary for different photomultipliers.)
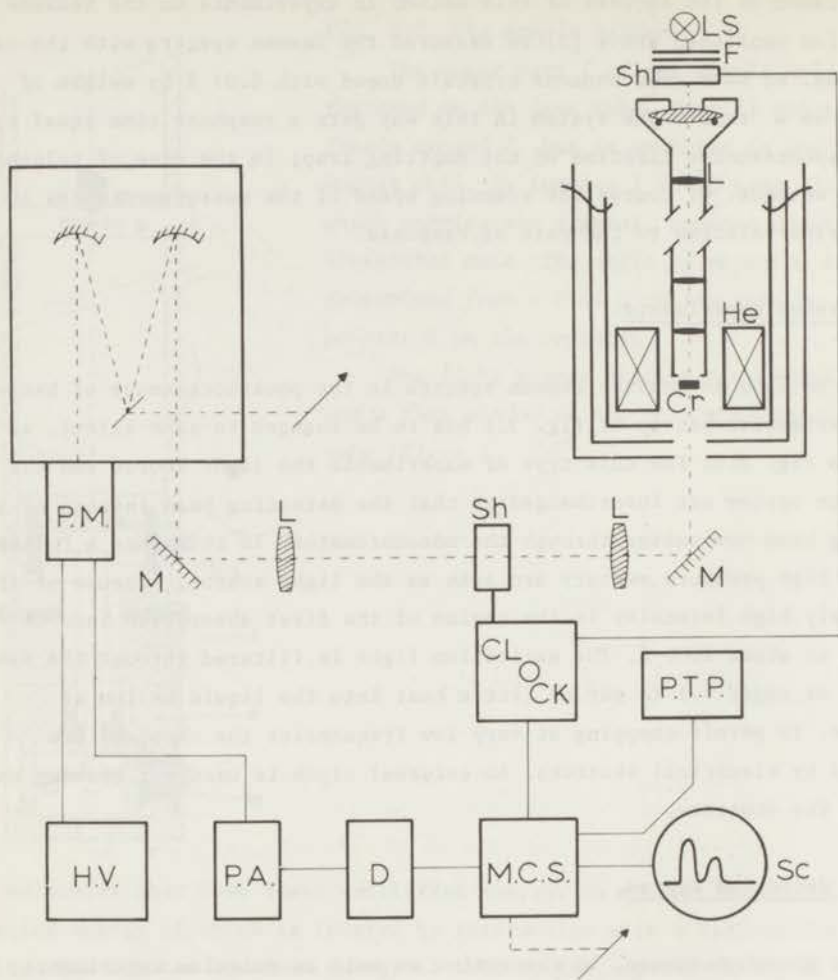
Fig. 3.3. The Zeeman spectrometer as used for the emission experiments.

The light source LS is a Philips SP-1000 mercury arc and is now placed on the top of the cryostat. The exciting light passes through the lens tube before reaching the crystal Cr. The photomultiplier is placed at the exit slit of the monochromator. For slow chopping frequencies the choppers are replaced by electrical shutters Sh.

The spectrum is recorded by scanning the spectrograph slowly through the appropriate region, while an external clock switches the Multi-Channel-Scaler from channel to channel (in the case of emission spectra this happens in phase with the shutters), every 5 or 10 seconds. The whole spectrum consists of 128 or 256 points. For further handling by a computer the spectra are punched on paper tape.

2. Principles of the Zeeman technique.

2.1 Introduction.

The purpose of the present Zeeman experiments is to solve the relative transition probabilities of the three spin sub-levels of the transition in question. The intensities of the Zeeman components are determined by the relative transition probabilities for the three zero-field states, the orientation of the molecules and, for emission spectra, the populations of the Zeeman levels.(This is already outlined in the example of fig. 1.2.) We shall in this section deduce the formulae for the absorption spectra and introduce the effect of the populations in emission at the very end of the deduction. If the orientations of the molecules are known and the intensities of the Zeeman components measured, the relative transition probabilities of the three zero-field states can be solved.

Inversely, it is also possible to draw conclusions from the Zeeman spectrum about the orientation of the molecules when the relative transition probabilities are known in advance. In this way conclusions were drawn about the orientation of Zn-porphin molecules in an n-octane crystal [4] which later were confirmed by ESR studies [5].

2.2 The spin Hamiltonian in zero-field.

By defining the principal axes in the benzene molecule in agreement with ESR results [6] as in fig. 2.1 the spin Hamiltonian can be written as [7]

$$\mathcal{H}_s = - X \, s_x^2 - Y \, s_y^2 - Z \, s_z^2 \, , \tag{3.1}$$

where X, Y, and Z are the eigenvalues of the spin energy of the three

eigenstates in zero-field. The corresponding triplet spin eigenfunctions τ_x, τ_y and τ_z are linear combinations of eigenfunctions of the S_z operator,

$$\tau_x = \sqrt{\tfrac{1}{2}} \, (\, |-\rangle - |+\rangle \,) \ ,$$
$$\tau_y = i\sqrt{\tfrac{1}{2}} \, (\, |-\rangle + |+\rangle \,) \tag{3.2}$$

and $\tau_z = |0\rangle$.

These triplet spin functions have the properties,

$$S_u \, \tau_u = 0$$

and $S_x \, \tau_y = - S_y \, \tau_x = i \, \hbar \, \tau_z$ etc. , $\tag{3.3}$

implying that for the state $|x\rangle$ (used as an abbreviation for the total eigenfunction of the triplet component with spin function τ_x) the spin angular momentum is aligned in the plane $x = 0$.

2.3 The spin Hamiltonian in an external magnetic field.

For the Hamiltonian of a triplet spin system interacting with an external magnetic field one has to add in (3.1) the Zeeman energy and obtains

$$\mathcal{H}_s = - X \, S_x^2 - Y \, S_y^2 - Z \, S_z^2 + g \, \beta \, \vec{H}.\vec{S} \ . \tag{3.4}$$

We neglect the small effects on g due to spin-orbit coupling which for aromatic molecules is a good approximation [8] and take the free electron value. The Zeeman term which depends on the magnetic field $\vec{H}$ will " mix " the triplet eigenfunctions (3.2). In the basis τ_u (u = x, y, z) one finds for the Hamiltonian matrix, using the relations (3.3),

$$\mathcal{H}_s = \begin{pmatrix} X & i \, B \, n & - \, i \, B \, m \\ - \, i \, B \, n & Y & i \, B \, l \\ i \, B \, m & - \, i \, B \, l & Z \end{pmatrix} \tag{3.5}$$

where B stands for $g \, \beta \, H_o$ and H_o is the magnetic field strength. The direction of $\vec{H}$ relative to the principal axes x, y, and z is determined by the direction cosines n, m and l, respectively. Diagonalization of (3.5) yields the eigenenergies of the three new spin states $|v\rangle$ (v = +, 0, -),

50

while the eigenvectors are the coefficients of τ_u (u = x, y, z) in the equations

$$T_v = \sum_u c_u \tau_u \quad , \qquad \begin{array}{l} u = x, y, z \\ v = +, 0, - \end{array} \qquad (3.6)$$

where T_v stands for the triplet spin eigenfunction of the high-field Zeeman level $|v\rangle$. If the transition probabilities for absorption or, in the case of emission, for the radiative decay, are denoted by k_u^r (u = x, y, z) then, because of the " mixing " expressed by (3.6), the transition probabilities of the Zeeman levels $|v\rangle$ are linear combinations of the k_u^r of the levels in zero-field,

$$k_v^r = \sum_u c_{uv}^* c_{uv} k_u^r \quad . \qquad (3.7)$$

For the example of fig. 1.2 one finds for a strong magnetic field $(g \beta H_0 \gg X, Y, Z)$ parallel to the y-axis of the molecule

$$k_+^r = k_-^r = \tfrac{1}{2}(k_x^r + k_z^r)$$

and $\quad k_0^r = k_y^r \quad .$ $\qquad (3.8)$

In practice it is much more reliable to measure relative intensities in one spectrum than absolute intensities over different spectra. A suitable quantity to determine is therefore the ratio of the intensities of the lower two components in the Zeeman spectrum. Using (3.7) we can express this ratio in the transition probabilities k_u^r. Denoting the intensity of the v'th component by I_v one finds

$$R_- = I_- / I_0 = \frac{\sum_u c_{u-}^* c_{u-} k_u^r}{\sum_u c_{uo}^* c_{uo} k_u^r} \qquad (u = x, y, z) \quad . \qquad (3.9)$$

The equation (3.9) holds for a single molecule, or for a set of molecules with the same orientation with respect to the magnetic field. However, in the case of a benzene crystal that is not placed with one of its crystal axes along the magnetic field direction, there are four inequivalent molecular sites with respect to the field direction. The spectra of all sites will coincide, because the variation in the positions of the lines due to the zero-field splitting term in (3.4) is negligible relative to the spectral line width. Therefore, the spectrum as detected is a superposition of four individual spectra. We can account for this by introducing an extra label and

summation in (3.9)

$$R_- = \frac{\sum\limits_{n}\sum\limits_{u} c_{u-n}^* c_{u-n} k_u^r}{\sum\limits_{n}\sum\limits_{u} c_{uon}^* c_{uon} k_u^r} \quad , \quad (u = x, y, z)$$ (3.10)

where n is the sum over the four different sites. The coefficients c_{uvn} will now differ for the various molecular sites, even for the same u and v.

The expression (3.10) not only can be used for analysing absorption spectra, but also for emission experiments if one introduces a population factor that takes care of the population differences between the Zeeman levels concerned. Assuming a Boltzmann equilibrium over the levels and eigenenergies that are equal for all sites (a good approximation in a 70 kG field where the Zeeman term of 7 cm^{-1} is large compared with the zero-field splitting of 0.1 cm^{-1}) one finds in the case of a phosphorescence Zeeman spectrum

$$R_- = \frac{\sum\limits_{n}\sum\limits_{u} c_{u-n}^* c_{u-n} k_u^r}{\sum\limits_{n}\sum\limits_{u} c_{uon}^* c_{uon} k_u^r} \exp\{ - (E_o - E_-)/kT\}$$ (3.11)

in which $(E_o - E_-)$ represents the energy separation between the Zeeman $|0\rangle$ and $|-\rangle$ levels.

2.4 Effect of the polarization of the transitions in zero-field.

As already outlined in chapter II the transitions to or from the triplet sub-levels must be linearly polarized along a molecular axis in those cases where there is no degeneracy. Since the detection system does not collect the light emitted in all directions, the effect of polarization has to be taken into account when applying (3.10) and (3.11) to an experimental situation. We shall deduce the formula for the emission situation, but a similar expression holds for absorption if unpolarized light is used for excitation.

The radiation density in an arbitrary direction that makes an angle β with the radiating dipole corresponding to the zero-field state $|u\rangle$ is [9]

$$I(\beta) = C k_u^r \sin^2\beta \quad .$$ (3.12)

Here C is a proportionality constant and k_u^r is the decay rate of the

zero-field state $|u\rangle$. The intensity measured in the experiment is proportional to this expression integrated over the aperture of the detection system.

In fig. 3.4 we have illustrated the situation. An axis system is chosen with $\vec{y}$ along the optical axis towards the detector. The radiating dipole lies in the x-y plane and makes an angle α with the y-axis. A unit vector
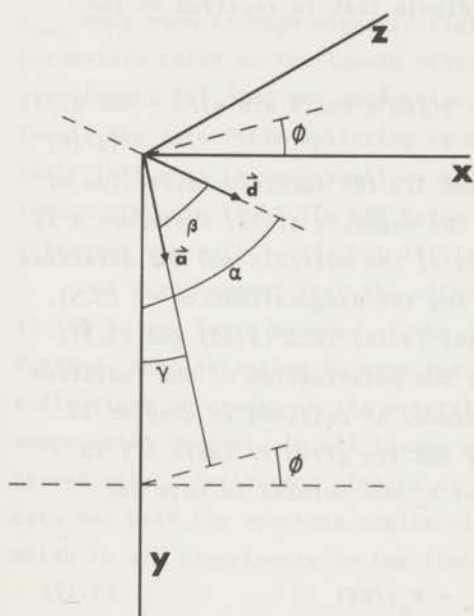
Fig. 3.4. Polarization effect in (3.11).

The radiating dipole $\vec{d}$ lies in the x-y plane and makes an angle α with the y-axis. An arbitrary ray $\vec{a}$ makes an angle β with $\vec{d}$ and an angle γ with the y-axis. The projection of $\vec{a}$ on the x-z plane makes an angle ϕ with the x-axis.

along an arbitrary ray received by the detector is indicated by $\vec{a}$, while $\vec{d}$ is the unit vector in the direction of the dipole. The angle between $\vec{a}$ and $\vec{d}$ is β as in (3.12) and that between $\vec{a}$ and $\vec{y}$ is γ. Finally the angle the x-axis makes with the projection of $\vec{a}$ on the x-z plane is denoted by ϕ.

In the x, y, z axis system the vectors $\vec{a}$ and $\vec{d}$ are represented by

$$\vec{a} = \begin{pmatrix} \sin\gamma\cos\phi \\ \cos\gamma \\ \sin\gamma\sin\phi \end{pmatrix} \quad \text{and} \quad \vec{d} = \begin{pmatrix} \sin\alpha \\ \cos\alpha \\ 0 \end{pmatrix} . \tag{3.13}$$

For the orientation dependent part in (3.12) we thus find using (3.13)

$$\sin^2\beta = 1 - \cos^2\beta = 1 - (\vec{a}.\vec{d})^2 = 1 - \sin^2\alpha\sin^2\gamma\cos^2\phi - \cos^2\alpha\cos^2\gamma +$$
$$-2\sin\alpha\cos\alpha\sin\gamma\cos\gamma\cos\phi . \tag{3.14}$$

In order to obtain the total intensity received by the detector (3.14) has to be integrated over ϕ and γ

$$\iint \sin^2\beta \, d\Omega = \int_{\gamma=0}^{\theta} \int_{\phi=0}^{2\pi} \sin^2\beta \, \sin\gamma \, d\gamma \, d\phi \qquad (3.15)$$

in which Ω is the solid angle and θ is determined by the aperture of the instrument. This finally yields the correction factor, which gives the fraction of the radiation emitted by the dipole that is received by the detector,

$$\iint \sin^2\beta \, d\Omega = 2\pi(1 - \cos\theta) - 2\pi\{1 - 3(\sin^2\alpha \, \cos\theta \, \sin^2\theta)/2 - \cos^3\theta\}/3. \qquad (3.16)$$

For the experimental set-up of fig. 3.1 and 3.3 the detection direction of fig. 3.4 coincides with the direction of the magnetic field. Therefore α is an angle between one of the principal axes of the molecule and the direction of the field, an angle one already needs for the diagonalization of (3.5).

We now introduce the correction factor (3.16) into (3.10) and (3.11) for each of the four sites to account for the polarization of the radiation emitted by the zero-field sub-level concerned. As outlined in chapter II these directions follow from group theory and are given in table 5.V in chapter V for the emission of benzene. For R_- one obtains in this way

$$R_- = \frac{\sum_n \sum_{u'} c_{u-n}^* \, c_{u-n} \, k_u^r \, P_{un}}{\sum_n \sum_u c_{uon}^* \, c_{uon} \, k_u^r \, P_{un}} \exp\{-(E_- - E_o)/kT\} \qquad (3.17)$$

where the exponential factor must be omitted for the absorption experiment, and P_{un} denotes the correction factor (3.16) for the u'th zero-field component of the n'th site in the unit cell.

2.5 Determination of the k_u^r.

In the Zeeman experiments the ratio R_- or, in absorption measurements sometimes the ratio R_+ defined as I_+/I_o is measured as a function of the orientation of the crystal. By rotating the crystal in steps of 10 or 20 degrees about an axis perpendicular to the magnetic field this orientation is varied. The position of the axis of rotation relative to the crystal axes is determined after the Zeeman experiments by X-ray crystallographic methods.

When rotating the crystal all quantities in equation (3.17) vary, except the k_u^r and the Boltzmann factor, but it is known how they vary. Thus, by measuring R_- (or R_+) for several orientations one obtains a set of independent equations in the unknowns k_u^r. The latter are then determined by a least-squares method, up to an unknown proportionality constant inherent in the form of equation (3.17).

The zero-field parameters X, Y, Z do not influence the coefficients c_{uvn} very much at high magnetic fields. In the emission experiments these parameters refer to the lowest vibronic level and are known from ESR experiments [6]. For the absorption measurements concerning higher vibronic levels the zero-field splitting is not known from experiment. However, since their influence is very small we have taken X, Y and Z equal to those of the lowest vibronic level (in ESR terms one expects $E = \frac{1}{2}(Y - X)$ to vary for different vibronic levels but little change in $D = -3Z/2$).

One might expect that the effect of the polarization as expressed in (3.16) is not large because of the averaging due to the four different sites. Further, depolarization is expected to a certain extent because of reflections at cracks in the crystal and because of strain in the optical components. However, in all Zeeman experiments reported in this thesis it proved that polarization effects do play a role; the fit to the experimental data was best for aperture angles close to the aperture of the monochromator, which in all experiments is the limiting component in the set-up.

3. Microwave Induced Delayed Phosphorescence (MIDP) experiments.

3.1 Introduction.

As will follow from the results of our Zeeman experiments to be reported in the chapters IV and V, the Zeeman technique does not supply unambiguous results for the k_u^r in the specific case of benzene. The reason for this lies in the crystal structure discussed in section 4 of the present chapter. To complete the results obtained with the Zeeman method we also used the MIDP technique. As shown by the work of Schmidt et al. [10] this method can be used with success in the investigation of the phosphorescence mechanism of aromatic molecules. For the principles of MIDP we refer to Schmidt's thesis [11].

In the case of a "symmetry allowed" transition the phosphorescence

mechanism is determined mostly by spin-orbit coupling and all information
is hidden in the three spin components of the lowest vibronic level of the
triplet state from which the radiation originates. In such a situation,
where most of the intensity is not vibronically induced it is efficient to
monitor the total phosphorescence intensity in MIDP experiments. In this
way most of the MIDP studies reported to date have been performed.

For a "symmetry forbidden" transition the radiation mechanism is
determined by both vibronic interaction and spin-orbit coupling and the
radiative decay rates may differ for each vibronic band in the spectrum.
Accordingly, we have followed the procedure suggested by El-Sayed et al.
[12] and in our MIDP experiments monitor the phophorescence intensity
emitted in separate vibronic bands.

3.2 Experimental set-up.

The experimental set-up is depicted in fig. 3.5. The crystal is
illuminated by the same light source and filter combination as used for the
Zeeman studies in emission.(See section 1.3 of this chapter.) The cryostat
for these experiments is a small glass one with several quartz windows at
the sides in the lower part, which has the advantage of short light paths.
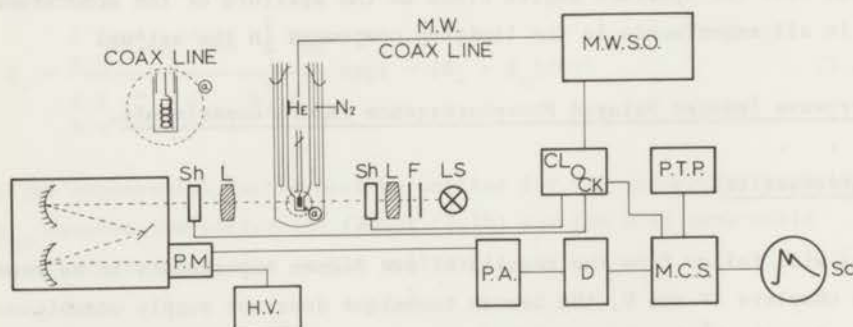
Fig. 3.5. Experimental set-up for MIDP experiments.

*The crystal is placed in a helix (see (a)) connected to the microwave
sweep oscillator. The sample is irradiated via filters F, lens L and shutter
Sh by a Philips SP-1000. The phosphorescence passes a second shutter and is
focussed on the slit of the monochromator. The emission in a particular band
is monitored with the photomultiplier PM and an averaging system. The results
can be displayed and are punched on paper tape.*

The inner part of this cryostat containing the helium ends in a three cm high square quartz cuvette (1 cm edges) in which the crystal is placed. A helix around the crystal is connected to the microwave source.

The phosphorescence is focussed on the slit of the monochromator, which selects one band of the spectrum, and monitored with the aid of a cooled photomultiplier. To prevent direct light from falling on the detection system two electrical shutters are placed, one in the exciting beam and the other one in the phosphorescence beam. These shutters are opened and closed via an external clock, which also triggers the microwave source (Hewlett-Packard HP 8690 B) and the Multi-Channel-Scaler. The 12 second cycle of the shutters is divided into three parts. During the first 4.5 seconds the crystal is irradiated with the light source. After the excitation period 3 seconds of rest follow to allow the system to reach an equilibrium situation in the decay. In the final period of 4.5 seconds the phosphorescence is monitored and the influence of microwave irradiation on its intensity observed.

4. The crystals.

4.1 Preparation.

The samples are prepared on a vacuum line as schematically drawn in fig. 3.6. In the case of Zeeman-absorption measurements samples are used of benzene (Phillips Research grade) doped with 0.01 % toluene (pro analysis quality). For emission experiments (Zeeman as well as MIDP) a solution of 0.2 % of C_6H_6 (Phillips) in C_6D_6 (Merck, uvasol quality) is used. The mixture, first dried on sodium, is refluxed for several hours over a potassium mirror in a reaction flask under vacuum on the line. It is then destilled four times, from the flask into three subsequent cold stages and finally into the crystal growing tube. If the sample has to be used for a Zeeman experiment this tube (pyrex) contains a small quartz tube (diameter about 2 mm, length about 15 mm). The crystal growing tube is sealed under vacuum. By lowering it into a mixture of water and ice the crystal is grown (rate about 5 mm per hour).

The day before a Zeeman experiment the quartz tube with the crystal inside is mounted in the small brass cup that fits into the rotation device of fig. 3.2 with zinc phosphate cement. This is allowed to harden in the
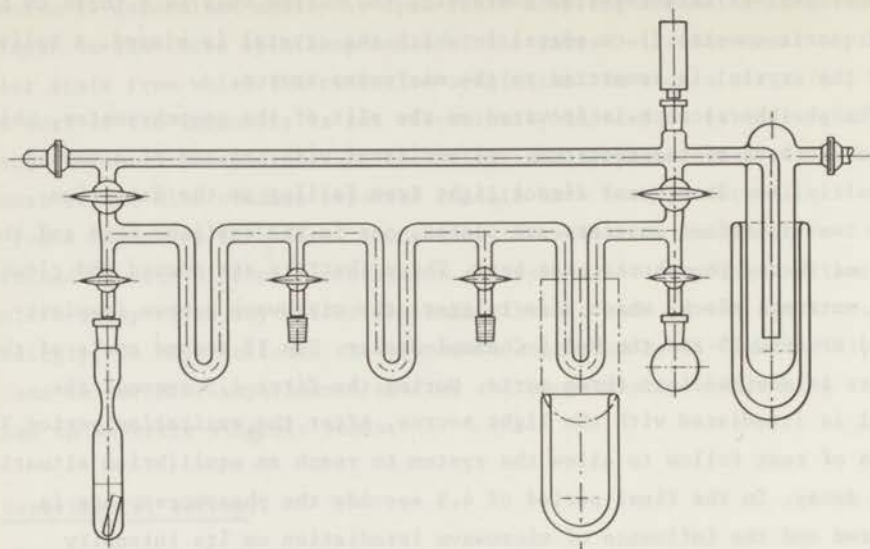
Fig. 3.6. Vacuum line for the preparation of the benzene samples.

The mixture is refluxed in the flask over a potassium mirror for several hours under vacuum. By cooling of the traps it is destilled, finally into the crystal growing tube. This tube is then sealed under vacuum. If the sample is needed for a Zeeman experiment the crystal growing tube contains a thin walled quartz tube. The latter tube is mounted with the crystal inside into the sample holder of fig. 3.2.

cold-room under a nitrogen atmosphere to prevent oxygen from diffusing into the crystal. After the experiment the crystal with brass cup is mounted on a goniometer head specially designed for the shape of the brass cup, and the positions of the crystal axes relative to the quartz tube are determined by X-ray methods.

4.2 Crystal structure.

Benzene crystals have space group P_{bca} with cell dimensions a = 7.46 Å, b = 9.67 Å and c = 7.03 Å [13]. The direction cosines of the molecular principal axes (chosen in agreement with the ESR experiments of de Groot et al. [6]) of the four different sites in the unit cell relative to the crystal axes are given in table 3.I. These data are used for the benzene crystal as

well as for the perdeuterobenzene crystal.

Table 3.I

axis	x	y	z
a	−0.3248	0.6397	0.6814
b	0.9456	0.1999	0.2532
c	−0.0339	−0.7265	0.6867

Table 3.I. Direction cosines of the molecular axes (x,y,z) with respect to the crystallographic axes (a,b,c) for one of the sites in the unit cell. Those of the three other sites are obtained by applying the symmetry operations of the crystal glide planes.

The ambiguity in the determination of the k_u^r from our Zeeman experiments arises from the particular crystal structure of benzene, in which two molecules occur in two almost perpendicular pairs in the unit cell. In fig. 3.7 we give a projection of the four sites along $\vec{b}$ on the a-c plane. While the x-axes of all four molecules are roughly parallel to the a-b plane it can be seen that the y-axis of one site is nearly parallel to the z-axis of another one in the unit cell. Accordingly, in a situation where the magnetic field is nearly parallel to the y-axis of one molecule the $|x\rangle$ and $|z\rangle$ states are heavily "mixed" (see fig. 1.2) but then for another site the field is almost parallel to the z-axis and for this molecule $|x\rangle$ and $|y\rangle$ are mixed. Therefore in equation (3.17) the product $c^*_{yvn}\,c_{yvn}$ will be almost equal to the product $c^*_{zvm}\,c_{zvm}$ if n and m number the two molecules considered. Because of this the observed radiation (absorption) in (3.17) can be interpreted by assuming it to come from the $|z\rangle$ level of molecule n and (or) from the $|y\rangle$ level of molecule m. The conclusion is apparent that for a benzene crystal one would only obtain a reliable set of k_u^r parameters if the measurements of R_- are extremely accurate and no difficulties arise because of hidden depolarization effects.
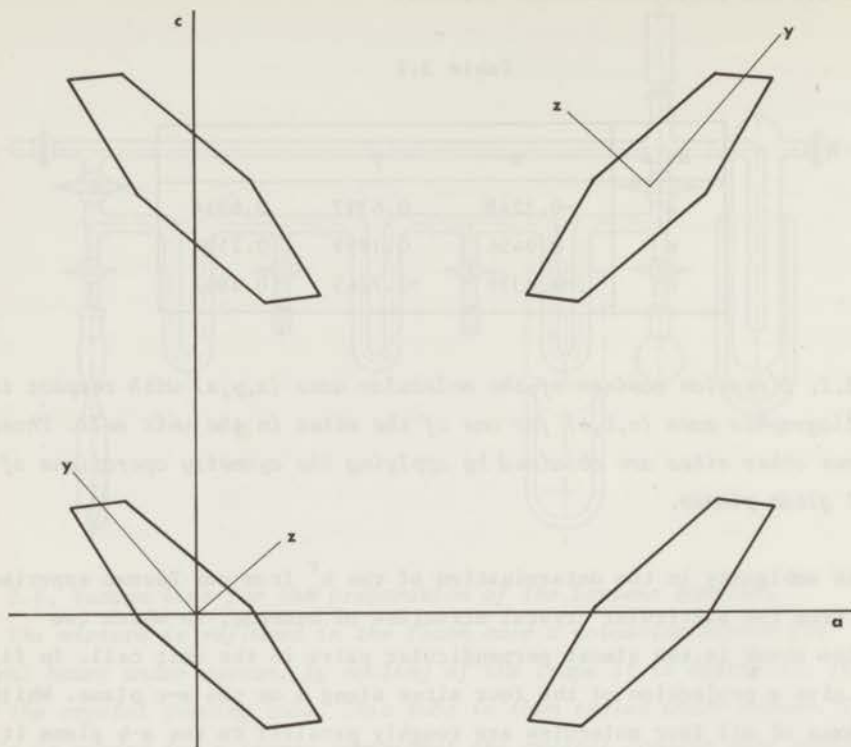
Fig. 3.7. The four benzene molecular sites projected on the a-c plane.

Only the carbon atoms are drawn in the figure. The x-axes of all molecules are near-parallel to the a-b plane. The z-axis of one site (bottom left) is almost parallel to the y-axis of another molecule (top right).

References.

[1] Avakian, P., Abramson, E., Kepler, R.G., and Caris, J.C., 1963, J. Chem.
    Phys., 39, 1127.
    Castro, G., and Robinson, G.W., 1969, J. Chem. Phys., 50, 1159.
    Marchetti, A.P., and Kearns, D.R., 1967, J. Am. Chem. Soc., 89, 768.

[2] Burland, D.M., Castro, G., and Robinson, G.W., 1970, J. Chem. Phys., 52,
    4100.

[3] Craig, D.P., Hollas, J.M., and King, G.W., 1958, J. Chem. Phys., 29, 974.

[4] Canters, G.W., van Egmond, J., Schaafsma, T.J., and van der Waals, J.H.,
    1972, Mol. Phys., 24, 1203.

[5] Kooter, J.A., van Dorp, W.G., and Soma, M., private communication.

[6] De Groot, M.S., Hesselmann, I.A.M., and van der Waals, J.H., 1967, Mol.
    Phys., 13, 583.
    De Groot, M.S., Hesselmann, I.A.M., and van der Waals, J.H., 1969, Mol.
    Phys. 16, 45.

[7] Stevens, K.W.H., 1952, Proc. Roy. Soc., 214, 237.

[8] Van der Waals, J.H., and de Groot, M.S., 1967, The Triplet State,
    ed. A.B. Zahlan (Cambridge Univ. Press, London).

[9] Stepanov, B.I., and Gribkovskii, V.P., 1968, Theory of luminescence,
    ILIFFE Books, London.

[10] Schmidt, J., and van der Waals, J.H., 1968, Chem. Phys. Lett., 2, 640.
     Schmidt, J., Veeman, W.S., and van der Waals, J.H., 1969, Chem. Phys.
     Lett., 4, 341.
     Schmidt, J., Antheunis, D.A., and van der Waals, J.H., 1971, Mol. Phys.,
     22, 1.

[11] Schmidt, J., Thesis, 1971, Leiden, The Netherlands.

[12] El-Sayed, M.A., Owens, D.V., and Tinti, D.S., 1970, Chem. Phys. Lett., 6,
     395.

[13] Cox, E.G., Cruickshank, D.W.J., and Smith, J.A.S., 1958, Proc. Roy. Soc.,
     A 247, 1.
     Bacon, G.E., Curry, N.A., and Wilson, S.A., 1964, Proc. Roy. Soc., A 279,
     98.

C H A P T E R   IV

THE ZEEMAN EFFECT IN THE BENZENE $^3B_{1u}$ STATE.
EVIDENCE FOR A DYNAMIC PSEUDO-JAHN-TELLER DISTORTION

J. van Egmond

and

D.M. Burland and J.H. van der Waals

The Zeeman effect in the phosphorescence photoexcitation spectrum of benzene is used to investigate the assignment of the intense vibronic doublet occurring in the $^3B_{1u} \leftarrow {}^1A_{1g}$ absorption spectrum. The results provide further evidence for a dynamic pseudo-Jahn-Teller vibronic coupling between the $^3B_{1u}$ and $^3E_{1u}$ electronic states.

1. Introduction.

Moffitt and Liehr predicted several years ago [1] that the lowest B_{1u} electronic states (both singlet and triplet) of benzene should be subject to strong "pseudo-Jahn-Teller" vibronic coupling to the nearby E_{1u} states. In a static picture such coupling, if indeed strong, would cause the hexagonal conformation to become unstable relative to certain nuclear displacements of e_{2g} symmetry. Unfortunately, until recently all of the experimental evidence for this effect [2-4] could also be attributed to a crystal field distortion of the benzene molecule.

Van der Waals et al. [5,6] analyzed the effect of this strong pseudo-Jahn-Teller coupling on the frequency of the vibrational normal mode

responsible for the vibronic coupling (the ν_8 e_{2g} mode[+]). Their calculations indicated a large decrease in the frequency of this normal mode in the $^3B_{1u}$ state as compared to its value in the ground and first excited singlet states (in the ground state its frequency is 1584 cm^{-1} [8] and in the first excited singlet state 1470 cm^{-1} [9]). Burland et al. [10] recently found that the singlet-triplet absorption spectrum of crystalline benzene could be consistently interpreted if one assumed that the ν_8 mode undergoes just such a large decrease in the $^3B_{1u}$ state and in addition is split into a closely spaced doublet with frequencies of 239 and 252 cm^{-1}. Lopez-Delgado [11] in a careful analysis of the $^3B_{1u} \rightarrow {}^1A_{1g}$ phosphorescence spectrum has observed this low-frequency vibration as a hot band but has attributed it to a b_{2g} vibration.

We have attempted to clarify the assignment of this low-frequency mode in the $^3B_{1u}$ state by studying the Zeeman effect in the phosphorescence photoexcitation spectrum of benzene [10,12]. In this manner [13,14] one should be able to obtain detailed information on the absorption character of the triplet sublevels of each component of this low-frequency doublet. In fig. 4.1 we have indicated the expected absorption properties of the doublet if it is indeed an e_{2g} vibration. For a regular hexagon the vibronic level would be degenerate and the $|x\rangle$ and $|y\rangle$ spin states indistinguishable. This situation is indicated on the left of the figure. (We neglect spin-dependent effects, which would partially lift the degeneracy of the hypothetical "hexagonal" situation.) The pseudo-Jahn-Teller effect would not alter this situation in a free molecule. It would only act to decrease the ν_8 vibrational frequency.

However in a benzene crystal the site symmetry is C_i, and the crystal field acting in conjunction with the strong vibronic coupling causes the excited benzene molecules to favour certain distorted conformations over others. The theory of this effect has been considered in [6] and from an analysis of the zero-field splitting and spin distribution observed in the lowest vibronic (i.e., vibrationally unexcited) level of the triplet state [2,4], a quantitative estimate of the crystal field parameters could be made. With this information and the wavefunction for the degenerate pair corresponding to one quantum of ν_8 vibrational excitation obtained in [6], it is then also possible to predict in what manner the doublet is split by

[+] For the numbering of the normal modes see ref. [7].
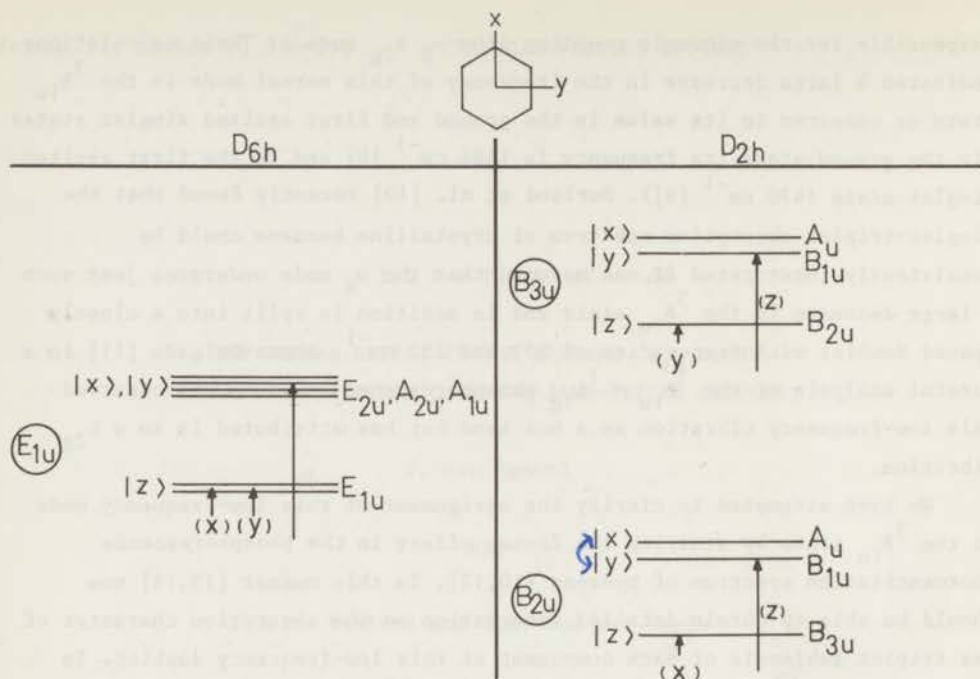
Fig. 4.1. The behaviour of the ν_8 vibronic level of the lowest triplet state of benzene in the "hexagonal" D_{6h} situation and under the influence of a distorting crystal field, which we here assume to have D_{2h} symmetry. The ordering of the two vibronic components on the right as well as the ordering of the individual sublevels within each component follows from the results of [6]. The expected absorption properties of the sublevels are indicated by arrows; intensities by the length and polarization by the label x, y or z. Circled symmetries indicate vibronic symmetry (vibrational and electronic); uncircled symmetries are total symmetries (vibronic and spin).

the crystal field. The result is shown on the right of fig. 4.1.

The principal axes of the zero-field tensor of the lowest vibronic level were found from ESR experiments to coincide with the axes drawn in fig. 4.1 to within an experimental error of a few degrees [2]. From this it then follows that the spin sublevel ordering and the absorption activity of the individual sublevels are as indicated on the right of fig. 4.1. For convenience we have labelled the states as if D_{2h} symmetry were preserved, but the present experiments give no proof of this. In fact the ENDOR results [4] show that the symmetry of the excited molecules is lower.

In this paper we will show that our Zeeman effect results are consistent

with the e_{2g} assignment. In a forthcoming publication, Hochstrasser et al.
[15] also report the use of the Zeeman effect to investigate the present
problem. Our results are essentially in agreement with theirs.

2. Experimental.

We have used the Zeeman effect to study the absorption properties of
the spin components of the benzene triplet state in a manner similar to that
described by Hammer et al. [14]. Benzene crystals doped with 0.01% by weight
of toluene are placed in a superconducting magnet (maximum field 75 kG) at
4.2° K. The $^3B_{1u} \leftarrow {}^1A_{1g}$ absorption is monitored by detecting the resulting
phosphorescence of toluene [9]. Measurements are taken every ten degrees as
the crystal is rotated about an axis perpendicular to the magnetic field.
For the crystal considered here 13 measurements were made. In fact, three
different crystals were investigated, with similar results.

The Zeeman spectrum of the doublet, now split into six components by
the field, is first corrected for the spectral sensitivity of the apparatus
and then fitted to a sum of gaussian lines. The positions of these lines are
known in advance from the field strength and the linewidths can be determined
from the lineshapes in the absence of a field. It is also known that the
$m = \pm 1$ sublevels for each component of the doublet must be equal. So the
only parameters to be varied are four intensities.

The field direction and the rotation axis are determined with respect
to the benzene crystal axes by X-ray crystallographic techniques after the
experiment has been completed. From the known orientations of the crystal in
the field, the relative absorption probabilities of the three zero-field
triplet sublevels (k_x^r, k_y^r and k_z^r) can be fit to the observed relative
intensities of the Zeeman sublevels for both doublet components [14]. In
these calculations of the relative intensities we have taken into account
the non-isotropic behaviour of the dipole absorption of the triplet
sublevels.

3. Results.

In fig. 4.2 we present the observed Zeeman spectra of the benzene
doublet for two orientations of the crystal in the magnetic field, which
differ from each other by a rotation over 40°. From these spectra it is clear
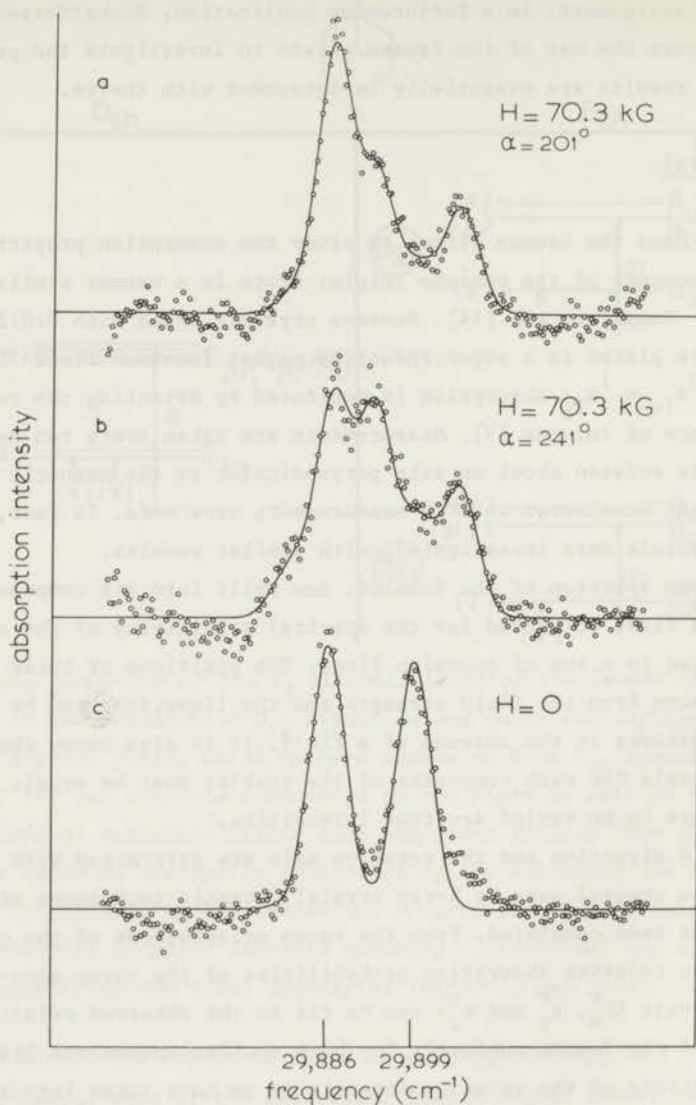
Fig. 4.2. A portion of the phosphorescence excitation spectrum of the $^3B_{1u} \leftarrow {}^1A_{1g}$ transition of benzene at 4.2° K. (a) and (b) are taken with a field of 70.3 kG. The angle α which specifies the direction of the field is defined in the caption to fig. 4.3. Part (c) gives the spectrum in the absence of a field. The dots indicate experimental measurements corrected for the spectral response of the apparatus; the drawn line is calculated as described in the text.

that the two components of the doublet have different absorption characters.
Consider first the low-energy component (the left-hand side of fig. 4.2). In
fig. 4.2a the $m = -1$ sublevel is nearly absent at the extreme left whereas
in fig. 4.2b it has <u>increased</u> at the expense of the $m = 0$ sublevel. By
contrast on the extreme right of fig. 4.2 the high-energy doublet component
shows just the opposite behaviour. The $m = +1$ sublevel (recall that $m = \pm 1$
sublevels have the same intensity) is larger than the $m = 0$ sublevel in fig.
4.2a and has <u>decreased</u> in intensity with respect to the $m = 0$ level in fig.
4.2b. These qualitative conclusions are confirmed in fig. 4.3a where we
display the experimental results of measurements of the relative intensities
of the $m = -1$ to $m = 0$ sublevels of the low-energy component for 13
different orientations of the crystal in the magnetic field. The line drawn
in the figure is the expected relative intensity as a function of orientation
when assuming $k_x^r = 1.0$ and $k_y^r = k_z^r = 0.0$. A least-squares fit of the data
indicates that k_y^r and k_z^r are both less than 10% of k_x^r.

It is more difficult to say something specific about the high-energy
component of the doublet for two reasons. Firstly, from the spectrum in the
absence of a field (fig. 4.2c) we see that this component is not gaussian,
but broadened asymmetrically to high energy. This means that our calculated
intensities are less appropriate for this component. Secondly, due to the
peculiarities of the benzene crystal structure [16,2], k_y^r and k_z^r occur in
the equations in such a way that there is an infinity of solutions, all of
which explain the data equally well. The reason for the coupling of these two
levels is easy to see. The x axes of all four benzene molecules in the unit
cell are within 17° of the crystal b axis. Rotating the crystal about any
arbitrary direction therefore affects the four molecular x axes in about
the same way. By contrast the y axis of one molecule is nearly parallel to
the z axis of another. This means that for any orientation of the crystal in
the magnetic field it is impossible to distinguish the absorption activity
of $|y\rangle$ for one molecule from the activity of $|z\rangle$ for another.

Nevertheless we find that one possible description of the absorption
probability for the high-energy component is given by assuming $k_y^r = 1.0$ and
$k_z^r = k_x^r = 0.0$, in agreement with the theoretical ideas schematically
presented in fig. 4.1. The relationship between experimental and calculated
results for this component is presented in fig. 4.3b. The agreement between
calculation and experiment is not nearly as good as in fig. 4.3a. The
agreement cannot be made better however by changing k_y^r, k_z^r or k_x^r. To improve
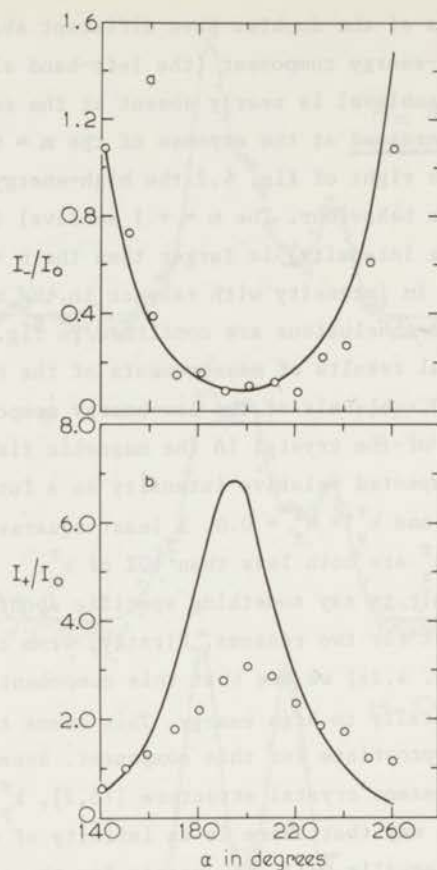
Fig. 4.3. (a) Relative intensity of $m = -1$ Zeeman sublevel to that of $m = 0$ level for the 29886 cm^{-1} component of the doublet. The drawn line has been calculated assuming $k_x^n = 1.0$, $k_z^n = 0.0$. (b) Relative intensity of $m = \pm 1$ Zeeman sublevel to that of $m = 0$ level for 29899 cm^{-1} component. The drawn line has been calculated for $k_x^n = 0.0$, $k_y^n = 1.0$, $k_z^n = 0.0$. In both cases the circles indicate experimental points. When the angle $\alpha = 0°$, the direction cosines of the field with respect to the crystal a, b and c axes are respectively -0.419, 0.902 and 0.055. The turning axis has direction cosines of 0.654, 0.263 and 0.701, respectively.

matters one must take into account the non-gaussian lineshape.

4. Conclusions.

In this paper we have presented experimental results which indicate that the absorption character of the two components of the 250 cm^{-1} vibronic doublet in the benzene $^3B_{1u} \leftarrow {}^1A_{1g}$ spectrum are consistent with the interpretation of this feature as due to the ν_8 e_{2g} vibrational mode. The low-frequency component of this doublet absorbs predominantly to the $|x\rangle$ sublevel and the high-frequency component to the $|y\rangle$ sublevel. (More properly we should say that the $|y\rangle$ sublevel activity is consistent with our results though not unambiguously dictated by the data.) Both the ordering of the doublet components and the absorption properties of the sublevels of each component are in agreement with theoretical results [6], that treat the effect on the $^3B_{1u}$ state of a dynamic pseudo-Jahn-Teller coupling acting in conjunction with a crystal field perturbation.

As mentioned earlier, Hochstrasser et al. [15] have also used the Zeeman technique and reached the same qualitative conclusions as we have. In addition they showed that the absorption of both doublet components was z-polarized as expected (see fig. 4.1). We think they must have the same ambiguity between the $|y\rangle$ and $|z\rangle$ sublevels as we have. Their polarization results would reflect a similar ambiguity.

Acknowledgement.

References.

[1] Moffitt, W., and Liehr, A.D., 1957, Phys. Rev., 106, 1195.
     Liehr, A.D., 1961, Z. Naturforsch., 16a, 641.

[2] De Groot, M.S., Hesselmann, I.A.M., and van der Waals, J.H., 1967, Mol.
     Phys., 13, 583.
     De Groot, M.S., and van der Waals, J.H., 1963, Mol. Phys., 6, 545.
     De Groot, M.S., Hesselmann, I.A.M., and van der Waals, J.H., 1969, Mol.
     Phys., 16, 45.

[3] Nieman, G.C., and Tinti, D.S., 1967, J. Chem. Phys., 46, 1432.

[4] Ponte-Goncalves, A.M., and Hutchison, C.A., 1968, J. Chem. Phys., 49,
     4235.

[5] Van der Waals, J.H., Berghuis, A.M.D., and de Groot, M.S., 1967, Mol.
     Phys., 13, 301.

[6] Van der Waals, J.H., Berghuis, A.M.D., and de Groot, M.S., 1971, Mol.
     Phys., 21, 497.

[7] Wilson, E.B., 1934, Phys. Rev., 45, 706.

[8] Bernstein, E.R., Colson, S.D., Tinti, D.S., and Robinson, G.W., 1968,
     J. Chem. Phys., 48, 4632.

[9] Garforth, F.M., Ingold, C.K., and Poole, H.G., 1948, J. Chem. Soc., 491.

[10] Burland, D.M., Castro, G., and Robinson, G.W., 1970, J. Chem. Phys., 52,
     4100.

[11] Lopez-Delgado, R., 1969, Thèse, Faculté des Sciences d'Orsay, Université
     de Paris.

[12] Castro, G., and Robinson, G.W., 1969, J. Chem. Phys., 50, 1159.

[13] Hochstrasser, R.M., and Lin, T.S., 1968, J. Chem. Phys., 49, 4929.

[14] Hammer, A., Schwoerer, M., and Sixl, H., 1970, Chem. Phys. Lett., 5, 434.

[15] Hochstrasser, R.M., Wessel, J., and Zewail, A.H., 1971, J. Chem. Phys.,
     55, 3596.

[16] Cox, E.G., Cruickshank, D.W.J., and Smith, J.A.S., 1958, Proc. Roy. Soc.,
     A 247, 1.
     Cox, E.G., 1958, Rev. Mod. Phys., 30, 159.
     Bacon, G.E., Curry, N.A., and Wilson, S.A., 1964, Proc. Roy. Soc.,
     A 279, 98.

C H A P T E R V

THE PHOSPHORESCENCE OF BENZENE:
ZEEMAN EFFECT AND MICROWAVE INDUCED EMISSION.

J. van Egmond

and

J.H. van der Waals

Results are given of Zeeman and Microwave Induced Delayed Phosphorescence experiments which determine the relative activities of the three zero-field spin components in the phosphorescence of benzene. The results allow one to decide which of the mechanisms proposed by Albrecht are responsible for the intensity of some of the most prominent bands in the phosphorescence spectrum. It is confirmed that vibronic coupling in the triplet manifold plays the dominant role for the phosphorescence bands that involve e_{2g} vibrations and it follows that the phosphorescence in these bands is almost purely out-of-plane polarized. Our results indicate that spin-orbit coupling occurs via the same mechanism as in other aromatic hydrocarbons.

1. Introduction.

As first pointed out by Craig [1], the phosphorescence of benzene cannot occur by spin-orbit coupling alone if the orbital symmetry of the lowest triplet state is B_{1u} in D_{6h}, an assignment now generally accepted [2] and in agreement with M.O. theory [3,4]. None of the three spin components of a $^3B_{1u}$ electronic state has a total (spin ⊗ orbit) symmetry which permits return to the ground state via emission of electric dipole radiation, and

though spin-orbit coupling mixes singlet character into the triplet components, it cannot change their symmetry. The experimental evidence for this situation is found in the structure of the phosphorescence spectrum, which clearly shows the emission to be vibronically induced.

Since the phosphorescence of benzene thus is "doubly forbidden" the mechanism by which the phosphorescent state acquires radiative activity must involve spin-orbit as well as vibronic interactions. Albrecht [5] analyzed this problem and has shown that, at least in principle, the coupling might occur along quite a number of different paths. At this stage his analysis may be reduced to two major questions:

(i)   does the relevant vibronic coupling occur in the singlet or in the triplet manifold;

(ii) is the dominant spin-orbit coupling (SOC) between $\pi\pi^*$ triplet and $\pi\sigma^*$ and $\sigma\pi^*$ singlet states, as in other aromatic hydrocarbons [6,7] or is benzene with its high symmetry an exceptional case where SOC within the π-electron system becomes effective?

In the discussion we shall give a summary of all coupling schemes considered by Albrecht [5] (Table 5.V). For the moment we refer to figures 5.1 and 5.2, where we have illustrated the most important possibilities without trying to be complete.

As to the first question, a comparison of the vibrational structure in the phosphorescence and fluorescence spectra provides very convincing evidence that it is the vibronic coupling within the triplet system that is responsible for most of the phosphorescence intensity. As shown by Moffitt [9] and Liehr [10] in their pioneering work, vibronic coupling in benzene should be particularly strong ("pseudo-Jahn-Teller interaction") between the fluorescent $^1B_{2u}$ and near-by $^1E_{1u}$ states (fig. 5.1), and between the phosphorescent $^3B_{1u}$ and near-by $^3E_{1u}$ states (fig. 5.2); these states arise from the lowest excited four-fold degenerate electron configuration of M.O. theory [3]. Both couplings occur via e_{2g} modes, but Moffitt also noted an important difference: from symmetry considerations it follows that skeletal bending modes ("even" vibrations in Moffitt's terminology) are most effective in coupling B_{2u} and E_{1u} states, whereas C-C stretching modes ("odd" vibrations) are most effective for coupling B_{1u} and E_{1u} states [8,9,10].

As is known [2], the vibronic structure of the fluorescence spectrum furnishes nice evidence for the correctness of Moffitt's ideas: it originates from a $^1B_{2u}$ electronic state, and indeed, the in-plane bending vibration ν_6

$^1E_{1u}$

$(e_{2g},$ mainly $\nu_6)$

$^1B_{2u}$

SOC

$^3B_{1u}$

$|x\rangle$
$|y\rangle$

$|z\rangle$

(x,y)

$h\nu(e_{2g})$

$^1A_{1g}$

Fig. 5.1. Possible phosphorescence mechanism involving vibronic interaction in the singlet manifold. The wavy line indicates vibronic coupling (pseudo-Jahn-Teller) between the $^1B_{2u}$ and the $^1E_{1u}$ pair. The most active vibration for this mechanism should be the dominant asymmetric mode in the fluorescence spectrum, ν_6. SOC in this case takes place between $\pi\pi^*$ states, which is known to be weak and leads to in-plane polarized phosphorescence. For simplicity the vibronic interaction is drawn between electronic states and the vibrational energies are neglected.

(E.B. Wilson's numbering of the modes [11]) is the prominent non-totally symmetric vibration that gives intensity to the transition. In the phosphorescence spectrum, on the contrary, the skeletal stretching mode ν_8 is dominant, whereas ν_6 is almost absent. This commonly is accepted [5,10] as a strong indication for vibronic coupling in the triplet manifold between the phosphorescent $^3B_{1u}$ state and the near-by $^3E_{1u}$ state of common M.O. parentage, as in fig. 5.2. The importance of this type of coupling is substantiated by the very characteristic $^3B_{1u} \leftarrow {}^1A_{1g}$ absorption spectrum [12]

$^1A_{2u}$ $(\pi\sigma,\sigma\pi)$

$\downarrow(z)$

$^1E_{1u}$ $(\pi\pi^*)$

$\downarrow(x,y)$

$^1B_{2u}$ $(\pi\pi^*)$

(SOC)

(SOC)

$^3E_{1u}$

$(e_{2g},\text{mainly }\nu_8)$

$^3B_{1u}$

$|x,y\rangle$

$|z\rangle$

$|x\rangle$ $|y\rangle$
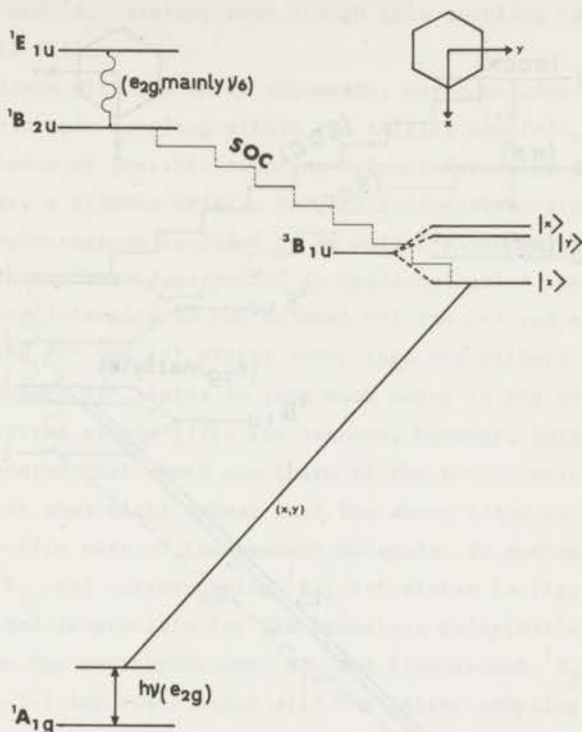
$|z\rangle$

(x) (x,y)

$h\nu(e_{2g})$

$^1A_{1g}$
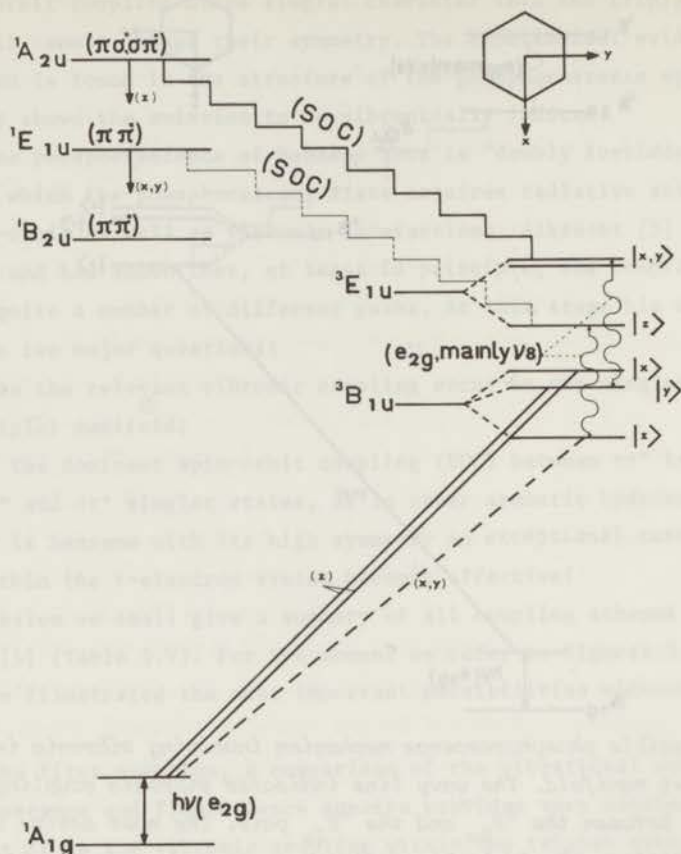
Fig. 5.2. Some phosphorescence mechanisms involving vibronic interaction in the triplet manifold. The wavy lines indicate vibronic coupling (pseudo-Jahn-Teller) between the $^3E_{1u}$ pair and the lowest triplet $^3B_{1u}$. The most active vibration for this coupling is known to be ν_8. Activity of the $|z\rangle$ component with in-plane polarized emission must be due to SOC with the $^1E_{1u}$ singlet state, which is expected to be weak. High energy $^1A_{2u}$ states involving σ MO's give z-polarized character to the $|x\rangle$ and $|y\rangle$ components of the triplet. For simplicity the vibronic interaction is drawn between electronic states and the vibrational energies are neglected.

and its Zeeman effect [13,14]. Further, the striking dissimilarity of the fluorescence and phosphorescence spectra seems to exclude intensity stealing by the phosphorescence from the fluorescence transition through direct SOC

between the $^3B_{1u}$ and $^1B_{2u}$ states, even though this coupling is symmetry allowed (fig. 5.1) [15].

If in accordance with the above arguments, one concludes with Albrecht [5] to dominant vibronic coupling within the triplet manifold, then one still is left with a choice of possible coupling schemes depending on the answer to question (ii). Here a dilemma arises. For all hydrocarbons studied, except benzene, the phosphorescence is found to be out-of-plane polarized [16]. This is consistent with current ideas on SOC in these molecules, which attribute the phosphorescence intensity to SOC between $\pi\pi^*$ and $\sigma\pi^*$ and $\pi\sigma^*$ states [6,7]. That highly excited $\sigma\pi^*$ and $\pi\sigma^*$ states enter into the picture is because SOC between non-degenerate $\pi\pi^*$ states is very weak owing to the characteristic symmetry of π-electron states [17]. For benzene, however, Russell and Albrecht [18] reported that about one third of the phosphorescence is in-plane polarized. It thus might appear that the above ideas on SOC are not valid for the specific case of the benzene molecule. Is perhaps the direct SOC between the $^3E_{1u}$ and corresponding $^1E_{1u}$ $\pi\pi^*$ states in fig. 5.2 stronger than anticipated and responsible for the anomalous polarization? Or, is the direct SOC between the phosphorescent $^3B_{1u}$ and fluorescent $^1B_{2u}$ states indicated in fig. 5.1 important after all? The latter coupling was considered by Hameka and Oosterhoff in their calculations [15] and also leads to in-plane polarized emission.

The present work was undertaken to provide an answer to these questions. As made clear in figs. 5.1 and 5.2, two types of experiment should be helpful in elucidating the mechanism(s) by which benzene acquires its phosphorescence intensity;

   a) Determination of the polarization of the emission in the various
      vibronic bands of the spectrum.
   b) Determination of the radiative activity of the three spin sublevels
      of the phosphorescent state for the individual bands.

The first approach (a) has been used by Russell and Albrecht [18], who did photo-selection experiments on benzene's phosphorescence in a glass at 77 K. They interpreted their results by the assumption of 30% in-plane polarized emission for the two intense bands (8_1^0) and $(9_1^0)^*$.

---

*
In this notation, first used by Callomon et al. [21], $(n_{v'}^v)$ indicates that for the vibrational mode ν_n the energy-quantum is changing from v in the excited state to v' in the ground state.

However, as noted already, these results appear anomalous in comparison with those on other aromatic molecules which all show almost purely out-of-plane polarized phosphorescence. For this reason it seemed worthwhile to approach the problem also via the second method (b).

We began our investigation by studying the Zeeman effect of the strongest band (8_1^0) in the emission spectrum of an isotopically mixed crystal of C_6H_6 in C_6D_6 at 4.2 K. The Zeeman technique has been used with success before by Hochstrasser and coworkers [19] for unravelling SOC mechanisms in a number of molecules and recently by Hammer et al. for quinoxaline [20].

Our Zeeman experiments are reported in the next section; from the results it will appear that owing to the particular structure of the benzene crystal, no unambiguous answers are obtained. Furthermore, problems arose because, contrary to our expectations and earlier experiences with e.g. quinoxaline in durene [22], spin-lattice relaxation proved too slow to maintain Boltzmann equilibrium between the spin states when the crystal is continuously excited in a 70 kG field at 4.2 K.

In the meantime the microwave-phosphorescence double resonance technique in zero-field had been realized by Schmidt et al. [23] in our laboratory and its potential for the vibronic analysis of phosphorescence spectra demonstrated by El-Sayed et al. [24]. These new methods appeared particularly suited for the present investigation. In zero-field one no longer suffers from the magnetic anisotropy of the crystal which is the cause of the ambiguity in the interpretation of the Zeeman spectra.

After a number of attempts we succeeded in observing so-called Microwave Induced Delayed Phosphorescence (MIDP) signals [23] for a number of vibronic bands in the phosphorescence spectrum. These experiments are described in section 3. The results, which for the o-o band agree with a report of Gwaiz et al. [25], establish that the phosphorescence of benzene derives its intensity almost entirely via vibronic coupling in the triplet manifold and SOC to highly excited $^1A_{2u}$ $\sigma\pi^*$ and $\pi\sigma^*$ states. Such a coupling scheme, indicated by the solid path in fig. 5.2, implies z-polarized emission. Russell and Albrecht [18], on the contrary, in photo-selection experiments on benzene in a glass at 77 K found a constant ratio of about 2:1 between out-of-plane and in-plane polarized emission for the strong bands involving e_{2g} modes. It is felt that their experiments must have been adversely affected by rotation of the excited molecules in the glass before decaying to the ground state.

2. Zeeman effect of the (8_1^0) band at 4.2 K

2.1 Experimental.

Crystals of perdeuterobenzene (MERCK, uvasol quality), doped with 0.2% of C_6H_6 (Phillips, research grade) are grown in a small open quartz tube. During crystallization this tube is held in a larger pyrex one, which has been sealed under vacuum. The sample tube is then placed in liquid helium within the bore of a superconducting solenoid (Oxford Instruments). A device is present by which the quartz tube with the crystal can be rotated about an axis perpendicular to the direction of the magnetic field. The crystal is illuminated by a Philips SP-1000 high pressure mercury arc through an aqueous solution of $CoSO_4$ and $NiSO_4$, and a Chance Pilkington OX-7 optical glass filter. The phosphorescence is focussed on the slit of a Jarrell-Ash spectrometer (75 cm Czerny-Turner) which selects the appropriate wavelength and is used in second order. The emission is counted by a combination of a cooled EMI-9634 photomultiplier and a Nuclear Data Pulse-Height Analyzer/ Multi Channel Scaling system (1100 series) which yields the spectra punched on paper tape for further handling by a computer.

For the interpretation of the spectra it is necessary to know the populations of the Zeeman-levels. In our first experiments we found that under steady-state illumination at 4.2 K there is no Boltzmann equilibrium between the three spin states; see the spectra in fig. 5.3. These spectra have been recorded with anti-phase chopping of the excitation and detection beams at a frequency of 42 Hz. For the temperature and the magnetic field strength (70 kG) of these experiments one calculates that at thermal equilibrium the ratio between the populations of the outer two Zeeman components of the triplet state should be about 90. Since, according to theory the radiative activity of these two components is equal it follows from the relatively high intensity of the high energy component, that under the present conditions thermal equilibrium is not established. It will also be clear from fig. 5.3 that the deviation from Boltzmann equilibrium is orientation-dependent, which indicates that the triplet state components are not populated with equal rates, a common finding in aromatic molecules.

To approximate a Boltzmann distribution we then replaced the choppers by a pair of electrical shutters which open and close with a cycle of 12 seconds. After 4.5 seconds of excitation the crystal is allowed to rest for
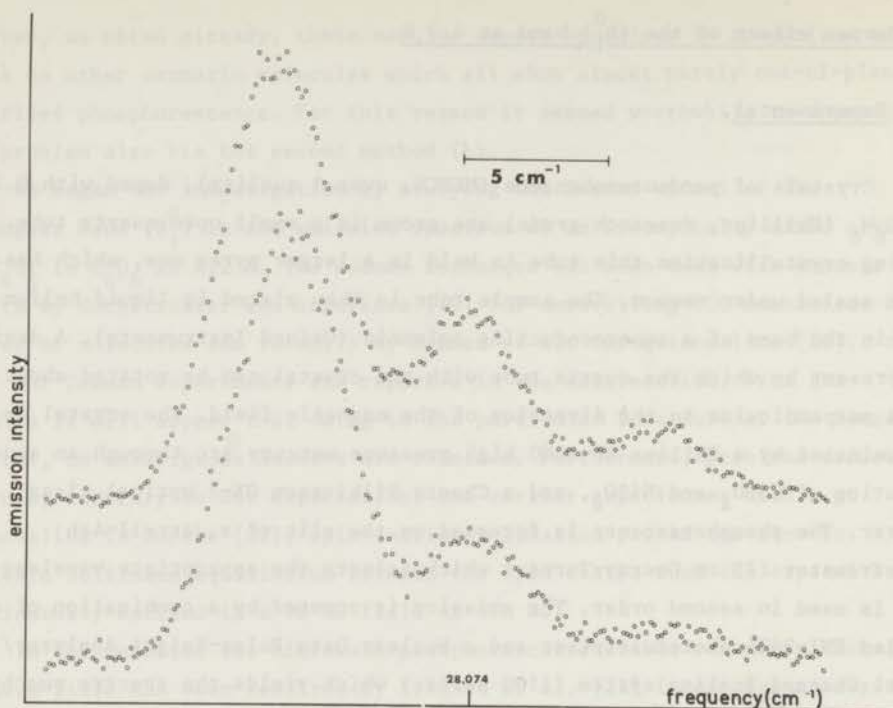
Fig. 5.3. The Zeeman effect in (8_1^0) for two different orientations of a crystal, recorded with the aid of anti-phase chopping of the excitation and phosphorescence beams at 42 Hz. From the relatively high intensity of the $|+\rangle$ component it follows that there is no thermal equilibrium under these conditions. The relative heights of these components also are orientation dependent which indicates that there is selective population of the zero-field spin states.

3 seconds in order to attain thermal equilibrium, after which 4.5 seconds of counting of the emission follows. Each cycle of the shutters corresponds to one channel of the Multi Channel Scaling system. As shown by the spectrum in fig. 5.4 the system now must be much closer to thermal equilibrium, since the top component no longer is observed. In the average case (depending on the quality of the particular signals) this implies that its intensity is less than 3 percent of that of the low energy one, and thus cannot be too far from the value of 1.1% at thermal equilibrium. Using the shutter cycle we recorded spectra for different orientations of the crystal, by rotation of the crystal about the quartz tube axis in steps of 10 or 20 degrees. After the
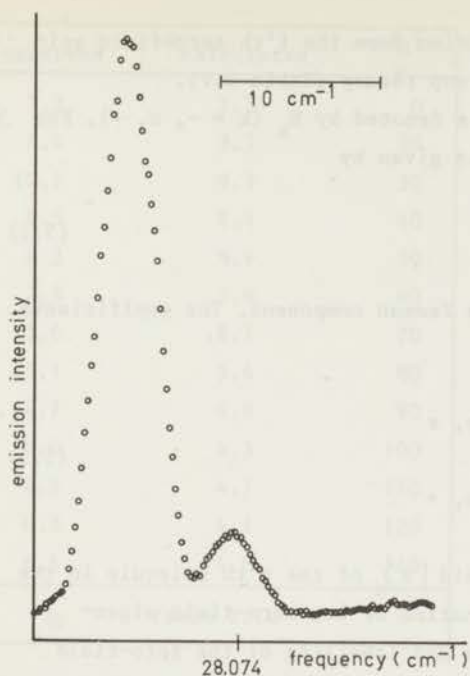
Fig. 5.4. Zeeman spectrum of (8_1^0) recorded with the shutter system. The $|+\rangle$ component does not appear anymore, and the system must be close to thermal equilibrium.

measurements the orientation of the crystal relative to the sample tube was determined by X-ray methods.

2.2 Interpretation of the spectra.

The ratio of the intensities of the two lower-energy components of the Zeeman spectrum, corresponding to $m = -1$ and $m = 0$, is given by [20]

$$R = I_-/I_o = \frac{N_- \sum\limits_n \sum\limits_i c^*_{-in} \, c_{-in} \, k^r_i \, p_{in}}{N_o \sum\limits_n \sum\limits_i c^*_{oin} \, c_{oin} \, k^r_i \, p_{in}} \qquad (5.1)$$

where $i = x, y, z$ labels the three zero-field spin states which we shall denote by $|x\rangle$, $|y\rangle$ and $|z\rangle$ and n is a summation index over the four molecules in the unit cell. The radiative decay rate of the i'th zero-field eigenstate is denoted by k^r_i, and p_{in} is a correction factor for the anisotropy introduced by its polarization. This factor represents the intensity of the radiation coming from the dipole integrated over the aperture of the instrument. In calculating p_{in} one has to postulate a

79

direction of polarization for the radiation from the i'th zero-field spin state; in our case this follows from group theory (Table 5.V).

The population of the k'th level is denoted by N_k (k = -, o, +). For Boltzmann equilibrium the ratio N_-/N_o is given by

$$N_-/N_o = \exp \{-(E_- - E_o)/kT\} \tag{5.2}$$

where E_k is the eigenenergy of the k'th Zeeman component. The coefficients c_{kin} follow from the equations

$$|k\rangle_n = \sum_i c_{kin} |i\rangle \qquad \begin{array}{l} i = x, y, z \\[4pt] k = -, o, + \end{array} \tag{5.3}$$

where the triplet component in high field $|k\rangle_n$ of the n'th molecule in the unit cell is written as a linear combination of its zero-field eigen-functions $|i\rangle$ (for the choice of axes and labelling of the zero-field states see fig. 5.1). These coefficients are determined from the known orientations of the molecules in the magnetic field by diagonalization of the Hamiltonian matrix in the basis $|i\rangle$. The elements of this matrix are given by

$$\mathcal{H}_{ij} = \langle i| \, g\beta \vec{H}.\vec{S} + \mathcal{H}_{ss} |j\rangle \qquad i,j = x, y, z. \tag{5.4}$$

Here, at high fields the zero-field splitting term $\mathcal{H}_{ss}$ is small compared to the Zeeman energy $g\beta \vec{H}.\vec{S}$ and may be neglected.

By measuring the ratio R as a function of the orientation of the crystal it is possible to fit two of the unknown radiative decay rates, say k_y^r and k_z^r to the experimental data by a least squares procedure, setting the third, k_x^r equal to 1.0.

2.3 Results.

In the tables 5.Ia and 5.IIa we give the observed R values as a function of the angle of rotation in two series of experiments on different crystals. When trying to fit rate constants to these observations an ambiguity arises that is characteristic for Zeeman studies on benzene and which we already

$R_{observed}$	$R_{calculated}$	angle
7.3	7.3	0
9.4	8.7	20
10.1	9.2	30
9.5	9.4	40
8.3	8.9	50
7.8	7.8	60
5.6	6.7	70
5.1	5.6	80
4.7	4.8	90
5.0	4.3	100
4.5	4.1	110
6.3	4.1	120
6.6	4.8	140
	Table 5.Ia	

Table 5.Ia. Intensity ratio R of the m = − 1 and m = 0 Zeeman components for a C_6H_6/C_6D_6 crystal at 4.2 K as a function of the angle of rotation. Experimental results and values calculated according to (5.1). The unit vector in the direction of the rotation axis in the a, b, c crystal axis system is given by (0.4573, 0.2934, −0.8394); further, an angle of rotation of 83.5° corresponds with the magnetic field parallel to the direction (0.6018, −0.7972, 0.0492).

$R_{observed}$	$R_{calculated}$	angle
6.8	8.8	0
5.3	7.5	20
5.4	8.1	40
9.1	8.8	60
7.5	8.1	80
6.6	7.6	90
7.9	8.0	110
13.6	10.5	130
7.7	10.3	150
11.0	7.9	170
11.5	7.6	190
	Table 5.IIa	

Table 5.IIa. Intensity ratio R as a function of the angle of rotation for a different crystal.
The direction of the rotation axis in this case is (−0.3547, 0.9285, 0.1097) while the magnetic field is parallel to (0.8565, 0.2756, 0.4364) when the rotation angle is 83.5°.

encountered in our experiments on the triplet←singlet absorption [14]. Because of the particular structure of the crystal [26,27] one only can determine a relation between k_y^r and k_z^r with confidence, rather than the two rates separately. This finds its origin in the relative orientation of the molecules: the y-axes of one set of molecules are almost parallel to the

z-axes of another set, related to the former by a crystal glide plane. The effect of this can clearly be seen in the second half of the tables 5.I and 5.II where we give a "map" of a reliability coefficient C_r x 100, with C_r defined as

$$C_r = \frac{\sum_i (R_{observed} - R_{calculated})^2}{\sum_i (R_{observed})^2} \quad , \text{ (i runs over the measurements)} \quad (5.5)$$

for various combinations of k_y^r and k_z^r with $k_x^r = 1.0$. In both tables a "valley" appears in the values of C_r for a series of combinations of k_y^r and k_z^r and therefore a reliable conclusion about their individual values cannot be drawn. The result of the two series of measurements may be summarized as:

$$k_y^r + 1.4 \ k_z^r = 0.7 \ (\pm \ 0.2) \quad \text{(Table I)}$$

with a "best" fit for $k_y^r = 0.7$ and $k_z^r = 0.0$

$$k_y^r + 1.3 \ k_z^r = 0.8 \ (\pm \ 0.3) \quad \text{(Table II)}$$

with the "best" fit for $k_y^r = 0.77$ and $k_z^r = 0.0$.
However, tables 5.Ib and 5.IIb show that one cannot use these "best" values with confidence because of the appearance of the valleys.

Table 5.Ib

k_z^r \ k_y^r	0.0	0.2	0.4	0.6	0.8	1.0	1.2
0.0	> 100	44.4	7.4	_1.8_	2.6	5.6	9.7
0.2	12.9	3.4	_1.9_	3.4	6.4	10.3	14.8
0.4	_2.7_	_2.5_	4.2	7.0	10.7	15.1	20.0
0.6	3.1	4.8	7.6	11.2	15.4	20.2	25.4
0.8	5.4	8.2	11.7	15.8	20.4	25.5	31.0
1.0	8.7	12.1	16.1	20.7	25.6	31.0	36.7

Table 5.Ib. Map of the reliability coefficient C_r x 100 for the data of table 5.Ia. C_r is defined in (5.5) and has been tabulated for various values of k_y^r and k_z^r; k_x^r is set equal to 1.0. A valley appears, which is indicated by underlining the numbers nearest to its bottom.

Table 5.IIb

k_z^r \ k_y^r	0.0	0.2	0.4	0.6	0.8	1.0	1.2
0.0	> 100	> 100	27.3	9.7	8.1	10.2	13.1
0.2	41.3	12.6	7.3	7.9	10.1	12.7	15.3
0.4	8.6	7.0	8.2	10.3	12.7	15.0	17.1
0.6	7.2	8.6	10.6	12.7	14.8	16.7	18.6
0.8	9.0	10.8	12.7	14.6	16.4	18.1	19.7
1.0	11.1	12.8	14.5	16.2	17.8	19.2	20.6

Table 5.IIb. Map of the reliability coefficient C_r x 100 for the data of table IIa.

At this stage we shall not draw conclusions from these data. We first discuss the MIDP experiments, which will be seen to yield unambiguious results, compatible with the above data.

3. Microwave Induced Delayed Phosphorescence experiments at 1.3 K.

3.1 Experimental.

Similar crystals as used for the Zeeman experiments are used for these measurements. The samples are cut to a size of about 3 x 3 x 10 mm and placed in a helix, which is mounted in a cryostat with four optical windows (suprasil) at right angles in the lower part. The helix is connected by a coaxial line to a Hewlett Packard HP 8690 microwave sweep oscillator. To make the population differences among the levels as large as possible the helium is pumped off to 1-1.2 torr, which corresponds to a bath temperature of 1.27-1.30 K. The crystal is irradiated with the same lamp/filter combination as used for the Zeeman experiments.

In fig. 5.5 we show the decay of the total phosphorescence at 1.3 K as a function of time from the moment we stopped the excitation. At a time $t = t_1$ the crystal is irradiated with microwaves resonant with the $y \leftrightarrow z$ transition. A "delayed phosphorescence signal" is induced which returns to the original exponential decay in a time which is short compared to the phosphorescence lifetime of about 10 seconds. From this picture it is clear
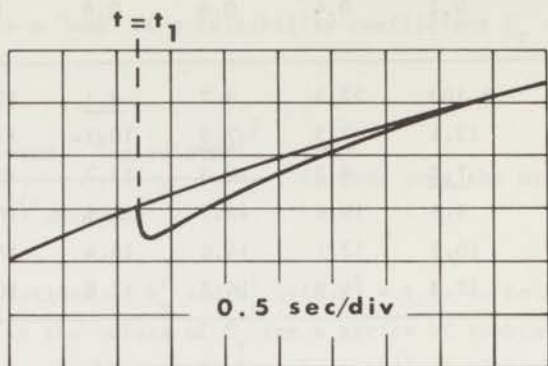
Fig. 5.5. Decay of the total phosphorescence of benzene at about 1.3 K. Two decay curves are superimposed:
a) normal decay
b) decay when sweeping through the y ↔ z transition at a time t = t₁. The baseline is below the horizontal axis. The time base is 0.5 sec/div and it is seen that after the microwave sweep the system returns to its unperturbed situation within 3 sec.

that there are relaxation mechanisms which account for the quick return to the original population distribution. We measured the height of this delayed signal as a function of the delay time t_1. It turns out that the height follows the same exponential as the total phosphorescence; that is to say, after a few seconds there is a constant ratio between the populations of the various levels. This implies that there is no "isolation" of the levels as in many other systems at this temperature [28,31] and large population differences will not occur. We shall see, that even without isolation, it remains possible to deduce conclusions from the MIDP signals.

As outlined in the introduction we are interested in the relative radiative activities of the different spin sublevels for individual vibronic bands. For this reason we did not monitor the total phosphorescence as in fig. 5.5, but did our experiments on specific vibronic bands. This was done by placing a monochromator (Jarrell-Ash 75 cm Czerny Turner) in the detection beam and analyzing the output of the photomultiplier with an averaging system.

84

Both photon counting (Nuclear Data Multi Channel Analyzer) and signal averaging (Hewlett Packard 5480 Signal Analyzer system) have been applied. The slits of the monochromator are set at about 400 μ (20 cm^{-1}) to gather as much light as possible. This implies that only those bands can be studied that are well separated from others. The photomultiplier (EMI 6256 or 9634) is cooled to -25°.

After 4.5 seconds of excitation (the same shutters are used as for the Zeeman experiments) the crystal is allowed to rest for 3 seconds. During the following observation period of 4.5 seconds a microwave sweep is triggered to equalize the populations of two levels. The same cycle is repeated until a reasonable signal to noise ratio has been obtained in the averaging system (100 - 1000 times). The delay between stopping excitation and sweeping through the resonant microwaves is always chosen to be about 5 seconds, which is considered sufficient to ensure a constant initial population ratio.

3.2 Results.

We have measured the height of the delayed phosphorescence signal relative to the total intensity just before the signal for five different vibronic bands in the phosphorescence. Three of these bands correspond to vibrations of e_{2g} symmetry, one to a b_{2g} mode and the last one to the o-o band. The behaviour of these bands is crucial for determining the path(s) by which intensity is "stolen" from the singlet manifold. The results are given in table 5.III.

Before giving a quantitative analysis of the results we may point out some characteristic features.

i)   When saturating the x ↔ z and y ↔ z transitions positive signals are observed for all bands (i.e. increase of the phosphorescence intensity); the effect of saturating the x ↔ y transition never was detected.

ii)   For the vibronically "allowed" bands, which involve one quantum of an e_{2g} vibration, the signals induced by the x ↔ z and y ↔ z transitions have about equal heights. It will prove significant that these signals are stronger for the (8_1^0) and (9_1^0) bands, the most active modes in the phosphorescence spectrum, than for (6_1^0) which is only weakly active in phosphorescence but very dominant in fluorescence (figures 5.1 and 5.2).

Table 5.III

band	vibration symmetry	z ↔ y transition	z ↔ x transition
(8_1^0)	e_{2g}	0.078 (0.005)	0.086 (0.005)
(9_1^0)	e_{2g}	0.08 (0.01)	0.10 (0.01)
(6_1^0)	e_{2g}	0.05 (0.02)	0.05 (0.02)
(4_1^0)	b_{2g}	0.08 (0.02)	0.08 (0.02)
o-o	a_{1g}	0.12 (0.02)	0.08 (0.02)

Table 5.III. Measured ratios h_{yz}/I and h_{xz}/I for the different vibronic bands in the phosphorescence spectrum.

Estimated possible maximum errors are given in parentheses.

iii) For the o-o band the y ↔ z signal is stronger than the x ↔ z signal. This is in agreement with a report by Gwaiz, El-Sayed and Tinti [25].

iiii) For the (4_1^0) band the x ↔ z and y ↔ z signals again are equally strong.

It is unlikely that impurities have contributed to the above results, since in all instances the induced signals occurred at the microwave frequencies of 4.93 and 4.54 GHz that follow from the zero-field splitting pattern determined in previous ESR experiments [29]. Also the positions of the various phosphorescence bands agreed with those reported by Colson et al. [30].

3.3 Interpretation of the measurements.

The relative contributions from the individual spin levels to the radiative intensity in a vibronic band can be determined from the ratio between the delayed signal and the total phosphorescence in the vibronic band in question. If h_{ij} is the height of the delayed signal for the i ↔ j transition (i,j = x, y, x), and I is the total light intensity just before the delayed signal, then according to the analysis given by Schmidt et al.

[31] the ratio of these two quantities is equal to

$$h_{ij}/I = \frac{f(N_j - N_i) \, (k_i^r - k_j^r)}{\sum\limits_{k=x,y,z} N_k \, k_k^r} \quad .$$ (5.6)

The factor f is the "transfer coefficient" of [31]. In this case it turns out that $f = \frac{1}{2}$; by the relatively slow microwave sweep the populations are equalized. The check for this is the observation that a second sweep through the transition, 0.1 sec. after the first one does not induce observable changes in the phosphorescence intensity.

Since relaxation is fast relative to the decay, the situation just before the microwave transition occurs must be close to Boltzmann equilibrium, which at the temperature of the experiments (1.3 K) is

$$N_x^o : N_y^o : N_z^o = 83 : 84 : 100 \ .$$

In the first instance one might substitute these values into (5.6) and use this equation to derive the relative radiative rates k_x^r/k_y^r and k_z^r/k_y^r from the experiments. However, a refinement is possible. In order to get more accurate information about the population distribution we did some further experiments on the strongest band, (8_1^0). In fig. 5.6 we show two pictures, made by sweeping through the $y \leftrightarrow z$ and $x \leftrightarrow z$ transitions in succession, 0.1 second after one another. It is clear that the pictures, which correspond to opposite sweep directions, are not identical.

From the heights of the delayed signals in fig. 5.6 relative to the total phosphorescence intensity we have calculated, with the aid of (5.6) and an analogous expression for the height of the second signal within a pair, that at the moment the microwave transition occurs the populations of the levels differ slightly from Boltzmann equilibrium;

$$N_x : N_y : N_z = 72 : 76 : 100 \ ,$$ (5.7)

and further that k_x^r and k_y^r are equal for this band within the experimental accuracy. That the $|x\rangle$ and $|y\rangle$ levels are underpopulated relative to the Boltzmann values must be due to the inactivity (both radiative and radiationless) of the $|z\rangle$ level and the only moderately fast relaxation
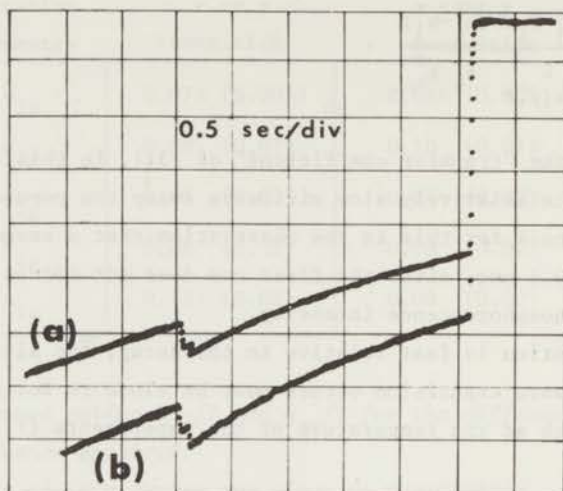
Fig. 5.6. Delayed signals in the phosphorescence of (8_1^0) produced by sweeping
subsequently through
  a) the $x \leftrightarrow z$ and $y \leftrightarrow z$ transitions;
  b) the $y \leftrightarrow z$ and $x \leftrightarrow z$ transitions.
The delay time between the two transitions is about 0.1 sec. These pictures
have been recorded with the aid of the shutter cycle and a Hewlett Packard
signal averager (about 150 sweeps). From the difference between the pictures
it is deduced that in the situation where excitation has been terminated for
serveral seconds the $|y\rangle$ level has a somewhat higher population than the
$|x\rangle$ level (see text). The time base is 0.5 sec/div.

observed in fig. 5.5. In the initial stages of the decay the populations of
the $|x\rangle$ and $|y\rangle$ levels decrease somewhat relative to that of the $|z\rangle$
level. This is observed experimentally; if one sweeps through the $x \leftrightarrow z$ or
$y \leftrightarrow z$ transition immediately after shutting off the exciting light, the
relative height of the induced signals is nearly 50% lower than in
experiments where 5 seconds of free decay have passed before the microwave
transition occurs. This is in accordance with very recent observations of
El-Sayed et al. [33] and the conclusion is apparent that the $|x\rangle$ and $|y\rangle$
levels are preferentially populated over the $|z\rangle$ level, as might have been

expected on theoretical grounds.

The time constant for the return of the delayed signal to the unperturbed phosphorescence decay observed in fig. 5.5, and in an almost identical picture for the $x \leftrightarrow z$ transition, is related to the relaxation processes between the three levels; it appears that the relaxation rates W_{xz} and W_{yz} for relaxation between $|x\rangle$ and $|z\rangle$ and between $|y\rangle$ and $|z\rangle$ both must be of the order of 0.5 sec^{-1}. As a check on the consistency of our observations we considered a model where $k_x = k_y = 0.15 \text{ sec}^{-1}$, $k_z = 0$ and $W_{xz} = W_{yz} = W_{xy} = 0.5 \text{ sec}^{-1}$. It was found that if such a system starts to decay with a Boltzmann distribution over the levels corresponding to a temperature of 1.3 K then the decay will be very nearly exponential with the observed lifetime of 10 seconds, while after 5 seconds the population distribution is equal to

$$N_x : N_y : N_z = 75 : 75 : 100 \; ,$$

in good agreement with (5.7). (This result is almost independent of the initial population distribution).

Using the values (5.7) for the population distribution we calculated the relative activities given in table 5.IV from the data of table 5.III. A difficulty arose in experiments on the very weak o-o band, where we were forced to use a relatively long response time in our detection system. This leads to a distortion of the delayed signals in which the steep rise in the beginning is smeared out. It is therefore to be expected that the delayed signal measured for the $x \leftrightarrow z$ transition is in fact too strong, and that part of the light increase does not originate directly from the microwave sweep, but is due to subsequent relaxation from the overpopulated $|x\rangle$ level into the radiative $|y\rangle$ level. The observed value of $h_{yz}/I = 0.12$ indeed suggests that this is the case. For a system where only $|y\rangle$ is radiating and with the population distribution (5.7) one expects a value of 0.16 for this quantity, while for the case that the $|x\rangle$ and $|y\rangle$ levels are both radiative $h_{yz}/I = 0.08$. Recalling that in the case where $|y\rangle$ only is radiating h_{yz} is decreased by the system reponse time it follows that k_x^r/k_y^r must be smaller than 0.5.

As a proof for the situation just described we show in fig. 5.7 the results of an experiment where the signals of the o-o band are compared directly with those of (9_1^0). Here we show the delayed signals of the $y \leftrightarrow z$

Table 5.IV

band	vibration symmetry	k_x^r	k_y^r	k_z^r
(8_1^0)	e_{2g}	1.00 (0.05)	1.0	0.0 (0.05)
(9_1^0)	e_{2g}	1.1 (0.2)	1.0	0.0 (0.1)
(6_1^0)	e_{2g}	1.0 (0.3)	1.0	0.7 (0.3)*
(4_1^0)	b_{2g}	1.0 (0.2)	1.0	0.0 (0.2)
o-o	a_{1g}	< 0.3†	1.0	0.0 (0.2)

*) This error is to one side only: k_z^r = 1.0 is not allowed, for the y ↔ z transition would not be observed then.

†) Because of the weakness of the o-o band this number was not determined from the data of table 5.III, but in a different manner (see text).

Table 5.IV. Radiative rates for the different vibronic bands.
Radiative rates for the individual bands calculated according to (5.6) from the data of table 5.III. The rate k_y^r is set equal to 1.0 for each vibronic band. Estimated maximum errors in parentheses.

and x ↔ z transitions with about one second interval in between for both bands. The x ↔ z transition for the o-o band can hardly be observed, while the results for the (9_1^0) band prove that there is a population difference for the $|x\rangle$ and $|z\rangle$ levels at the moment the resonant microwaves of the x ↔ z transition hit the crystal. In this experiment the effect of the relaxation from $|x\rangle$ to $|y\rangle$ on h_{xz} is reduced; 1 second after the y ↔ z transition the $|y\rangle$ level should be slightly overpopulated relative to the undisturbed situation and relaxation from $|x\rangle$ to $|y\rangle$ is less probable. From this figure one concludes that k_x^r for the o-o band cannot be larger than 0.3.
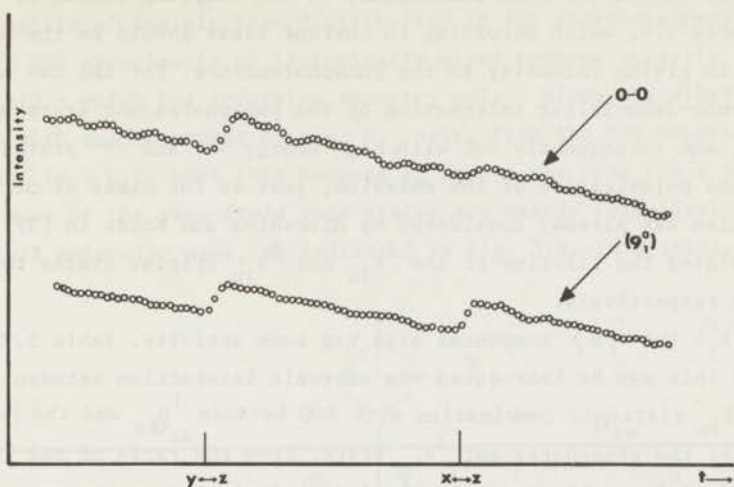
Fig. 5.7. MIDP signals corresponding to the y ↔ z and x ↔ z transitions in the phosphorescence decay of

a) (9_1^0)

b)   the o-o band.

The delay time between the two transitions in both cases is about 1 second. From the positive signal in the (9_1^0) band caused by the x ↔ z transition it follows that there is a population difference for $|x\rangle$ and $|z\rangle$ at the moment the second transition occurs. The corresponding signal for the o-o band is much weaker, indicating that the $|x\rangle$ level here does not have much radiative character.

3.4 Discussion.

First it is noted that within the experimental accuracy the results of the Zeeman experiments on (8_1^0) are consistent with the more subtle MIDP technique. The microwave experiments prove that for the (8_1^0) band k_x^r and k_y^r are equal to within 5%. When turning to tables 5.I and 5.II of the Zeeman effect, the equality $k_x^r = k_y^r$ indeed requires that k_z^r is very small, which is in perfect agreement with table 5.IV.

Let us now look at the results for the various bands with reference to table 5.V which gives the possible mechanisms derived by Albrecht [5] from group theory. First it is apparent that for the intense bands involving the vibrations ν_8 and ν_9 of e_{2g} symmetry the $|x\rangle$ and $|y\rangle$ components are by

far the most radiative. This corresponds to the coupling scheme of the top line of table 5.V, which according to current ideas should be the most effective in giving intensity to the phosphorescence. For the two modes strong pseudo-Jahn-Teller interaction of the phosphorescent state occurs* with $^3E_{1u}$, and subsequently SOC with high energy $\sigma\pi^*$ and $\pi\sigma^*$ states leads to out-of-plane polarization of the emission, just as for other aromatics. This SOC mechanism was already considered by Mizushima and Koide in [37], where they calculated the lifetime of the $^3E_{1u}$ and $^3B_{1u}$ triplet states to be 0.14 and 14 sec respectively.

For (6_1^0) the $|z\rangle$ component also has some activity. Table 5.V(fig. 5.1) shows that this may be introduced via vibronic interaction between the $^1B_{2u}$ and $^1E_{1u}$ states in combination with SOC between $^1B_{2u}$ and the $|z\rangle$ component of the phosphorescent $^3B_{1u}$ state. From the ratio of the intensity of (6_1^0) and (8_1^0) and the activity k_z^r of (6_1^0) derived from the present experiments it follows that this mechanism is about 100 times weaker than the dominant path of the top line in table 5.V. This is in agreement with the lifetime (3500 sec) of the $^3B_{1u}$ triplet calculated by Hameka and Oosterhoff [15] on the basis of SOC between the $^3B_{1u}$ and $^1B_{2u}$ states.

For the (4_1^0) band, which involves a b_{2g} mode, $|x\rangle$ and $|y\rangle$ also are the only active components. This supports the $^3B_{1u}$ assignment of the lowest triplet state of benzene: as mentioned by Albrecht [5] activity of the $|z\rangle$ component (or, in other words, out-of-plane polarization of the emission) in this band would only be compatible with a $^3B_{2u}$ assignment for the lowest triplet (see bottom line of the two sections of table 5.V, where Albrecht's [5] coupling scheme for a $^3B_{2u}$ assignment of the phosphorescent state is given, an assignment which is ruled out by the present experiments). The emission of the (4_1^0) band is thought to be "stolen" from the $^1E_{1u} \rightarrow {}^1A_{1g}$ $\pi\pi^*$ transition.

The results for the o-o band, which confirm an earlier observation by Gwaiz et al. [25], show that here the $|y\rangle$ level is most active. This is

---

* The simultaneous activity of ν_8 and ν_9 in this interaction gives rise to the appearance of combination bands (2 quanta of one and 1 of the other) in the phosphorescence spectrum. We have made a quantitative analysis of this problem and the intensity of these bands. This will be reported in another paper [32].

in very nice agreement with the explanation put forward to account for the
non-hexagonality of the electron distribution in the phosphorescent state
observed in ESR experiments on isotopically mixed benzene crystals [29]. The
crystal field – which has inversion symmetry only – mixes the vibrationless
$^3B_{1u}$ state with one component of the $^3E_{1u}$ pair. From the ESR experiments it
follows that in a C_6D_6 host this happens in such a way that the x and y
principal axes of the zero-field spin states are nearly coincident with in-
plane twofold molecular axes, as indicated in fig. 5.8. In a static picture
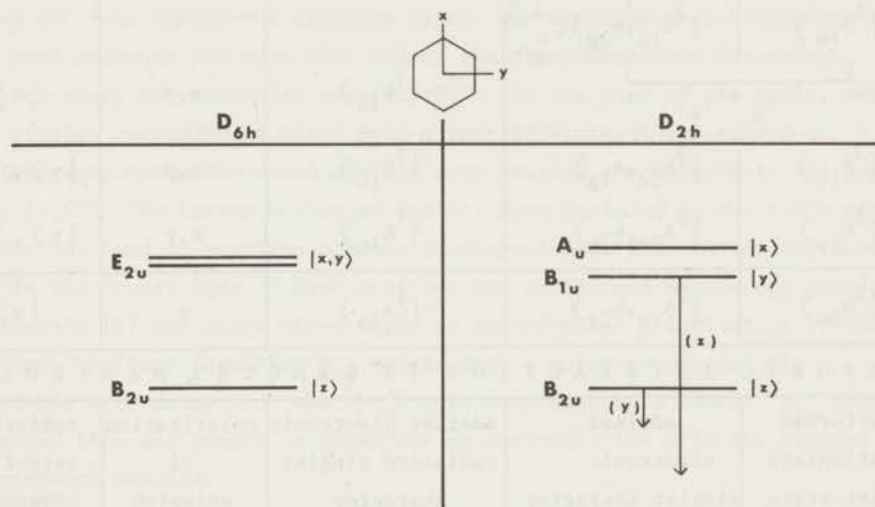
Fig. 5.8. The lowest vibronic level of the $^3B_{1u}$ state
   a) in the free molecule of D_{6h} symmetry
   b) in the benzene crystal.
The zero-field splitting and orientation of the principal axes are known from
ESR experiments, which indicate that D_{2h} symmetry is approximately preserved.
The total symmetry labels at the right and radiative decay modes are those
predicted by group theory for the D_{2h} situation.

of the situation one might say that the crystal field "locks" the molecule in
a distorted conformation of approximate D_{2h} symmetry. It then follows from
group theory that, if the D_{2h} symmetry were perfect with the set of axes as
fixed by the ESR results, all out-of-plane intensity would originate from the
$|y\rangle$ state. That the $|x\rangle$ state also posesses some activity is an
indication of the lower symmetry of the situation.

VIBRONIC INTERACTION IN TRIPLET MANIFOLD

unperturbed vibrationless triplet state	admixed triplet character by vibronic coupling	admixed electronic singlet character	polarization of emission	radiative zero-field component
VIBRONIC COUPLING		SPIN–ORBIT COUPLING		
$\|^3B_{1u}\rangle$	$\|^3E_{1u}, e_{2g}\rangle$	$\|^1A_{2u}\rangle$	z	$\|x\rangle, \|y\rangle$
$\nu_8 > \nu_6$		$\|^1E_{1u}\rangle$	x,y	$\|z\rangle$
$\|^3B_{1u}\rangle$	$\|^3E_{2u}, e_{1g}\rangle$	$\|^1E_{1u}\rangle$	x,y	$\|y\rangle, \|x\rangle$
$\|^3B_{1u}\rangle$	$\|^3A_{2u}, b_{2g}\rangle$	$\|^1E_{1u}\rangle$	x,y	$\|y\rangle, \|x\rangle$
$\|^3B_{2u}\rangle$	$\|^3A_{1u}, b_{2g}\rangle$	$\|^1A_{2u}\rangle$	z	$\|z\rangle$

VIBRONIC INTERACTION IN SINGLET MANIFOLD

unperturbed vibrationless triplet state	admixed electronic singlet character	admixed electronic radiative singlet character	polarization of emission	radiative zero-field component
SPIN–ORBIT COUPLING		VIBRONIC COUPLING		
$\|^3B_{1u}\rangle$	$\|^1B_{2u}\rangle$	$\|^1E_{1u}, e_{2g}\rangle$	x,y	$\|z\rangle$
		$\nu_6 > \nu_8$		
		$\|^1E_{1u}, e_{1g}\rangle$	x,y	$\|y\rangle, \|x\rangle$
$\|^3B_{1u}\rangle$	$\|^1E_{2u}\rangle$	$\|^1E_{1u}, b_{2g}\rangle$	x,y	$\|y\rangle, \|x\rangle$
		$\|^1A_{2u}, e_{2g}\rangle$	z	$\|x\rangle, \|y\rangle$
$\|^3B_{2u}\rangle$	$\|^1B_{1u}\rangle$	$\|^1A_{2u}, b_{2g}\rangle$	z	$\|z\rangle$

Table 5.V

Table 5.V. Mechanisms allowed by group theory for the appearance of benzene phosphorescence by a combination of vibronic interaction and SOC, according to Albrecht [5].

    The direction of polarization for electric dipole radiation and the spin component from which the emission originates are given in the last two columns. The first line in each part of the table corresponds to "pseudo-Jahn-Teller" vibronic coupling, which is known to be particularly strong [9,10] and the most effective modes have been indicated. The top line represents the only path in which strong vibronic coupling is combined with strong SOC (one centre-one electron type). Our experiments substantiate that this path accounts for more than 90% of the phosphorescence intensity.

    For every SOC-mechanism considered in the top part of the table, whereby some singlet character is mixed into a triplet state, there exists a complementary mechanism which admixes some triplet character into the ground state [7,36]. The latter mechanism has not been included in the table since it does not lead to coupling schemes distinguishable from those considered.

    In the lowest line of both sections two additional mechanisms considered by Albrecht [5] are given where there is out-of-plane polarization of the emission for lines involving b_{2g} modes. Such a polarization is only compatible with decay from the $|z\rangle$ spin component of a lowest $^3B_{2u}$ triplet state and this assignment is therefore in contradiction with the present experimental results.

4. Conclusions.

The present work shows again that the Zeeman and MIDP techniques may be very useful for studying phosphorescence mechanisms in aromatic molecules at low temperature. In the particular case of benzene they allow us to conclude that the phosphorescence must be out-of-plane polarized for more than 90%, as for other aromatic molecules. Further, there seem to be no contradictions left between the results of electron resonance on the vibrationless triplet state of benzene and spectroscopy of its $T_o \leftrightarrow S_o$ transitions. The present work once again corroborates the importance of the strong vibronic coupling that arises between the $^3B_{1u}$ and $^3E_{1u}$ states. Some aspects of this coupling are dealt with in a subsequent paper [32].

There is a major problem that needs clarification. In the "pseudo-cylindrical" model for vibronic coupling [34,35] the energy difference between the $|x\rangle$ and $|y\rangle$ zero-field spin states (-2E in the ESR terminology) and the direction of the corresponding principal axes are strongly dependent on the crystal field. If, however, the higher order "hexagonal" terms in the vibronic coupling were more important than previously thought [35], then the crystal field would merely try to select one of the conformations of lowest energy arising from the hexagonal terms in the molecular problem. In order to determine whether the zero-field splitting and radiative behaviour of the vibrationless $^3B_{1u}$ state of benzene are mainly determined by external or intramolecular effects, it therefore is important to study the molecule in environments other than a C_6D_6 crystal. Thus we have tried to extend our present studies to systems where the guest molecule is diluted in other hosts: n-hexane, n-octane, 1,4- dioxane and cyclopentane. In all these systems we saw positive MIDP signals corresponding to the x ↔ z and y ↔ z transitions. However, these signals proved to be broad and unsuitable for quantitative analysis *). The broadness of the microwave transitions indeed shows that the zero-field splitting parameters are environment dependent, but rigorous conclusions cannot be drawn. Though a

---

* In a very recent publication El-Sayed et al. [33] have reported very weak MIDP signals for the (8^0_1) and the o-o bands of benzene in a cyclohexane host which may indicate that the zero-field splitting pattern is different in this host.

quantitative treatment was not possible we think that the appearance of positive MIDP signals proves that in other environments the main phosphorescence mechanism is the same as in a C_6D_6 crystal (top line in table 5.V), and that the anomalous results obtained by Russell and Albrecht [18] are are not influenced by the special environment they chose (3-methyl-pentane glass), but by rotation of the phosphorescent molecules.

Acknowledgement.

References.

[1] Craig, D.P., 1950, J. Chem. Phys., 18, 236.

[2] Herzberg, G., 1966, Molecular Spectra and Molecular Structure, Vol. 3
     (D. van Nostrand).

[3] Goeppert-Mayer, M., and Sklar, A.L., 1938, J. Chem. Phys., 6, 645.

[4] Parr, R., Craig, D.P., and Ross, I., 1950, J. Chem. Phys., 18, 1561.

[5] Albrecht, A.C., 1963, J. Chem. Phys., 38, 354.

[6] Henry, B.R., and Siebrand, W., 1969, Chem. Phys. Lett., 3, 90.
     Henry, B.R., and Siebrand, W., 1969, J. Chem. Phys., 51, 2396.

[7] Veeman, W.S., and van der Waals, J.H., 1970, Mol. Phys., 18, 63.

[8] Albrecht, A.C., 1960, J. Chem. Phys., 33, 169.

[9] Moffitt, W., 1954, J. Chem. Phys., 22, 320.

[10] Liehr, A.D., 1961, Z. Naturf. A, 16, 641.

[11] Wilson, E.B., 1934, Phys. Rev., 45, 706.

[12] Burland, D.M., Castro, G., and Robinson, G.W., 1970, J. Chem. Phys.,
     52, 4100.

[13] Hochstrasser, R.M., Wessel, J.E., and Zewail, A.H., 1971, J. Chem. Phys.,
     55, 3596.

[14] Van Egmond, J., Burland, D.M., and van der Waals, J.H., 1971, Chem.
     Phys. Lett., 12, 206.

[15] Hameka, H.F., and Oosterhoff, L.J., 1958, Mol. Phys., 1, 358.

[16] Azumi, T., and McGlynn, S.P., 1962, J. Chem. Phys., 37, 2413.
     Krishna, V.G., and Goodman, L., 1962, J. Chem. Phys., 37, 912.
     El-Sayed, M.A., 1963, Nature, 197, 481.
     Gropper, H., and Dörr, F., 1963, Ber. Bunsenges. Physik. Chem., 67, 46,
     193.

[17] McClure, D.S., 1952, J. Chem. Phys., 20, 682.

[18] Russell, P.G., and Albrecht, A.C., 1964, J. Chem. Phys., 41, 2536.

[19] Castro, G., Clarke, R.H., Marzacco, C.J., Shafer, M., Whitemen, J., and
     Hochstrasser, R.M., The Triplet State, ed. A.B. Zahlan (Cambridge Univ.
     Press, London, 1967) p. 29.

[20] Hammer, A., Schwoerer, M., and Sixl, H., 1970, Chem. Phys. Lett., 5,
     434.

[21] Callomon, J.H., Dunn, T.M., and Mills, I.M., 1966, Phil. Trans. R. Soc.
     A, 259, 499.

[22] Van der Waals, J.H., and de Groot, M.S., The Triplet State, ed. A.B. Zahlan (Cambridge Univ. Press, London, 1967) p. 101.

[23] Schmidt, J., and van der Waals, J.H., 1968, Chem. Phys. Lett., 2, 640. Antheunis, D.A., Schmidt, J., and van der Waals, J.H., 1970, Chem. Phys. Lett., 6, 255.

[24] El-Sayed, M.A., Owens, D.V., and Tinti, D.S., 1970, Chem. Phys. Lett., 6, 395.

[25] Gwaiz, A.A., El-Sayed, M.A., and Tinti, D.S., 1971, Chem. Phys. Lett., 9, 454.

[26] Cox, E.G., Cruickshank, D.W.J., and Smith, J.A.S., 1958, Proc. Roy. Soc. A., 247, 1.

[27] Bacon, G.E., Curry, N.A., and Wilson, S.A., 1964, Proc. Roy. Soc. A., 279, 98.

[28] Schmidt, J., Veeman, W.S., and van der Waals, J.H., 1969, Chem. Phys. Lett., 4, 341.

[29] De Groot, M.S., Hesselmann, I.A.M., and van der Waals, J.H., 1969, Mol. Phys., 16, 45.

[30] Bernstein, E.R., Colson, S.D., Tinti, D.S., and Robinson, G.W., 1968, J. Chem. Phys., 48, 4632.

[31] Schmidt, J., Antheunis, D.A., and van der Waals, J.H., 1971, Mol. Phys., 22, 1.

[32] Van Egmond, J., and van der Waals, J.H., to be published.

[33] El-Sayed, M.A., Moomaw, W.R., and Chodak, J.B., 1972, J. Chem. Phys., 57, 4061.

[34] Van der Waals, J.H., Berghuis, A.M.D., and de Groot, M.S., 1967, Mol. Phys., 13, 301.

[35] Van der Waals, J.H., Berghuis, A.M.D., and de Groot, M.S., 1971, Mol. Phys., 21, 497.

[36] Goodman, L., and Krishna, V.G., 1963, Rev. Mod. Phys., 35, 541.

[37] Mizushima, M., and Koide, S., 1952, J. Chem. Phys., 20, 765.

C H A P T E R   VI

VIBRONIC INTERACTION IN THE LOWER ELECTRONIC STATES OF BENZENE:

TWO ACTIVE VIBRATIONAL MODES IN THE PSEUDO-CYLINDRICAL APPROXIMATION.

1. Introduction.

In chapter V we have reported the results of MIDP and Zeeman experiments
on benzene designed to determine the spin-orbit and vibronic coupling
mechanisms through which its phosphorescence acquires intensity. The results
of these experiments confirm the idea, first put forward by Mizushima and
Koide [1], that the vibronic coupling which in combination with SOC makes the
emission "allowed", occurs between the phosphorescent $^3B_{1u}$ state and the
near-by $^3E_{1u}$ pair.

Since the work by Moffitt and Liehr [2] the vibronic coupling between
the $^3B_{1u}$ and $^3E_{1u}$ states in benzene ("pseudo Jahn-Teller interaction") has
been the subject of many theoretical papers [3-5]. The calculations reported
by van der Waals et al. [5] were aimed in particular at providing a
quantitative interpretation of two observations made in recent low-
temperature work on isotopically mixed benzene crystals: the non-hexagonality
of the electron spin distribution in the phosphorescent triplet state [6,7]
and the remarkable low-frequency doublet in the triplet-singlet absorption
spectrum [8]. With a model, in which only the dominant e_{2g} mode ν_8 (mainly
C-C stretching) was considered, these seemingly different phenomena could be
explained from a single point of view. But, it also was noted that the model
was too simple to give a satisfactory account of spectral intensities. In
particular, since only one vibrational mode was considered, the model could
not be used to give an explanation for the characteristic combination bands
(2 times ν_8 plus ν_9 and 2 times ν_9 plus ν_8) that appear in the
phosphorescence spectrum of benzene. Further, in a recent study Katz et al.
[4] questioned the quantitative aspects of the previous analysis [5] and

indicated that inclusion of more coupling modes might have a noticeable effect on the position of the low-frequency doublet in the triplet←singlet absorption spectrum. Calculations of Sloane and Silbey [9] on the dynamic Jahn-Teller effect involving more active modes also suggest that the vibronic spacing and intensity distribution is influenced by the introduction of a second active mode.

In the course of our experiments on the phosphorescence of benzene described in chapter V, and the coupling between the $^3B_{1u}$ and $^3E_{1u}$ states that is an essential element in its mechanism, the question therefore arose: if one extends the model of part I and II [5] by including coupling via two active e_{2g} modes, ν_8 and ν_9, is it then possible to give a satisfactory account of the relevant features of the $^3B_{1u} \leftrightarrow {}^1A_{1g}$ transitions, both in absorption and emission? The present chapter gives the results of such a calculation, which appear to be in good agreement with experiment.

The procedure which we use is a straightforward extension of the classical papers on the dynamic Jahn-Teller coupling by Longuet-Higgins, Öpik, Pryce and Sack [10] and Moffitt and Thorson [11] to the situation for the phosphorescent state of benzene. For the sake of brevity we shall not repeat the basic formulation, but refer to [5] and the short introduction in chapter II. Because of the size of the variational problem which arises for two active modes we have treated the problem in the "pseudo-cylindrical approximation" of [5].

2. The Hamiltonian and the construction of its approximate solutions.

In the pseudo-cylindrical approximation one considers the coupling of the $^3B_{1u}$ Crude-Born-Oppenheimer (CBO) state with the members of the corresponding $^3E_{1u}$ pair and restricts oneself to coupling that is linear in the vibrational coordinates (see chapter II section 7). By a simple extension of (2.34) to coupling via two active modes, we obtain for the Hamiltonian of our problem

$$\mathcal{H} = \mathcal{H}^o + \tilde{\mathcal{H}}(\rho_8, \phi_8) + \tilde{\mathcal{H}}(\rho_9, \phi_9) + K_8 \rho_8 U(\phi_8) + K_9 \rho_9 U(\phi_9) \ . \qquad (6.1)$$

The first term $\mathcal{H}^o$ is the Hamiltonian for the electronic problem and the zero superscript indicates that it is considered independent of the nuclear coordinates and refers to the hexagonal conformation of lowest energy. The

next two terms are the Hamiltonians of two isotropic two-dimensional harmonic oscillators representing the active modes, expressed in the nuclear polar symmetry coordinates (ρ_8, ϕ_8) for ν_8 and (ρ_9, ϕ_9) for ν_9. The last two terms in (6.1) introduce coupling between the electronic states and K_8 and K_9 are parameters that determine the strength of the coupling. In the basis of the relevant eigenfunctions of $\mathcal{H}^o$

$$\psi^{o+}_{E_{1u}} \equiv E_+ \quad , \qquad \Lambda = 1 \quad ,$$

$$\psi^{o}_{B_{1u}} \equiv B \quad , \qquad \Lambda = 3 \qquad\qquad\qquad (6.2)$$

and $\psi^{o-}_{E_{1u}} \equiv E_- \quad , \qquad \Lambda = 5 \quad ,$

the operators $\mathcal{H}^o$ and $U(\phi)$ are represented by the matrices

$$\mathcal{H}^o = \begin{pmatrix} C & \cdot & \cdot \\ \cdot & \cdot & \cdot \\ \cdot & \cdot & C \end{pmatrix} \quad \text{and} \quad U(\phi) = \begin{pmatrix} \cdot & \exp(-i\phi) & \cdot \\ \exp(i\phi) & \cdot & \exp(-i\phi) \\ \cdot & \exp(i\phi) & \cdot \end{pmatrix}. \quad (6.3)$$

Λ in (6.2) relates to the electronic angular momentum in ψ^o (see below). Energies are expressed in the vibrational quantum ε_o of the mode ν_8 ($\varepsilon_o = 1483$ cm^{-1}) as in [5].

The eigenfunctions of (6.1) are solved by a variational procedure and developed in the basis of the eigenfunctions of the first three terms of (6.1),

$$| \Lambda; v_8, l_8; v_9, l_9 \rangle . \qquad\qquad\qquad (6.4)$$

This notation expresses that each basis function is a product of three functions: an electronic function ψ_Λ of the set (6.2), an eigenfunction of $\tilde{\mathcal{H}}(\rho_8, \phi_8)$ for the mode ν_8 with v_8 quanta and associated vibrational angular momentum l_8, and a similar eigenfunction of $\tilde{\mathcal{H}}(\rho_9, \phi_9)$ for ν_9 specified by the quantum numbers v_9 and l_9. (For given v the angular momentum can take the values $l = v, v-2, \ldots\ldots\ldots, 2-v, -v$.)

As in the earlier work on the Jahn-Teller effect [10,11] the computational problem is greatly simplified by noting that under the symmetry operator R corresponding to a rotation of the system over $2\pi/6$ about

the hexagonal axis the basis functions (6.4) transform as

$$R|\Lambda; v_8, l_8; v_9, l_9\rangle =$$

(6.5)

$$= \omega^{\Lambda + 2l_8 + 2l_9} |\Lambda; v_8, l_8; v_9, l_9\rangle = \omega^{-2j} |\Lambda; v_8, l_8; v_9, l_9\rangle$$

Here the quantum number j is defined as

$$j = \tfrac{1}{2}(\Lambda - 3) + l_8 + l_9 \quad .$$

(6.6)

The structure of the coupling terms in the pseudo-cylindrical Hamiltonian (6.1) is such that R commutes with $\mathcal{H}$, hence j is a good quantum number and $\mathcal{H}$ has no elements between states with different j. Accordingly, the space spanned by the basis (6.4) separates into a number of sub-spaces, characterized by their j-values, between which there are no coupling terms in the pseudo-cylindrical approximation. We shall be interested in the vibrationless $^3B_{1u}$ state which has j = 0 and in the states with j = $\pm$ 1, which correspond to "allowed" transitions in absorption from the ground state (see fig. 2 in [5b]).

In constructing the eigenvectors $\underset{\sim}{a}(j)^{(k)}$ of $\mathcal{H}$ by the variational method in the basis (6.4) one has the following selection rules. When denoting a general matrix element by

$$\langle \Lambda; v_8, l_8; v_9, l_9 | \mathcal{H} | \Lambda'; v_8', l_8'; v_9', l_9'\rangle \quad ,$$

(6.7)

and expressing energies in units of the vibrational quantum ε_o of ν_8 the diagonal elements are given by

$$(\tfrac{\Lambda - 3}{2})^2 C + (v_8 + 1) + a(v_9 + 1) \quad .$$

(6.8)

The first term in (6.8) represents the electronic energy, with the level of the B_{1u} state as the zero energy level. The next two terms give the vibrational energy due to the motion along Q_8 and Q_9 respectively, where a is the vibrational quantum of ν_9. The electronic energy C of the E_{1u} state and the quantum a are parameters determined from experiment (see below).

103

The only non-vanishing off-diagonal elements are those for which

  i) a pair of vibrational quantum numbers, say (v_9, l_9) is equal on both
       sides, $(v_9, l_9) = (v_9', l_9')$

  ii) $|\Lambda - \Lambda'| = 2$

  iii) one has, because of the conservation of j, for the other pair of
       vibrational quantum numbers (v_8, l_8) the relations

$$l_8 - l_8' = \tfrac{1}{2}(\Lambda' - \Lambda)$$

       and $|v_8 - v_8'| = 1$.

These matrix elements are calculated by extending the relations for the
vibrational integrals (2.36b) to two modes

$$\langle v_8+1, l_8+1; v_9, l_9 | \rho_8 \exp(i\phi_8) | v_8, l_8; v_9', l_9' \rangle =$$

$$= \langle v_8, l_8; v_9, l_9 | \rho_8 \exp(-i\phi_8) | v_8+1, l_8+1; v_9', l_9' \rangle =$$

$$= \delta_{v_9 v_9'} \, \delta_{l_9 l_9'} \, [\tfrac{1}{2}\{v + l + 2\}]^{\frac{1}{2}} \tag{6.9}$$

and

$$\langle v_8-1, l_8+1; v_9, l_9 | \rho_8 \exp(i\phi_8) | v_8, l_8; v_9', l_9' \rangle =$$

$$\langle v_8, l_8; v_9, l_9 | \rho_8 \exp(-i\phi_8) | v_8-1, l_8+1; v_9', l_9' \rangle = \delta_{v_9 v_9'} \, \delta_{l_9 l_9'} \, [\tfrac{1}{2}\{v - l\}]^{\frac{1}{2}}$$

with similar expressions for those matrix elements that have the pair (v_8, l_8)
equal.

The $j = 0$ problem is solved in a basis of 70 functions (all members of
(6.4) for which $v_8 + v_9 \leqslant 6$ and $j = 0$). The $j = 1$ problem is solved in a
basis of 94 functions ($v_8 + v_9 \leqslant 7$ and $j = 1$); the solutions for $j = -1$ are
the complex conjugates of those for $j = 1$. The order in which the basis
functions are taken will become clear from the tables that follow.

3. Parameters.

  From fig. 1 of [5b] it is found that the ratio of the reduced

intensities of (8_1^0) and (8_3^0) is strongly dependent on K_8 and only weakly on the other parameter C. We therefore chose K_8 equal to 1.2, the value that fits this ratio best in [5b], and subsequently fitted K_9 to the ratio of the intensities of (8_1^0) and (9_1^0). Further, there is an apparent relation between the parameter C, the distance between the B_{1u} and E_{1u} electronic states in the absence of vibronic coupling, and Γ, the energy separation between the o-o transition in the absorption spectra to these two electronic states [8,12]. (For meaning of the different parameters and the notation used for the various observables see also fig. 6.1.) The ratio a between the vibrational quanta of the two active vibrations in the excited states is assumed to be equal to this ratio in the ground state,

$$a = \nu_8/\nu_9 \simeq 0.75 \quad . \tag{6.10}$$

By trial and error it was found that the number of functions of the type (6.4) that is required for convergence is quite substantial. For instance, by increasing the basis from 45 functions (i.e. $\nu_8 + \nu_9 \leqslant 5$) to 94 functions ($\nu_8 + \nu_9 \leqslant 7$) the vibrational quantum of ν_8 in the lowest triplet state (Δ in fig. 6.1) is decreased by 0.03 ε_0, i.e. by 15% of its final value. In the language of perturbation theory this means that higher order terms are far from negligible.

4. Results.

In table 6.I we give the first parts of the eigenvectors of lower energy and of spectroscopic interest for the above choice of the parameters. The left hand section of table 6.I contains the coefficients of the eigenvector $\underset{\sim}{a}(0)^{(1)}$ with j = 0 of lowest energy and parentage $|B;0,0;0,0\rangle$, the vibrationless level of the lowest triplet state. Its coefficients express the distribution of intensity over the lines in the phosphorescence spectrum. For example the reduced intensity ratio

$$I(8_3^0)/I(8_1^0)$$

is determined by the square of the ratio of the coefficients of the basis functions $|E_\pm;3,\pm1;0,0\rangle$ and $|E_\pm;1,\pm1;0,0\rangle$ respectively,
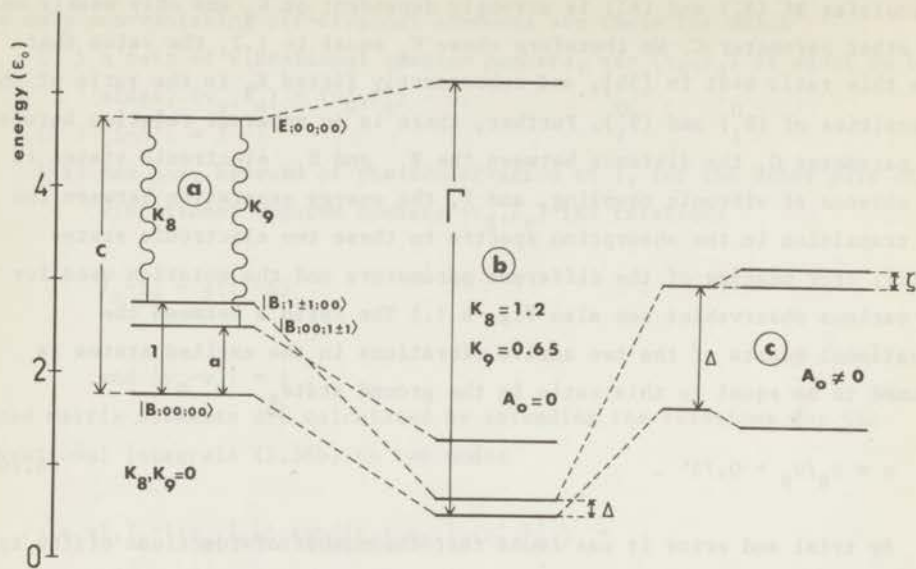
Fig. 6.1. The various parameters and observables which appear in the calculations.

(a) The imaginary situation where there is no vibronic coupling ($K_8 = K_9 = 0$) which illustrates the parameters that enter in the calculation. C is the energy separation between the vibrationless electronic states while the vibrational quanta are $\underline{1}$ and $\underline{a}$ for ν_8 and ν_9 respectively, because all energies are expressed in ε_o, the vibrational quantum of ν_8. The vibronic matrix elements between the vibrationless E states and the vibronic levels of the B state corresponding to one quantum of ν_8 and ν_9 are K_8 and K_9.
(b) The real situation with the observable levels when there is vibronic coupling. The values of the coupling parameters are as indicated in the figure. The vibronic level of the B state corresponding to one quantum of ν_8 is lowered in energy to a distance Δ from the lowest level and for a free molecule it is double degenerate. The energy gap between the o-o transitions of the absorption spectra to the two different electronic states is Γ.
(c) The degeneracy of the vibronic level in the B state with a single quantum of ν_8 is lifted by the interaction with the crystal field. The splitting is denoted by ζ.

$$I(8^0_3)/I(8^0_1) = \{a(0)^{(1)}_{10} / a(0)^{(1)}_2\}^2 \tag{6.11}$$

For the combination bands one has to sum over two terms of different parentage reflecting the degeneracy of a vibronic level with several quanta, for instance

$$I(8^0_2 9^0_1)/I(8^0_1) = \{a(0)^{(1)}_{12}/a(0)^{(1)}_2\}^2 + \{a(0)^{(1)}_{14}/a(0)^{(1)}_2\}^2 \tag{6.12}$$

because all states $|E_\pm;2,0;1,\pm1\rangle$ and $|E_\pm;2,\pm2;1,\mp1\rangle$ contribute to the phosphorescence intensity of $(8^0_2 9^0_1)$.

In the right hand section of table 6.I we give the eigenvectors of the lower two vibronic states for $j = \pm1$ and of total symmetry E_{1u}, which stem from $|B;1\pm1;0,0\rangle$ and $|B;0,0;1,\pm1\rangle$. It is clear from the coefficients in these eigenvectors that the two vibronic levels corresponding to ν_8 and ν_9 are heavily mixed which results in a lowering of the energy of the lowest state. A comparison of calculations and experimental results is made in table 6.II. The last column of this table gives the results of the earlier calculations with one active mode [5b].

5. The interaction with a crystal field.

We have made calculations on the influence of the crystal field in a way similar to that used in [5b]. The anisotropy of the interaction with the crystal field tentatively is approximated by the simple potential

$$V_{cr} = A_o(2\rho_8 \cos\phi_8 + K_9/K_8 \ 2\rho_9 \cos\phi_9) . \tag{6.13}$$

The physical idea behind this potential can be described as follows. Both ν_8 and ν_9 are thought to be decomposed in the "pure" stretching and bending modes as formulated in internal molecular coordinates [13]. The pure stretching mode S_8 [13,5a] is now supposed to be responsible for the vibronic coupling of the electronic states. A very elementary picture of this coupling is given by Salem [14], using the influence of bond stretching on the exchange integrals β in the Hückel picture. It is now to be expected that on decomposing ν_8 and ν_9 into the "pure" modes, the ratio of S_8 character present in the normal modes ν_8 and ν_9 is reflected in the ratio of the

Table 6.I

Parameters used			C = 3.00			$K_8 = 1.2$		$K_9 = 0.65$		$a = 0.75$	
eigenvector			$a(0)^{(1)}$				$a(1)^{(1)}$			$a(1)^{(2)}$	
j-value			0				1			1	
energy (ε_0)			0.475				0.663			1.299	
	function				coeff.	function				coeff.	coeff.
CBO state coeff.	Λ	v_8 l_8	v_9 l_9			Λ	v_8 l_8	v_9 l_9			
a_1	B	0 0	0 0		0.6439	E_-	0 0	0 0		-0.2166	0.0703
a_2	E_+	1 1	0 0		-0.2547	B	1 1	0 0		0.5124	-0.4503
a_3	E_+	0 0	1 1		-0.1612	B	0 0	1 1		0.4162	0.4582
a_4	E_-	1 -1	0 0		-0.2547	E_+	2 2	0 0		-0.2075	0.2200
a_5	E_-	0 0	1 -1		-0.1612	E_+	0 0	2 2		-0.1104	-0.1788
a_6	B	2 0	0 0		0.3469	E_+	1 1	1 1		-0.2170	-0.1003
a_7	B	0 0	2 0		0.1644	E_-	2 0	0 0		-0.1967	0.1640
a_8	B	1 1	1 -1		0.2372	E_-	0 0	2 0		-0.1024	-0.1254
a_9	B	1 -1	1 1		0.2372	E_-	1 1	1 -1		-0.1233	0.0982
a_{10}	E_+	3 1	0 0		-0.1140	E_-	1 -1	1 1		-0.1627	-0.1912
a_{11}	E_+	0 0	3 1		-0.0352	B	3 1	0 0		0.2415	-0.2685
a_{12}	E_+	2 0	1 1		-0.1060	B	0 0	3 1		0.0964	0.1989
a_{13}	E_+	1 1	2 0		-0.0757	B	2 0	1 1		0.2659	0.1570
a_{14}	E_+	2 2	1 -1		-0.0808	B	1 1	2 0		0.1776	0.1169
a_{15}	E_+	1 -1	2 2		-0.0489	B	1 -1	2 2		0.1430	0.2789
a_{16}	E_-	3 -1	0 0		-0.1140			.			
a_{17}	E_-	0 0	3 -1		-0.0352			.			
a_{18}	E_-	2 0	1 -1		-0.1060			.			
a_{19}	E_-	1 -1	2 0		-0.0757			.			
a_{20}	E_-	2 -2	1 1		-0.0808			.			
a_{21}	E_-	1 1	2 -2		-0.0489			.			
.								.			
.								.			
.		70 functions					94 functions			94 functions	

Table 6.1. Parts of the eigenvectors of lower energy $\underset{\sim}{a}(0)^{(1)}$, $\underset{\sim}{a}(1)^{(1)}$, $\underset{\sim}{a}(1)^{(2)}$. The basis functions are characterized by B, E_+, or E_- and the two sets of vibrational quantum numbers. The first column gives the coefficients of the lowest vibronic level of the B state, from which the phosphorescence originates; it is of B_{1u} vibronic symmetry and the coefficients determine the intensity distribution over the different bands in the phosphorescence spectrum. The eigenvectors in the last two columns are the two lower solutions of E_{1u} vibronic symmetry and have a parentage $|B;1,\pm1;0,0\rangle$ and $|B;0,0;1,\pm1\rangle$ respectively.

coupling parameters K_8/K_9. In this very simple reasoning the crystal field interaction of formula (3.1) in [5b] has to be extended to the form (6.13) above.

   The potential (6.13) for the crystal field interaction gives non-zero matrix elements between the state $\underset{\sim}{a}(0)^{(1)}$ and the real combination of the $j = \pm1$ states $\underset{\sim}{r}(1)^{(k)}$ defined as*

$$r(1)^{(k)} = \sqrt{\tfrac{1}{2}}\,\{\underset{\sim}{a}(1)^{(k)} + \underset{\sim}{a}(-1)^{(k)}\} \tag{6.14}$$

Using similar formulae as given in [5b] we calculated the following experimental observables: ζ (the splitting of the vibronic doublet (8_0^1) in the absorption spectrum, see fig. 6.1), $I_{o-o}/I(8_1^0)$ (the relative reduced intensity of the o-o transition in emission); $I_{o-o}/I(8_0^1)$ (the same quantity in the absorption spectrum), E (the zero-field splitting parameter equal to half the energy separation between the $|y\rangle$ and $|x\rangle$ spin components of the phosphorescent state $\underset{\sim}{a}(0)^{(1)}$) and ε (characterizing the deviation from hexagonal symmetry of the electron spin distribution $\underset{\sim}{a}(0)^{(1)}$, as defined in [6]). The results are given in table 6.III for two different values of the crystal field parameter A_o.

---

*
It is noted that in the corresponding formule (3.2) in [5b] the normalization constant $1/\sqrt{2}$ has been misprinted as $\sqrt{2}$. However, this mistake has not been carried through in the rest of the calculations.

Table 6.II

Parameters used	C = 3.00	K_8 = 1.2	K_9 = 0.65	a = 0.75
quantity	calculated from table 6.I	experiment	reference	earlier calculations one active mode ν_8
$I(8_1^0)\equiv 1.0$				
$I(9_1^0)$	0.40	0.37	[17]	-
$I(8_3^0)$	0.20	0.16	[17]	0.19
$I(9_3^0)$	0.019	0.015	[17]	-
$I(8_2^0 9_1^0)$	0.27	0.32	[17]	-
$I(8_1^0 9_2^0)$	0.13	0.13	[17]	-
Γ	4.71	4.64	[8,12]	4.3
Δ	0.188	0.165	[15b]	0.32
$I(9_0^1)/I(8_0^1)$	0.11	0.43	[8]	-

Table 6.II. Calculated and experimental values of some observables in the triplet ↔ singlet spectra of benzene.

In the first five rows we compare the intensities of bands in the phosphorescence spectrum involving the active modes. Then two energy gaps observed in the absorption spectrum are given. Finally we calculate a reduced intensity ratio obtained from the absorption spectrum; the corresponding experimental value suffers from Fermi-resonance with another line in the spectrum (see text).

For comparison those results from the calculations with one active mode are given that reappear in the present calculations.

Table 6.III

parameters used	$C = 3.00$	$K_8 = 1.2$	$K_9 = 0.65$		$a = 0.75$
observable	calculated ($A_o = 0.014$)	calculated ($A_o = 0.007$)	experiment	ref.	
A.					$h(0,1)=2.01$
ζ (cm^{-1})	12.5	3.1	13.0($\pm$0.2)	[15b]	
$I_{(o-o)}/I(8_0^1)$	0.022	0.005	0.03($\pm$0.01)	[8]	$\lambda = 10.7$
$I_{(o-o)}/I(8_1^0)$	0.016	0.004	0.017($\pm$0.002)		
B.					$P = -0.62$
E (cm^{-1})	-0.013	-0.0065	-0.0064	[6]	
2ϵ	0.044	0.022	0.015, 0.020	[7]	

Table 6.III. Calculated and observed values of observables induced by the interaction with the crystal field.
Tabulated are the values calculated for some spectroscopic (A) and ESR (B) quantities, for two different values of the crystal field parameter A_o. Some parameters that appear in the calculation of these quantities are given at the right of the table. For their meaning we refer to the earlier calculations [5b].

6. Discussion.

a. The phosphorescence spectrum.

From the data in table 6.II it is clear that the present model with two "pseudo-Jahn-Teller" active vibrations can account for a characteristic feature of the phosphorescence spectrum; the bands involving 3 quanta of vibrational energy are calculated to have intensities close to the observed values.

b. The $^3B_{1u} \leftarrow {}^1A_{1g}$ absorption spectrum.

i) The remarkable shift to lower energy of the first vibronic level to which a transition from the ground state is allowed (parentage

$|B;1,\pm1;0,0\rangle$) becomes even more pronounced by the introduction of a second active mode, as can be clearly seen from table 6.II. The experimental value for the energy separation Δ between the o-o band and the (8_0^1) band as reported in [8] is still somewhat smaller than the calculated value. However, one expects the calculated value to decrease further upon introducing the "hexagonal" terms in the Hamiltonian, as shown in the earlier investigations [5b].

ii) From the coefficients in table 6.I one also can make an estimate of the ratio of the oscillator strengths of the $^3B_{1u} \leftarrow {}^1A_{1g}$ and $^3E_{1u} \leftarrow {}^1A_{1g}$ spectra by assuming this ratio to be equal to the ratio of the reduced intensities of the origins of the spectra, in the sense that one takes the false origin (8_0^1) of the $^3B_{1u} \leftarrow {}^1A_{1g}$ spectrum,

$$f(^3B_{1u})/f(^3E_{1u}) \simeq \{a(1)_1^{(1)}\}^2 = 0.04 \quad,$$

in agreement with the order of magnitude given by Colson and Bernstein [12].

iii) The calculated splitting ζ of (8_0^1) into two components by the interaction with a crystal field of the form (6.13) is consistent with the assignment of this band proposed by Burland, Castro and Robinson [8] and later confirmed by Zeeman studies [15].

It also might be understood why this splitting disappears on adding one quantum of ν_1, i.e. in the band $(8_0^1 1_0^1)$. Using the numbers reported by Burland et al. [8] one expects this band at about 1170 cm^{-1} from the o-o transition. However, it is found at about 1140 cm^{-1}. This relatively large shift is thought to be due to Fermi-resonance with the higher (9_0^1) band which is much stronger than the interaction with the crystal field. This would also explain the deviation of the experimental intensity of (9_0^1) from the calculated value (table 6.II) and the decrease in intensity of $(8_0^1 1_0^1)$ compared with the corresponding bands $(6_0^1 1_0^1)$ and (1_0^1).

iiii) The intensity of the o-o transition in the absorption spectrum is not known as accurately as that of the phosphorescence spectrum. The experimental value must be in the order of 3% of the intensity of (8_0^1) as can be measured from the spectrum given in [8]. The calculated and experimental values of these quantities are compared in table 6.III, for

two different values of the crystal field potential parameter A_o.

c. The ESR parameters.

From table 6.III we see that the present model is too simple to account for both the ESR quantities and the spectroscopic features of the excited benzene molecule in a crystal. A crystal field of the form (6.13) can explain the spectroscopic properties of the molecule, but the non-hexagonality of the spin distribution then is exaggerated. A possible explanation for this is the neglect of quadratic terms in the crystal field potential [5b]. Inprovement by taking more parameters in the calculation does not look realistic, however, because of the small amount of experimental data available.

d. The activity of ν_6 in the spectra.

We have extended the calculations to three active modes of e_{2g} symmetry (ν_8, ν_9 and ν_6 in the order of decreasing activity) in an attempt also to account for the emission and absorption intensities of the lines involving ν_6. In order to calculate the right intensity for the (6_1^0) band in the phosphorescence spectrum one has to introduce a coupling parameter K_6 of about 0.13 in the calculations. However this value of K_6 cannot explain the relatively high intensity of (6_0^1) in the absorption spectrum; for this one would have to take K_6 much larger. It might be that for this bending vibration higher order terms ("hexagonal terms") play a more important role, and that the effect of the different terms is such that there is interference between them causing a difference in the relative intensities of (6_0^1) and (6_1^0). In table 6.IV we give the reduced intensities of some bands involving ν_6 in the phosphorescence spectrum. These intensities were calculated with a value of 0.17 for K_6. Experimental data for these lines are not available, but some of them are reported to be visible [16]. The order of magnitude of the calculated intensities is such, that one expects them to be very weak in the spectrum, in accordance with the experimental report [16].

7. Conclusions.

In this chapter we have presented some calculations in a simple model to account for certain spectroscopic features of the benzene molecule in the

parameters used	$C = 3.00$	$K_8 = 1.2$	$K_9 = 0.65$
	$a = \nu_9/\nu_8 = 0.75$	$\nu_6/\nu_8 = 0.375$	

quantity	calculated	experimental	reference
$I(8_1^0) \equiv 1.0$			
$I(6_1^0)$	0.048	0.03	[17]
$I(8_2^0 6_1^0)$	0.036	very weak	[16]
$I(9_2^0 6_1^0)$	0.008	–	
$I(8_1^0 9_1^0 6_1^0)$	0.029	very weak	[16]

Table 6.IV. Calculated reduced intensities for bands in the phosphorescence spectrum involving ν_6. The parameter K_6 for these calculations has been chosen as 0.17.

triplet state. As is clear from the results in the tables 6.II and 6.III it is possible to explain the most salient spectroscopic features of the molecule in the simple "pseudo-cylindrical approximation". The most striking phenomenon, the energy decrease of the ν_8 mode in the excited state, can be understood in the model with two active vibrations. These calculations again prove that the assignment given by Burland et al. [8] of the strong doublet in the triplet ← singlet absorption spectrum as (8_0^1) is right and that the splitting into two components is due to the interaction with the crystal field. Another characteristic phenomenon for the excited state of benzene is the appearance of the combination bands in the phosphorescence spectrum. The calculated reduced intensities tabulated in table 6.II are in good agreement with the experimental values, and the conclusion can be drawn that for these quantities the neglected higher order terms in the Hamiltonian are relatively less important and that the pseudo-cylindrical approximation works nicely for the modes ν_8 and ν_9. For other quantities these terms might be non-negligible and perhaps an extension of the approximation methods introduced by Sloane and Silbey [9] for the Jahn-Teller case might make calculations in this direction feasible.

The crystal field also is responsible for the intensities of the o-o

transitions in the spectra. The description with the simple form of the crystal field potential (6.13), however, does not succeed in giving compatible results for both the spectroscopic and the ESR quantities with a single value of the parameter A_o.

Although it follows from this chapter that the main conclusions of the former calculations were right [5] the present results prove that the activity of a second mode has a marked effect on the vibronic level spacing as mentioned by Katz et al. [4].

[1] Griffith, J.S., 1956, J. Chem. Phys., 17, ...
[2] Soules, T.F., 1965, J. Chem. Phys., 42, ...
Perrin, M.H., and Gouterman, M., 1967, J. Chem. Phys., 46, 1019.
[3] Reedy, A., Kulel, DH., Chari, N., and Bersohn, R., 1976, J. Chem. Phys., 65, 60.
[4] ...
[5] Van der Waals, J.H., Berghuis, A.M.D., and de Groot, M.S., 1967, Mol. Phys., 13, 301.
Van der Waals, J.H., Berghuis, A.M.D., and de Groot, M.S., 1971, Mol. Phys., 21, 497.
[6] de Groot, M.S., Hesselmann, I.A.M., and van der Waals, J.H., 1967, Mol. Phys., 13, 583.
[7] Davis-Searles, A.H., and Gouterman, C.A., 1969, J. Chem. Phys., 51, 1163.
[8] Burland, D.M., Castro, G., and Robinson, G.W., 1970, J. Chem. Phys., 52, 4100.
[9] Sloane, C.S., and Silbey, R., 1972, J. Chem. Phys., 56, 6031.
[10] Langhoff-Stephen, S.C., Quinn, R., Pizza, M.G.J., and Bree, R.A., 1974, Proc. R. Soc., A 340, 17.
[11] Sixl, H., and Thomas, W.E., 1970, Mol. Phys., C.N.R.S., Paris, November.
[12] Colson, S.D., and Bernstein, E.R., 1965, J. Chem. Phys., 43, 2661.
[13] McClure, D.S., 1952, Phil. Trans. R. Soc., A 256, 131.
[14] Salem, L., 1966, The Molecular Orbital Theory of Conjugated Systems (New York W.A. Benjamin).
[15] Hochstrasser, R.M., Wessel, J.E., and Zewail, A.H., 1971, J. Chem. Phys., 55, 5344.
a) Van Egmond, J., Burland, D.M., and van der Waals, J.H., 1971, Chem. Phys. Lett., 12, 206.
[16] Sloane, C.S., and Robinson, G.W., 1967, J. Chem. Phys., 74, 1516.
[17] Sloane, C.S., 1965, J. Chem. Phys., 50, 1440, 1478.

References.

[1] Mizushima, M., and Koide, S., 1952, J. Chem. Phys., 20, 765.

[2] Moffitt, W., 1954, J. Chem. Phys., 22, 320.
     Liehr, A.D., 1961, Z. Naturf., 16a, 641.
     Moffitt, W., and Liehr, A.D., 1957, Phys. Rev., 106, 1195.

[3] Donath, W.E., 1964, J. Chem. Phys., 41, 626.
     Donath, W.E., 1965, J. Chem. Phys., 42, 118.
     Perrin, M.H., and Gouterman, M., 1967, J. Chem. Phys., 46, 1019.

[4] Katz, B., Brith, M., Sharf, B., and Jortner, J., 1970, J. Chem. Phys.,
     52, 88.

[5] a) Van der Waals, J.H., Berghuis, A.M.D., and de Groot, M.S., 1967, Mol.
     Phys., 13, 301.
     b) Van der Waals, J.H., Berghuis, A.M.D., and de Groot, M.S., 1971, Mol.
     Phys., 21, 497.

[6] De Groot, M.S., Hesselmann, I.A.M., and van der Waals, J.H., 1969, Mol.
     Phys., 16, 45.

[7] Ponte-Goncalves, A.M., and Hutchison, C.A., 1968, J. Chem. Phys., 49,
     4235.

[8] Burland, D.M., Castro, G., and Robinson, G.W., 1970, J. Chem. Phys., 52,
     4100.

[9] Sloane, C.S., and Silbey, R., 1972, J. Chem. Phys., 56, 6031.

[10] Longuet-Higgins, H.C., Öpik, U., Pryce, M.H.L., and Sack, R.A., 1958,
     Proc. R. Soc., A 244, 1.

[11] Moffitt, W., and Thorson, W.R., 1958, Rec. Mém., C.N.R.S., Paris,
     November.

[12] Colson, S.D., and Bernstein, E.R., 1965, J. Chem. Phys., 43, 2661.

[13] Whiffen, D.H., 1955, Phil. Trans. R. Soc., A 248, 131.

[14] Salem, L., 1966, The Molecular Orbital Theory of Conjugated Systems (New
     York W.A. Benjamin).

[15] a) Hochstrasser, R.M., Wessel, J.E., and Zewail, A.H., 1971, J. Chem.
     Phys., 55, 3596.
     b) Van Egmond, J., Burland, D.M., and van der Waals, J.H., 1971, Chem.
     Phys. Lett., 12, 206.

[16] Nieman, G.C., and Robinson, G.W., 1963, J. Chem. Phys., 39, 1298.

[17] Nieman, G.C., 1969, J. Chem. Phys., 50, 1660, 1674.

SUMMARY

This thesis gives the results of some experiments at liquid helium temperature and calculations concerning the lowest triplet state of benzene. Our first task was to build a Zeeman spectrometer and study the optical transitions between the triplet state and the ground state of this molecule.

It appeared that for the special case of a benzene crystal the Zeeman technique suffers from shortcomings due to the relative orientation of the different molecules. Hence the experiments were extended with the study of benzene by microwave induced delayed phosphorescence (MIDP). In this method there is no external magnetic field which leads to the anisotropy that is the cause of the ambiguity in the Zeeman technique. The results of our experiments then directed our attention to the calculations by van der Waals, Berghuis and de Groot on the vibronic coupling in the triplet manifold of benzene. With a simple extension, which for the computational problem has considerable consequences, we were able to account for some characteristic features of the phosphorescence spectrum.

In chapter I a general introduction is given in which the history of the experiments on molecular triplet states is sketched and in which the Zeeman technique appears as a recent development. A theoretical introduction to the problems which occur for the benzene molecule follows in chapter II. A description of the Zeeman spectrometer then is given in chapter III, where also the theoretical model by which the experimental results have to be interpreted is considered.

The Zeeman-absorption experiment discussed in chapter IV was started to confirm Burland, Castro and Robinson's interpretation of the strong doublet which these authors observed in the triplet←singlet absorption spectrum of benzene. They assigned it as the band in which one quantum of ν_8 is excited and which is split into two components by the crystal field. Since the assignment of this band is essential for a proper understanding of vibronic coupling in the triplet manifold of benzene we tried to check it by investigating which of the spin sublevels is involved in the absorption for the two components of the doublet. From the experiment it followed that for one component the $|x\rangle$ triplet sublevel is responsible for the absorption. For the other component it proved impossible, because of the crystal structure, to get unambiguous results with the Zeeman technique, but our results are not in contradiction with the theoretical prediction that only the

$|y\rangle$ sublevel has absorption probability. Therefore, the results as a whole can be seen as a confirmation of Burland et al.'s assignment.

In chapter V Zeeman and MIDP experiments are described on benzene's phosphorescence. As demonstrated in chapter II one can investigate the phosphorescence mechanism by determining which triplet sublevels are responsible for the radiation in the various bands of the spectrum. For benzene, where vibronic interaction is important, one might expect different results for bands in the spectrum in which different vibrations are active. Because the Zeeman effect did not yield unambiguous results, the experiments were extended with MIDP studies and five of the stronger bands in the phosphorescence spectrum were studied with this technique. The results prove that, in contradiction to Albrecht's interpretation of photo-selection experiments, the phosphorescence must be almost purely out-of-plane polarized. It is also confirmed that vibronic interaction in the triplet manifold plays the dominant role in the phosphorescence mechanism.

In chapter VI we give the results of some calculations on this vibronic interaction in which two active modes are taken into consideration. It appears that one can account for the characteristic bands in the phosphorescence spectrum which involve three quanta of the active modes distributed in different ways over the two vibrations (3-0, 2-1, 1-2 and 0-3 of ν_8 and ν_9, respectively).

SAMENVATTING

Dit proefschrift geeft de resultaten van enige experimenten, bij de
temperatuur van vloeibaar helium, en berekeningen aangaande de laagste
triplettoestand van benzeen. Onze eerste taak was een Zeemanspectrometer te
bouwen en de optische overgangen tussen de triplettoestand en de grondtoe-
stand van dit molecule te bestuderen. Het bleek dat voor het speciale geval
van een benzeenkristal de Zeemantechniek lijdt aan tekortkomingen die voort-
vloeien uit de onderlinge ligging van de verschillende moleculen. Daarom
werden de experimenten uitgebreid met de bestudering van benzeen door middel
van microgolf-geïnduceerde-vertraagde-fosforescentie-experimenten (microwave
induced delayed phosphorescence, MIDP). Bij dit soort metingen is niet het
uitwendige magneetveld aanwezig, dat leidt tot de anisotropie die de dubbel-
zinnigheid bij de Zeemantechniek veroorzaakt. De resultaten van onze
experimenten vestigden onze aandacht op berekeningen door van der Waals,
Berghuis en de Groot aan de vibronische koppeling tussen de triplettoestanden
van benzeen. Met een eenvoudige uitbreiding, die voor de omvang van het
rekenprobleem aanzienlijke consequenties heeft, zijn we in staat geweest
enige karakteristieke trekken van het fosforescentiespectrum te verklaren.

In hoofdstuk I wordt een algemene inleiding gegeven waarin de
geschiedenis van experimenten aan de triplettoestand van moleculen wordt
geschetst en waarin de Zeemantechniek als een recente ontwikkeling naar
voren komt. Een theoretische inleiding op de problemen die zich voordoen
bij benzeen volgt in hoofdstuk II. Een beschrijving van de Zeemanspectrometer
wordt daarna in hoofdstuk III gegeven, waar ook het theoretische model wordt
besproken aan de hand waarvan de experimentele resultaten moeten worden
geïnterpreteerd.

Het Zeeman-absorptie-experiment dat besproken wordt in hoofdstuk IV werd
ondernomen om een bevestiging te verkrijgen van Burland, Castro en Robinson's
interpretatie van het sterke doublet dat door hen in het triplet←singulet
absorptiespectrum werd waargenomen. Zij kenden dit doublet toe aan de band
waarbij één quant van v_8 wordt aangeslagen en die door het kristalveld in
twee componenten wordt opgesplitst. Daar de toekenning van deze band
essentieel is voor een juist begrip van de vibronische koppeling tussen de
triplettoestanden van benzeen, hebben we getracht van deze interpretatie een
bevestiging te krijgen door te onderzoeken welke tripletsubniveaus

betrokken zijn bij de absorptie van elk van de componenten van het doublet.
Uit het experiment volgde dat voor één component het $|x\rangle$ tripletsubniveau
verantwoordelijk is voor de absorptie. Voor de andere component bleek het
vanwege de kristalstructuur onmogelijk ondubbelzinnige resultaten te krijgen,
maar deze zijn niet met de theoretische voorspelling in tegenspraak, dat
voor deze component alléén het $|y\rangle$ niveau absorptiewaarschijnlijkheid heeft.
Het resultaat als geheel kan daarom als een bevestiging van Burland et al.'s
toekenning gezien worden.

CURRICULUM VITAE

Na in 1964 het HBS-B diploma behaald te hebben aan de Rijks-HBS te Den Helder begon ik in september van dat jaar de Scheikundestudie aan de Rijksuniversiteit te Leiden. In januari 1967 werd het candidaats-examen (letter E) afgelegd waarna de studie met hoofdrichting Organische Chemie werd voortgezet onder leiding van Prof. Dr. E. Havinga en Dr. C. Altona. Als bijvak werd Röntgen-diffractie gekozen, en in overleg met Prof. Havinga werd ook een groot gedeelte van de hoofdvak practicumtijd op deze afdeling besteed, onder leiding van Dr. C. Romers. Als derde richting werd Theoretische Organische Chemie gekozen bij Prof. Dr. L.J. Oosterhoff. Na het behalen van het doctoraal examen in januari 1969 werd mij de gelegenheid geboden een promotieonderzoek te beginnen als assistent in dienst van de Rijksuniversiteit in de werkgroep "Moleculen in de Aangeslagen Toestand" die onder leiding staat van Prof. Dr. J.H. van der Waals. Januari 1970 trad ik in dienst bij de stichting Scheikundig Onderzoek Nederland als wetenschappelijk medewerker.